POLITECNICO DI MILANO

Facoltà di Ingegneria Industriale

Corso di Laurea in Ingegneria Meccanica

Design of an innovative shape memory actuator for fluidic applications

Relatore Interno: Prof. Gaetano Cascini

Relatori Esterni: Ing. Francesco Butera, Prof. Ferdinando Auricchio

Tesi di Laurea di:

Carlo Blu STEINER

Matr. n. 804436

Anno Accademico 2014/2015

Contents

Nomenclature

M^s	Martensite transformation start temperature	$[K]$
M^f	Martensite transformation finish temperature	$[K]$
A^s	Austenite transformation start temperature	$[K]$
A^f	Austenite transformation finish temperature	$[K]$
T_m	Inflection point of the logistic curve	$[Year]$
K	Saturation point of the logistic curve	
Kv	Flow rate of the valve	$[m^3/h]$
V	Overall volume of the valve	$[mm^3]$
E_A	Austenitic Elastic Modulus	$[MPa]$
ν_A	Austenitic Poisson's ratio	
E_M	Martensitic Elastic Modulus	$[MPa]$
ν_M	Martensitic Poisson's ratio	
ε^L	Transformation strain	
$(\delta\sigma/\delta T)_L$	Loading $(\delta\sigma/\delta T)$	$[MPa/K]$
σ_L^S	Start of transformation stress during loading	$[MPa]$
σ_L^E	End of transformation stress during loading	$[MPa]$
T_0	Reference temperature	$[K]$
$(\delta\sigma/\delta T)_U$	Unloading $(\delta\sigma/\delta T)$	$[MPa/K]$
σ_U^S	Start of transformation stress during unloading	$[MPa]$
σ_U^E	End of transformation stress during unloading	$[MPa]$
σ_{CL}^S	Start of transformation stress during compressive loading	$[MPa]$
ψ_{el}	Elastic strain energy	$[J]$
ψ_{ch}	Chemical energy	$[J]$
ψ_{tr}	Transformation strain energy	$[J]$
ψ_{id}	Free energy	$[J]$
$\varphi_{\varepsilon L}(e^{tr})$	Indicator function	
p	Volumetric part of the stress	$[MPa]$
s	Deviatoric part of the stress	$[MPa]$
η	Entropy	$[J/K]$
X	Thermodynamic force	
E_B	Young's modulus of the beam	$[MPa]$

E_S	Young's modulus of the spring	$[MPa]$
K_S	Spring's stiffness	$[N/mm]$
l_S	Free length of the spring	$[mm]$
l_B	Free length of the beam	$[mm]$
η_S	Y-displacement of the spring (bottom node)	$[mm]$
η_B	Y-displacement of the end of the beam	$[mm]$
A_S	Section of the spring	$[mm^2]$
A	Section of the beam	$[mm^2]$
R	Recovery parameter	$[mm]$
U_C	Value of the vertical displacement at low temp.	$[mm]$
U_H	Value of the vertical displacement at high temp.	$[mm]$
R_s	R parameter considering stress	$[mm]$
σ_C	Stress at low temperature	$[MPa]$
F	Force parameter	$[N]$
F_C	Value of the F parameter at low temperature	$[N]$
F_H	Value of the F parameter at high temperature	$[N]$
Δ	Deflection of the lever's beam	$[mm]$
P	Load in terms of actuator force	$[N]$
I	Area moment of inertia	$[mm^4]$
M_f	Moment due to deflection of the beam	$[Nmm]$
b	Distance between point load and strain gauge	$[mm]$
h	Thickness of the beam	$[mm]$
GF	Gauge factor of the strain gauge	
V_r	Voltage ratio of the strain gauge	
V_{EX}	Excitation voltage	$[V]$
V_{CH}	Measure signal voltage	$[V]$

List of figures

List of tables

Acknowledgement

This work would not have been possible without the precious expertise of Professor. Auricchio and PhD. Mauro Ferraro in the field of FEM analysis and modeling of Shape Memory Alloys. I acknowledge, on the side of the production, Eng. Christoph Bechtold and Eng. Rodrigo Lima de Miranda, from Acquandas. I hereby want to thank Fluid-o-tech, particularly Eng. Butera and Eng. Andrea Coccia, for being the living heart of the project, and helping me accomplish this work. I want to give a special thanks to Professor Gaetano Cascini who with patience, kindness and knowledge provided me guidance to start, develop and complete this project. As for my odd family and all its extensions, whether animals or human beings ("filappere"), friends included, a simple acknowledgement would not be enough, so I hope my future actions and decisions will show how much I love you all.

"Lala ya tu sabes..."

Abstract

Nowadays, the field of micro-technology is being increasingly explored. Regardless the particular type of technology, production is pushed toward designing smaller and more efficient products. Especially today, every kind of actuator has to be both more energy efficient and smaller than its previous versions. Therefore, materials play an outstanding role in the design process, especially those defined as smart materials. Amongst them, Shape Memory Alloys (SMA), play a remarkable role, since they have the largest output energy density and can provide the greatest displacements and strokes [1]. Fluid-o-tech, a company delivering innovation in the field of valves and pumps, proposed the case study of this work consisting in designing a valve with outstanding performance. The aforementioned SMA technology is used in the following research, brought about by Acquandas, a German company specialized in microsystem technology and sputtering process, that produced the NiTi thin film prototypes for the valve. In order to gain a better understanding of solenoid valve's technology the first step is to perform a thorough patent analysis, so as to understand if technology is ready for a leap in terms of innovation. Then, after searching through old and new catalogues and studying the performance gathered from them, a target is chosen based on the desired flow rate and overall volume of the new valve. The SMA's technology is embedded in the actuation part of the valve, which eliminates the volume occupied by the solenoid, maintaining the fluidic part. This allows reducing the occupied space while maintaining the original performances. An optimization process is provided via finite element simulation with different models, to achieve the best performance in terms of the shape of the actuator. The experimental setup, intended to test the material and to asses the capability of the valve is described in the final part of this thesis.

Sommario

Al giorno d'oggi, il campo delle micro tecnologie è sempre più esplorato. A prescindere dal particolare tipo di tecnologia, l'industria è spinta a progettare prodotti con sempre più ridotte dimensioni e minori consumi energetici. In particolare, tutti i tipi di attuatore devono essere sempre più efficienti e miniaturizzati. Per raggiungere questi obiettivi i materiali svolgono un ruolo fondamentale nel processo di progettazione, specialmente quelli definiti materiali intelligenti. Tra questi si distinguono le leghe a memoria di forma (SMA), dato che posseggono la maggiore densità di energia e possono fornire le maggiori corse di attuazione [1]. Fluid-o-tech, un'azienda innovatrice del settore di valvole e pompe, propone il caso studio di questo elaborato, che consiste nel progettare una valvola innovativa con prestazioni superiori rispetto a quelle del mercato attuale. La tecnologia SMA è messa a disposizione per questa ricerca da Acquandas, un'azienda tedesca specializzata in microsystem technology e nel processo di sputtering, che produce i prototipi di film di NiTi per la valvola. Per capire meglio lo stato attuale delle valvole a solenoide, si esegue, per prima cosa, una ricerca brevettuale per verificare se la tecnologia è sufficientemente matura per compiere un salto in termini di innovazione. Successivamente, dopo una ricerca attraverso cataloghi attuali e passati ed uno studio delle performance estrapolate dagli stessi, si sceglie un target basato sul flusso ed il volume totale che deve possedere la nuova valvola. La tecnologia SMA, incorporata nella parte di attuazione della valvola, permette di eliminare il volume occupato dal solenoide pur mantenendo intatte le prestazioni della parte fluidica. In tal modo si riduce lo spazio occupato, mantenendo le performance originali. Successivamente si è eseguito, un processo di ottimizzazione attraverso simulazioni ad elementi finiti, per ottenere la forma dell'attuatore che garantisce i migliori risultati. Nella parte finale dell'elaborato è descritto un setup sperimentale per testare il materiale e le capacità della valvola.

Introduction to the case study

Fluid-o-tech, a company delivering innovation in the field of valves and pumps, proposed the case study of this work consisting in designing a solenoid valve with outstanding performances. The idea is to design a novel valve, by an unconventional process, with better performance with respect to the normal characteristics of a solenoid valve. Knowing that shape memory alloys (SMA) are a group of metal alloys that can return to their original shape or size, in response to an adequate external stimulus (temperature), the goal of this work is to understand how this self-actuated material can be implemented in the field of valves. This material can be triggered to change shape also with direct-heating, which consists in an electric current passing through the material, heating it by joule effect. If the size of the actuator is small, the current needed is low, which allows low power consumption. There are two main production processes that can be used to give shape to a possible SMA actuator: casting combined with rolling and laser cutting or sputtering. Experimental tests proved that the outcome of sputtering technology is a pure material without heat-affected zone, which ensures a better performance in terms of stress, fatigue behavior and damping. The purpose of this work is to insert a new technology in the market in order to compete with and replace current solenoid valves products. The ambition is to create a novel pilot solenoid valve because of its low actuation forces compared with its flow rate. Once the goal is defined, it is fundamental to demonstrate that the field of solenoid valve is luckily to be chosen for a process of innovation. To show this possibility, an analysis of patents filed from 1946 to January 2014 is provided. After choosing five relevant producers of solenoid valves, old and recent catalogues are collected and relevant data fitted in a diagram showing the present market of solenoid valves and its trend over the time. Defined a target in terms of performances of the new valve, it is fundamental to detail the design specifications to create a competitive product. To achieve the specification needed an actuator of sputtered NiTi thin film is used instead of the solenoid actuation part. Starting from the specific SMA film's function in the valve, technical requirements for the actuator are obtained using the experience of Fluid-o-tech to define the working pressure, the stroke, the force needed, so as to regulate the flow of the valve. To ensure said characteristics, it is decided to start a process to search for the optimum shape of the actuator. FEM analyses are performed by applying

mathematical models of shape memory alloys to various possible shapes. Simulations starts from the simplest design, which is a cantilever beam, whose length is optimized to reach the best stroke and force while the actuator is being warmed up. The best shape obtainable is achieved for the case study described by increasing the complexity of the above mentioned actuator by optimizing parameter after parameter such as number of cantilevers, width and thickness of the material. The entire process leads to define the designs to be produced, that increases strokes and forces of actuation. Considering that the purpose is to develop a product, the process is completed by designing an experimental setup suitable to validate the results of the proposed simulations, to observe the real behavior of the actuator and to evaluate if it can be sold on the market.

1 CHAPTER State of the art Shape Memory Alloys and review of the sputtering process

1.1 State of the art Shape Memory Alloys

Introduction

Shape memory alloys (SMA) are a group of metal alloys that can return to their original shape or size, when subjected to a memorization process, by changing between two non-diffusive transformation phases [2]. As shown in Figure 1 below, SMA can "memorize" and recover the given shape only if heated. Arne Olander first discovered shape memory alloy or smart alloy in 1932, however the importance of shape memory materials was not recognized until William Buehler and Frederick Wang revealed the shape memory effect (SME) in a nickel titanium (NiTi) alloy in 1962. Since then, the demand for SMAs for engineering and technical application has been increasing in various commercial fields [3]

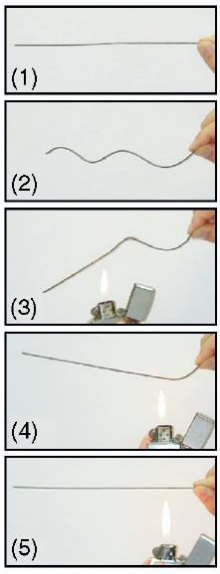

Figure 1 Example of shape memory effect [4]

The mechanical characteristic of SMA can be regulated by the transitions temperatures of the phases that are adjustable by changing both the chemical composition of the alloys and varying the heat treatment. This allows having different properties and phases at different temperature ranges, which is fundamental to fit the material into the chosen application. At different temperatures the

mechanical behavior of the material varies from plastic to superelastic and shape memory (see Figure 2)

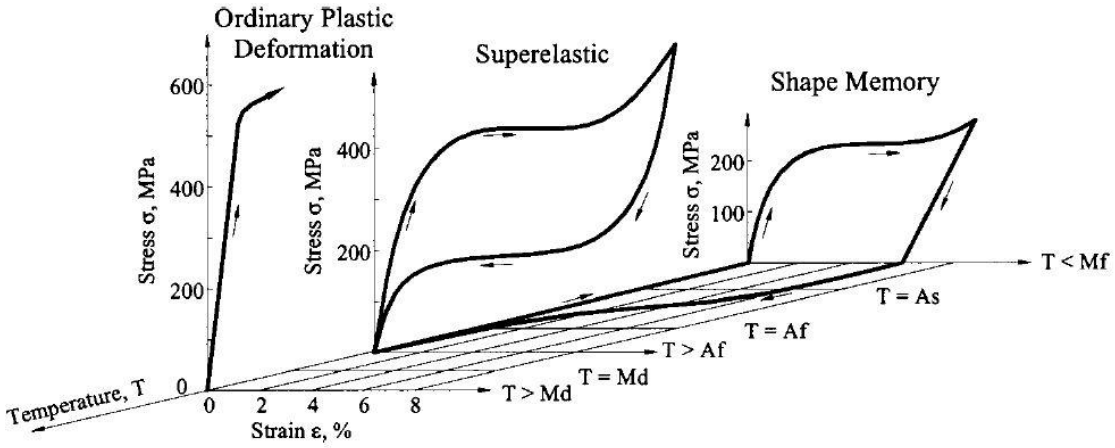

Figure 2 Three-dimensional stress–strain temperature diagram showing deformation and shape memory behavior of NiTi shape memory alloy [5]

Nowadays there are various alloys obtained by the combination of Nickel, Titanium and Copper mostly. They are divided in three groups: Cu-based (mainly CuAlNi and CuZnAl), NiTi-based and Fe-based (FeMnSi, FeNiC and FeNiCoTi) alloys, which show of course different properties [6].

Although iron-based and copper-based alloys are low cost and commercially available, due to their instability and poor performance, NiTi-based SMAs are much more preferable for most applications [3]. Concerning the last group, beyond their exclusive shape memory performances, excellent mechanical properties, good corrosion and biocompatibility it is possible to meet specific needs by using ternary alloys [1]. To achieve a narrow hysteresis copper is a substitute for nickel by more than 7.5%, at this point a new phase appears (orthorhombic R-phase), which reduces the transformation hysteresis to less than 10K and increases the damping capacity. On the other hand, to obtain a wider hysteresis, niobium is added to the binary alloy, which depresses the M_S temperature allowing a transformation hysteresis of 150K. The last group is high-temperature SMAs when in NiTi is substituted by palladium, platinum and gold up to 50% or Ti is substituted by hafnium and zirconium by up to a 20%, the transformation temperatures could be increased as high as 873K [1].

1.1.1 Crystalline Structure and transformation among the phases

Thermo-responsive SMAs are characterized by four temperatures: Martensite Start and finish, Austenite start and finish that are ordered as shown in the Figure 3 below.

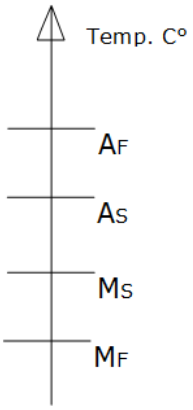

Figure 3 Relative positioning of the Phases

The peculiarities of this kind of alloys are the crystalline structure that allows having more than one stable phase at a certain temperature.

Depending on the composition of the alloy the latter temperatures can shift, which is fundamental to reach the necessary flexibility to fit in most of the engineering applications.

The possible structure for SMA alloys are austenite, martensite and Twinned martensite. Austenite is characterized by a cubic close-packed structure (ccp) while martensite is characterized by hexagonal close-packed (hcp) organization of the atoms.

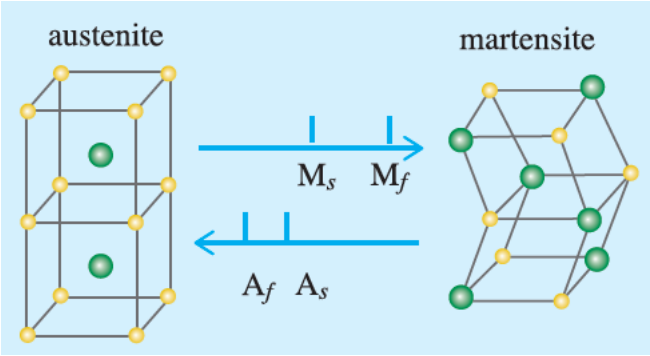

Figure 4 Austenite to martensite transformation [7]

The stability of these two phases depends on the temperature of the material. Austenite is stable at higher temperatures and martensite is stable at lower ones. Having an idea of how much the structure changes, it is possible to look at the micrograph of Figure 5, the phase transformation temperature may be determined quantitatively from the surface roughness [1].

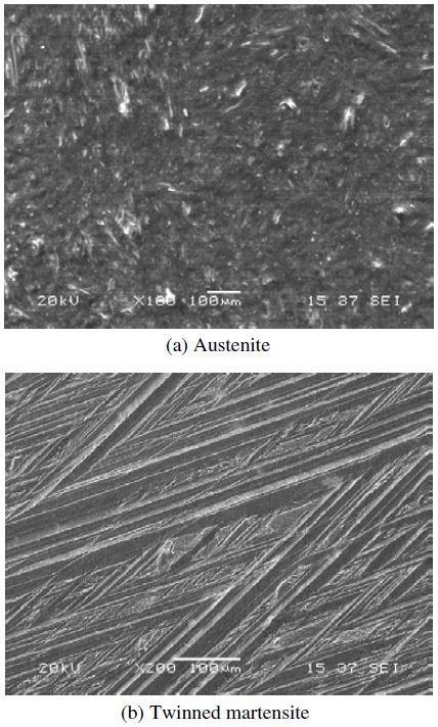

(a) Austenite

(b) Twinned martensite

Figure 5 Surface of a CuAlNi single crystal showing austenite and martensite phases [8]

Martensite has two different configurations: Twinned martensite and detwinned martensite. The former is visible when there is no stress applied to the material, the latter is a transformation of the former when a stress is applied.

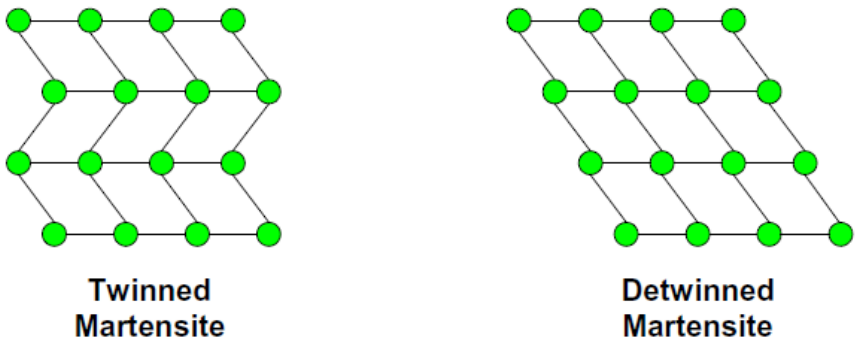

Figure 6 Structure of twinned and detwinned Martensite [6]

Among these phases, there are six possible transformations [6]:

- Austenite transforms into detwinned martensite upon loading
- Detwinned martensite transforms back to austenite upon loading at high temperatures or upon heating without any applied load or with a very small applied load
- Detwinned martensite transforms into another detwinned martensite upon loading (R-phase, not always present)
- Twinned martensite transforms into detwinned martensite upon loading
- Austenite transforms into twinned martensite upon cooling
- Twinned martensite transforms into austenite upon heating

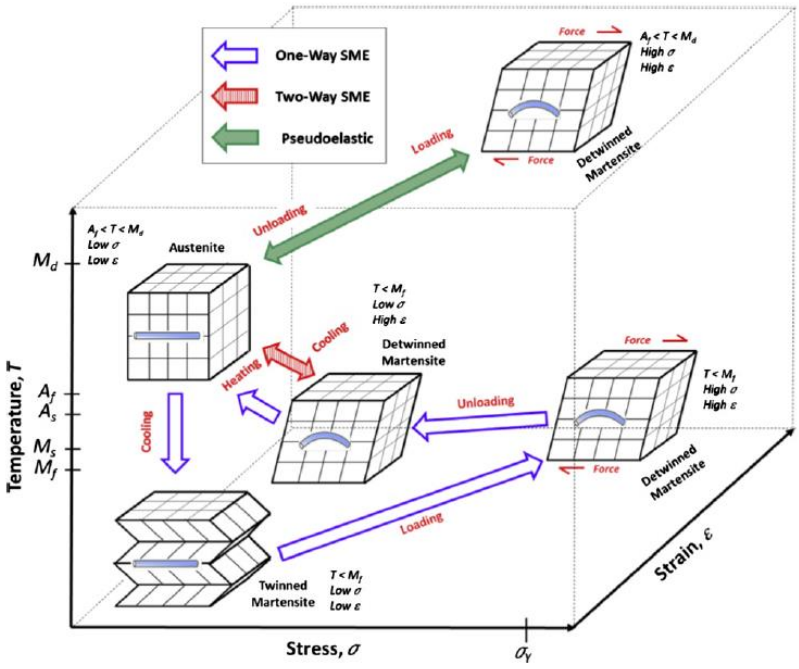

Figure 7 Phases transformations [3]

The transformation between Martensite and Austenite occurs by changing the temperature or the stress applied. This structure change is not instantaneous; this is why the four characteristic temperatures exists:

M^s M^f A^s A^f

This temperature creates two bands in which the transformation of each structure starts and ends.

As the free energy of a phase is related with the temperature it is possible to see how at low temperature the favored structure is martensite while, at higher temperatures is austenite [4]. This creates a hysteresis loop (Figure 8) which consists in a different behavior while heating or cooling the material.

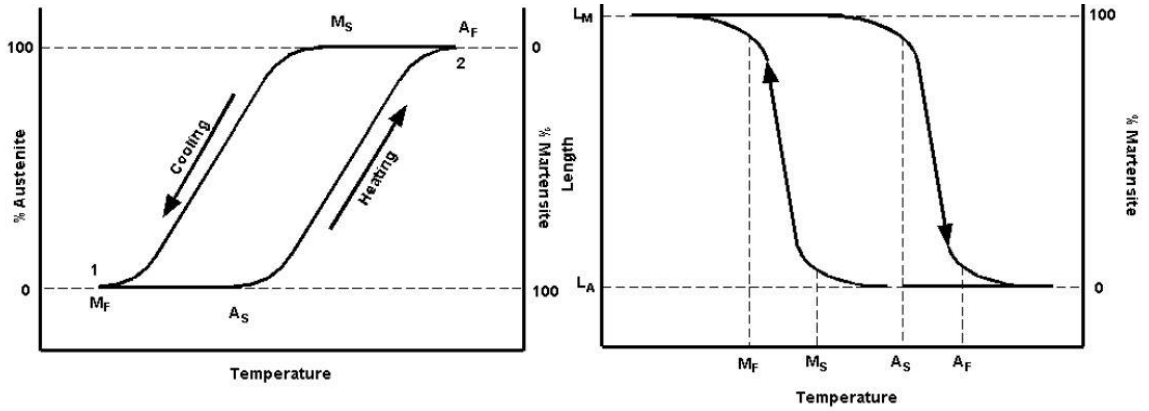

Figure 8 Hysteresis loops in shape memory alloys

The last two transformations are thermally induced without any macroscopic shape change, but with significant surface relief. As such, a flat surface in austenite becomes rough upon cooling to twinned martensite, and vice versa [6].

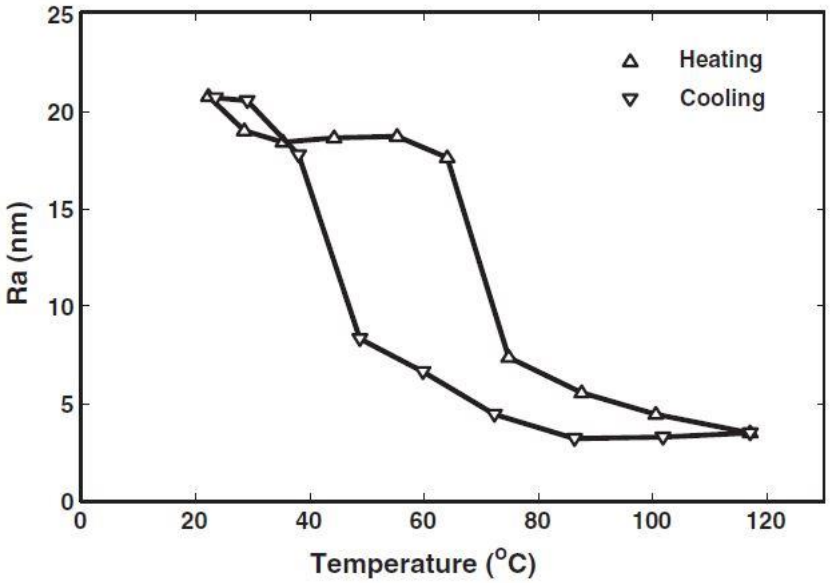

Figure 9 Relationship of Ra versus temperature in a thermal cycle [9]

It is remarkable that stress induced martensite transformation is exothermal [6], this allows by measuring the heat flow of the material to determine the transformation temperatures.

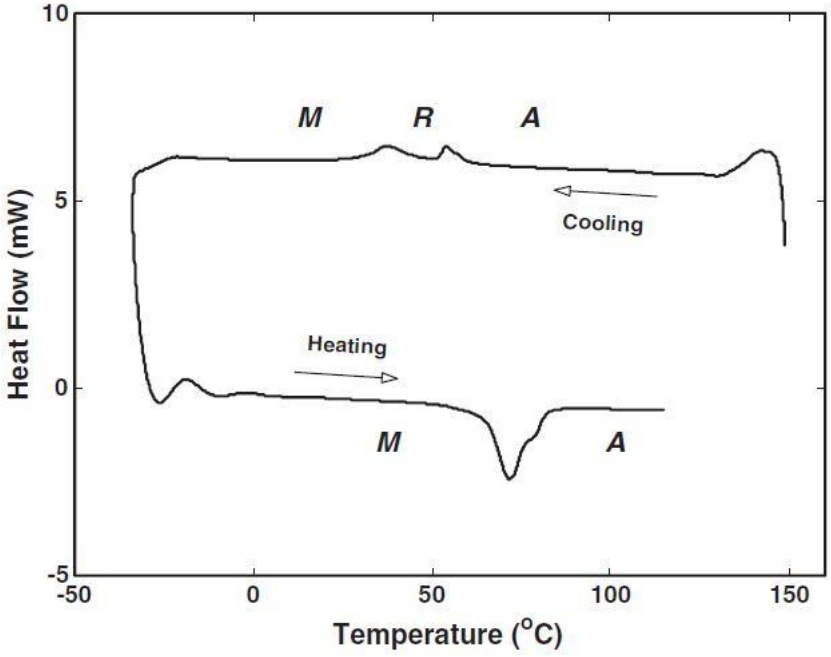

Figure 10 Graph representing the heat flow recorded during phase transformation [9]

These transformations allow different behavior changing with the stress and temperature applied, the most important are: shape memory and superelasticity (or pseudoelasticity).

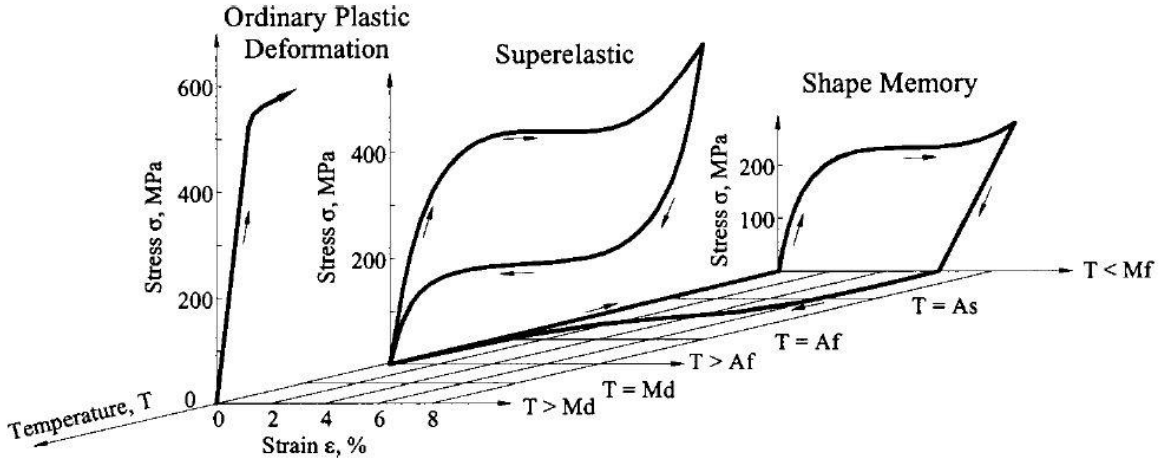

Figure 11 Three-dimensional stress-strain temperature diagram showing deformation and shape memory behavior of NiTi shape memory alloy [5]

Among the phase transformation presented there is one, which shows an orthorhombic phase (R-phase), which is a martensitic transformation which competes with the subsequent one with austenite. This transformation is revealed in:

Ni-rich Ti-Ni alloys if they are heat-treated at proper temperatures so as to produce Ti3Ni4 precipitates, in a few % of Ni in Ti-50Ni alloy is substituted by Fe or Al, heat treatment of Ti-Ni alloys after cold-working to create rearranged dislocation structures [10]. The lattice deformation is smaller than for the martensitic transformation. The amount of transformation strain is smaller than in the martensitic one. Another remarkable point is that the hysteresis loop is smaller than the one between austenite and martensite, so the transformation temperature are closer [11].

1.1.2 Shape memory effect

Shape memory effect (SME) means the ability of a material once deformed to recover its original shape after being heated, which is made possible by non-diffusive transformation of the lattice structure (see Figure 12).

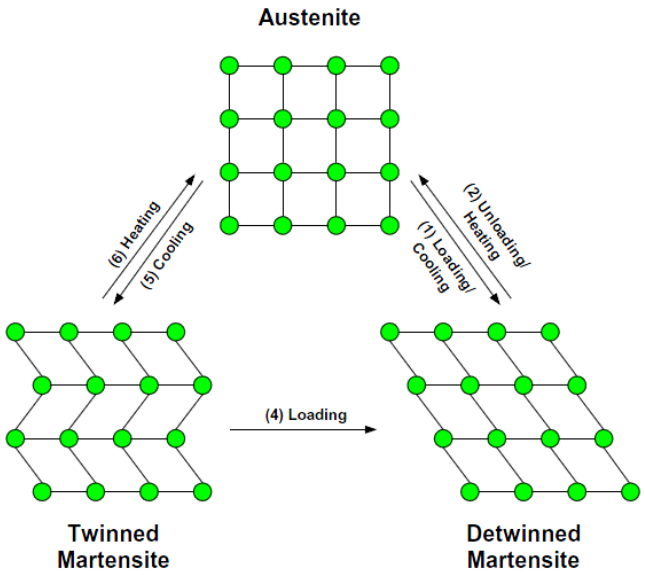

Figure 12 Change in lattice structure [12]

Depending on the alloy and on the heat treatment received there are two different types of SME. The former is called one-way shape memory effect which consist in retain a deformed state after the removal of an external force and then recover to its original shape upon heating. The latter is the two-way SME that means the ability to "remember" the shape at both high and low temperature. [3]

In order to show these behaviors the alloy has to be "trained". The shape has to be set by adding bonds so as to prevent the free movement of the material. After it has been heated above the A^f temperature, the shape is set in the austenitic structure. Then it is cooled down rapidly below the M^s temperature. Now the material has a Martensitic twinned structure. By stressing it applying a force the T-Martensite is forced to transform into detwinned martensite. In order to recover to the original shape the alloy is heated up, it happens that martensite starts to transform into austenite, which provides the wanted shape, so the metal starts to regain the original shape. After the complete transformation in austenite the alloy, is cooled down and the phase is now transformed into detwinned martensite. Successively below M^s

temperature, it maintains the shape and detwinned martensite changes into twinned martensite. By heating the material if there is no load applied the strain recovery is at zero stress. The stress strain diagram for one-way SME is illustrated below (Figure 13).

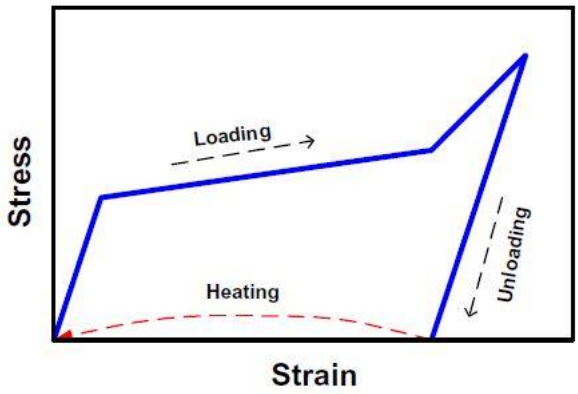

Figure 13 Stress-strain diagram for one-way shape memory effect. [6]

The training for the two-way effect it is more complicated because the alloy needs to "remember" also the low temperature shape. Usually means a thermo-mechanical cycling under constraints and isothermal mechanical cycling in the austenite phase [13].

This two effects lead to different ways of designing actuator. With two-way SME the solution are more space-efficient and elegant, but one-way SME provides twice the recovery strain provided by the same material [14]. In addition, the strain of the former rapidly deteriorates with high temperatures and due to the complex training process are less cost effective than the latter.

Resuming the intrinsic method deals with tailoring the microstructure of the material to obtain two-way SME, the extrinsic method uses additional mechanical elements to provide the necessary force to promote the nucleation of stress-induced variants.

1.1.3 Superelasticity

The terms "superelasticity" and "pseudoelasticity" are interchangeably used to describe the ability of shape memory alloys to undergo large deformations without the onset of plasticity [15].The deformation can be up to ten times more than a conventional material [16]. This unusual elasticity it is called pseudoelasticity because it not only originates from Hookian elasticity, it is caused by a stress induced phase transformation, from austenite to martensite [16].

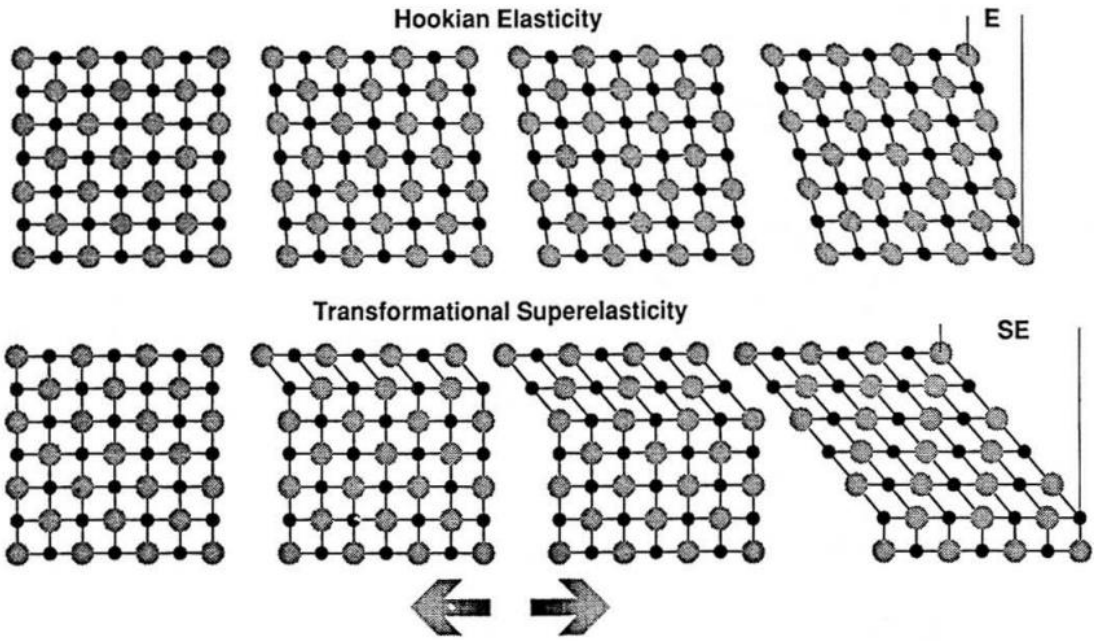

Figure 14 Tensile behavior of steel and Ni-Ti superelastic alloy and mechanism of elastic deformation [16]

In Figure 14 it is possible to see how the lattice changes gradually its structure from austenite to martensite if a strain is applied; this allows the material to have superior elongation due to the combination of Hookian and pseudo elasticity.

In comparison with normal metallic materials such as steel, it allows to have one order of magnitude more strain as shown in Figure 15.

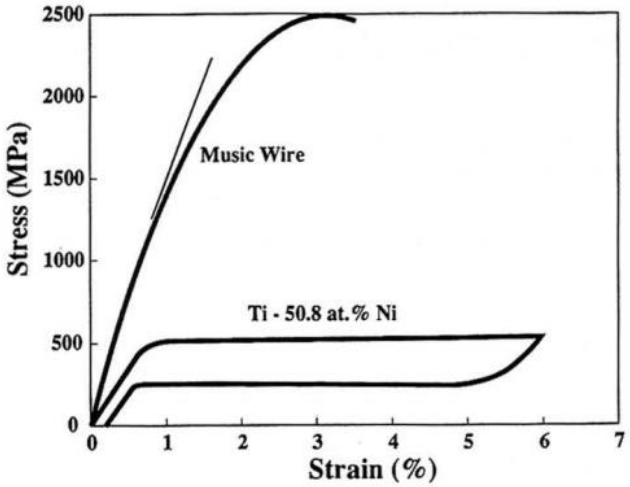

Figure 15 Stress/strain curves for a conventional material and a superelastic Ni-Ti alloy [16].

The pseudoelasticity has some limits in terms of stress that it is possible to apply and also in terms of temperature. Superelastic effect only occurs above A^f but the stress needed to induce martesite must be less than that to induce slip [17]. If the stress limits are passed there will be permanent deformation in the alloy with, of course, no recovery in shape. In Figure 16 below are shown the particular conditions where it is possible to found superelasticity.

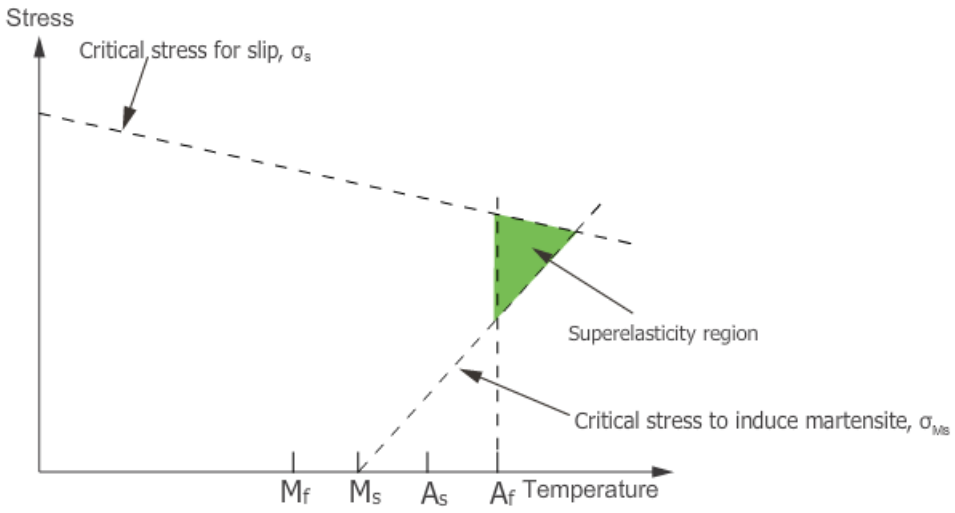

Figure 16 Narrow window of superelasticity [17]

1.1.4 Magnetic and Martensitic phase transformation

Magnetic shape-memory alloys (MSMA), or ferromagnetic shape-memory alloys (FSMAs), are ferromagnetic materials which exhibit large strains under the influence of an applied magnetic field due to a martensitic phase transformation. Large magnetic-field-induced strains have been observed in Heusler alloys (such as NiCoMnIn) with a body-centered cubic structure and have been explained by the rearrangement of martensite structural variants due to an external magnetic field [9]. Instead of heating a Shape Memory alloy it is possible (with MSMAs) to induce a recovery in shape, not only by heating it, but also applying a correct magnetic field. More specifically, in the transformed martensite state, the microstructure of Heusler alloy consists of ferroelastic domains which are twin orientation with respect to each other across the tetragonal {101} planes. Due to the magnetoelastic coupling between the ferroelastic and magnetic domains, the free energy minimization during magnetization reversal requires a reconfiguration of the ferroelastic domains when the geometry of the magnetic domains is altered by application of magnetic field [18].

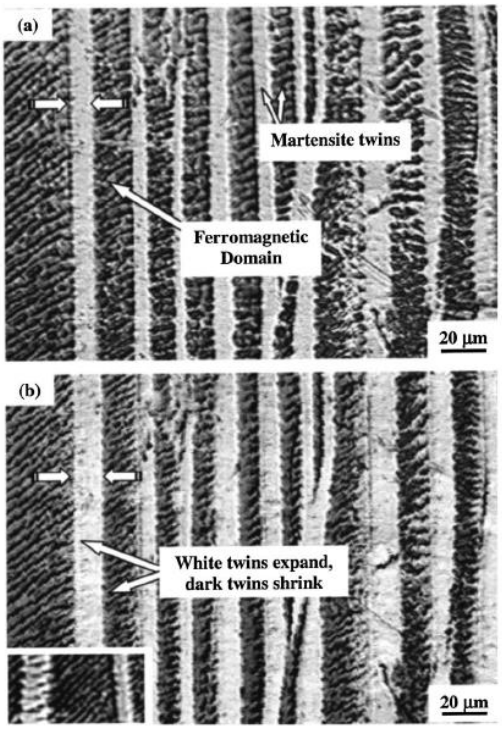

Figure 17 Magnetic domains superimposed on martensite twins in a Ni2+x Mn1-x Ga SMA single crystal. (a) Applied field strength H=400 Oe, (b) applied field strength H=1800 Oe. The field direction points from left to right in the micrographs [19].

1.1.5 Traditional applications of shape memory alloys

From the past twenty years until today a process of innovation started using new materials to fit in electro-magnetic actuator reducing size, weight, costs, optimizing the movement and offering the opportunity to implements new functions [20].

Having an idea of the main application of shape memory materials helps to understand the innovation brought by those material in engineering product. New way of designing products and actuators are available for the simplicity and effectiveness of a smart material who does not need many energy transformations to perform a movement.

Essentially, there are three way of actuation for SMA devices: (a) one-way, (b) biased, (c) two-way.

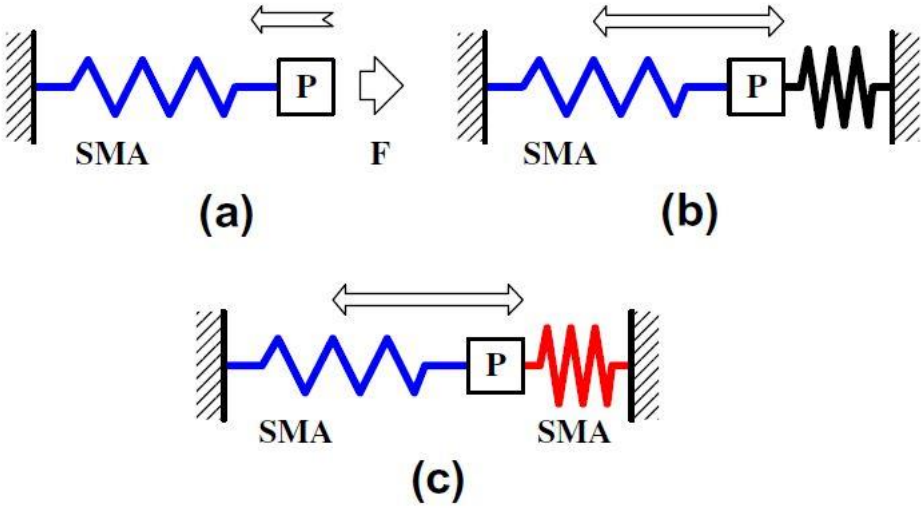

Figure 18 Three basic types of SMA actuator based on the SME.(a) One-way actuator; (b) biased actuator; (c) two-way actuator [21]

As presented in Figure 18 one-way actuation (a) assume the presence of a force which can be overcome by one-way shape memory effect, in case (b) the force is provided by a spring, the last case (c) is composed by either two antagonist SMA material or by a two-way actuator. Focusing on the designing process Belluard([13]) describes two manners, one called intrinsic (based on the tailoring of the material properties), the second extrinsic based on other mechanical forces to provide the initial deformation of the material.

Neglecting the several existing application in biomedical field, some examples are listed.

Focusing on intrinsic application, it is remarkable the example of Figure 19 in which the two-way SME is used to perform the movements of a microgripper.

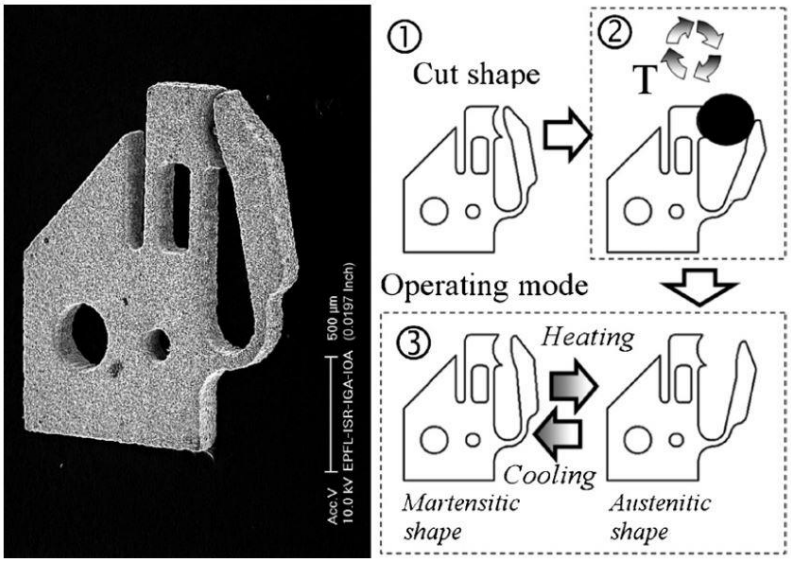

Figure 19 Microgripper for submillimeter lens handling [22]

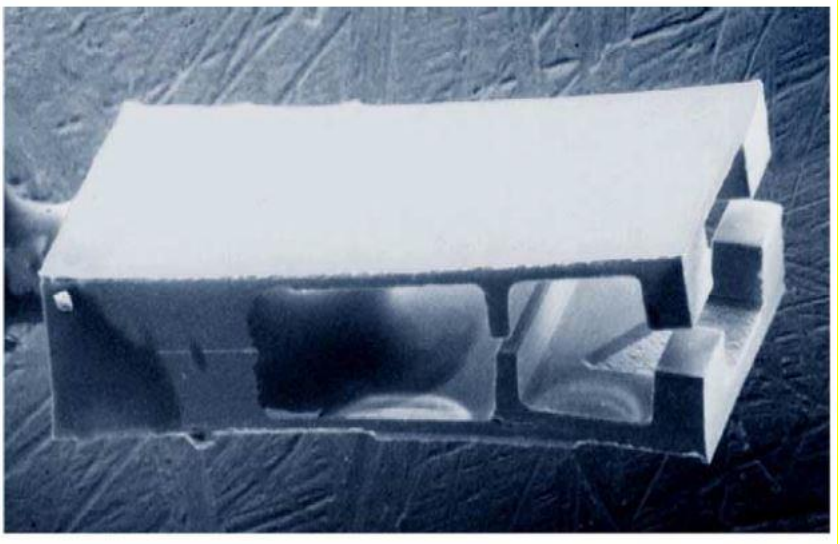

Figure 20 TiNi/Si microgripper with cantilever structure with out-of-plane bending mode: (a) microgripper [23];

Regarding the extrinsic application, a typical way is to use bias springs as described in Figure 21; by using two equilibrium configurations at two different point of the stroke it is possible to have different position at different temperatures.

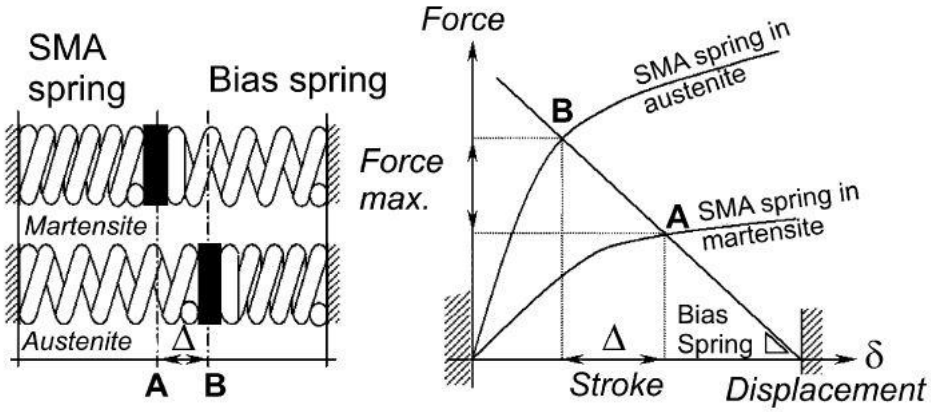

Figure 21 General principle of a spring based design [13]

The same principle is applied in Figure 22 by varying the properties of the material with heat treatment (annealing). The spring here is given by different microstructure of the material (non-annealed part).

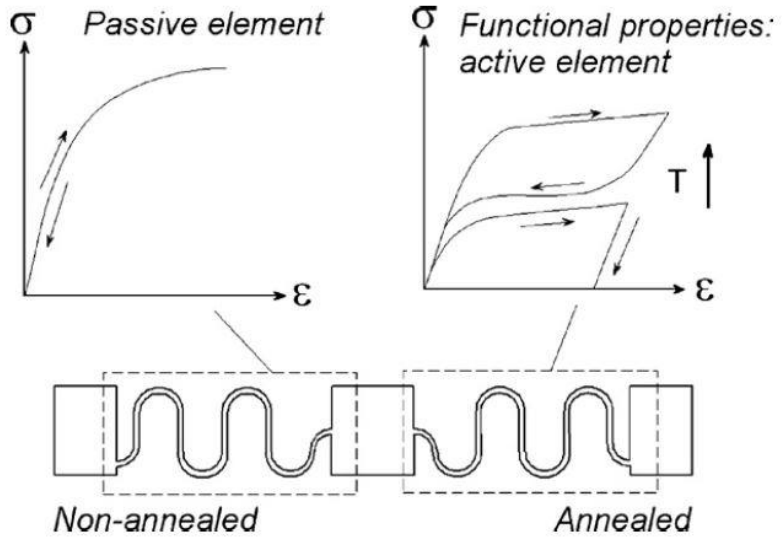

Figure 22 Schematics of monolithic integration. By locally annealing the material, mechanical properties are distributed across the material [13]

An example of integration of more functionalities in the same substrate is given by Figure 23, which shows that the actuator is made by a laser annealed part of the material which provides the actuation force to move the gripping jaws.

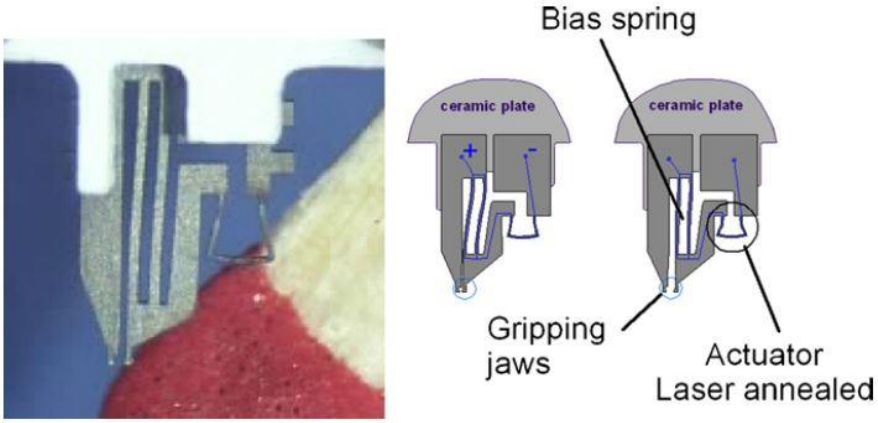

Figure 23 Laser-annealed monolithic micro-gripper [24]

Other interesting application are biased actuator for valves (see Figure 24Figure 25), the principle is the same presented before. Here the inner fluid when reaches the desired temperature by heating the SMA coil makes it transform and generate the necessary force to either open or close the valve. The first example is a fire check valve, if the environment reaches a certain temperature the valves opens and allows water to comes out and extinguish the fire.

Figure 24 Firecheck industrial safety valve [25]

In the figure below the same actuation concept is used to let passing through only a liquid flow of chosen temperature.

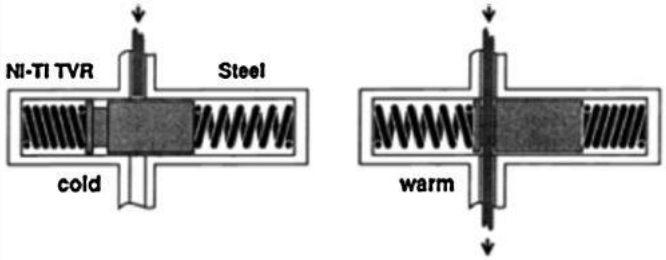

Figure 25Mercedes-Benz automatic transmission valve [26]

By regulating the heating treatment, the material composition and the stiffness of the spring is possible to obtain the perfect configuration that fits in the industrial application.

1.2 Sputtering technology for producing NiTi films

Introduction

Nowadays technology is exploring more and more the field of micro, especially in terms of dimensions. As it is possible to see, every producer of no matter what technology is trying to design more efficient and smaller product. Especially today, every kind of actuator has to be both efficient and smaller than the previous version of it. In this vision sputtered thin film would help to reach these goals, because of the purity of the material created and the fact that almost every metal could be sputtered. Recently thin film SMAs have been recognized as a new type of promising and high-performance material for microelettromechanicalsystem (MEMS) and in biological applications. Among these SMA films, TiNi based films are the most promising ones. [27] They are typically produced by sputtering.

In the sputtering process, atoms removed from a target material by the sputtering gas condense onto various substrates such as silicon wafers, polyimide films, and glass plates to form a thin film [28].

Magnetron sputtering process is divided in three phases:

- Sputter
- Three dimensional photo lithography
- Wet etching

The first phase is used to deposit the material on a substrate, the second is necessary to print the design on the raw material and with the last the surplus of material is chemical etched.

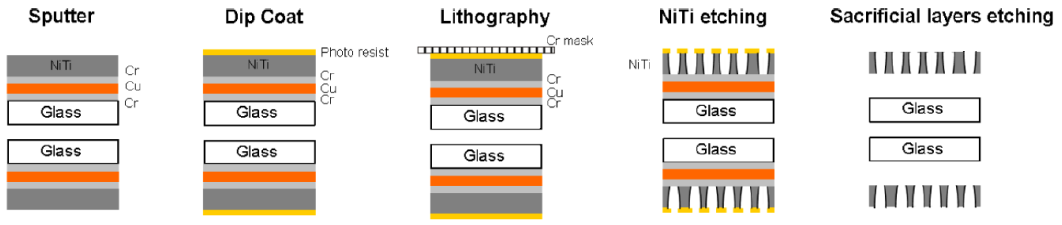

Figure 26 Sputtering overall process [29]

1.2.1 Magnetron sputtering

Magnetron sputtering machine is composed by four fundamentals parts: vacuum chamber, substrate holder, metal target, and magnetron.

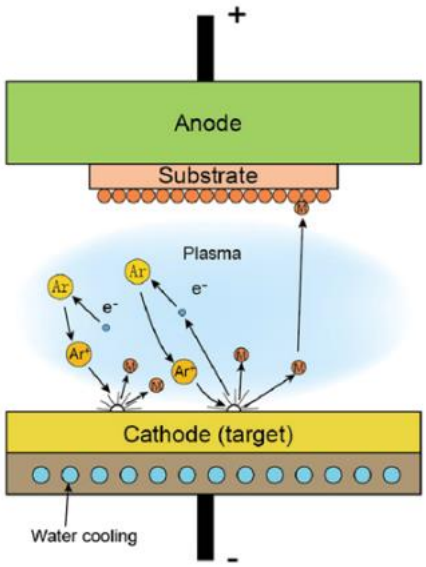

Figure 27 DC diode sputtering system [30]

Usually argon is used as ionizing gas. When a sufficient difference of potential is created between the plate where the substrate is fixed and the metal target, argon starts to transform into plasma. The magnetic field created by the magnetron, forces the argon's positive ion to impact the surface of the metal. If the energy is sufficient, atoms removed from a target material by the sputtering gas condense onto various substrate such as silicon wafers, polyimide films, and glass plates to form thin films. [31] In this phase of the overall process sacrificial layers of Cu and Cr are sputtered, to allow the chemical etching.

Usually thin films of TiNi are deposited on unheated substrates that result in an amorphous microstructure of the film. Subsequently, the samples is crystallized in a high vacuum chamber in order to avoid oxidation during the annealing process. The annealing temperature is held constant at the maximum temperature to crystallize amorphous TiNi, this result in better crystalline structure and mechanical properties [29]. There are also experience of sputtered films (with an excess of titanium) on heated substrate, providing crystallized structure without annealing [32]

1.2.2 Three dimensional photo lithography

After the sputtering process the film is dip coated with photo resistant material (few microns), then it is soft baked order to fix the coat. Then for the photo lithography a chromium covered quartz mask is used with a feature resolution if 500nm. A trade off considering feature resolution and diffraction effects of the light determines the precision of the process. After the exposition few seconds) the resist is developed with a suitable solution. [29]

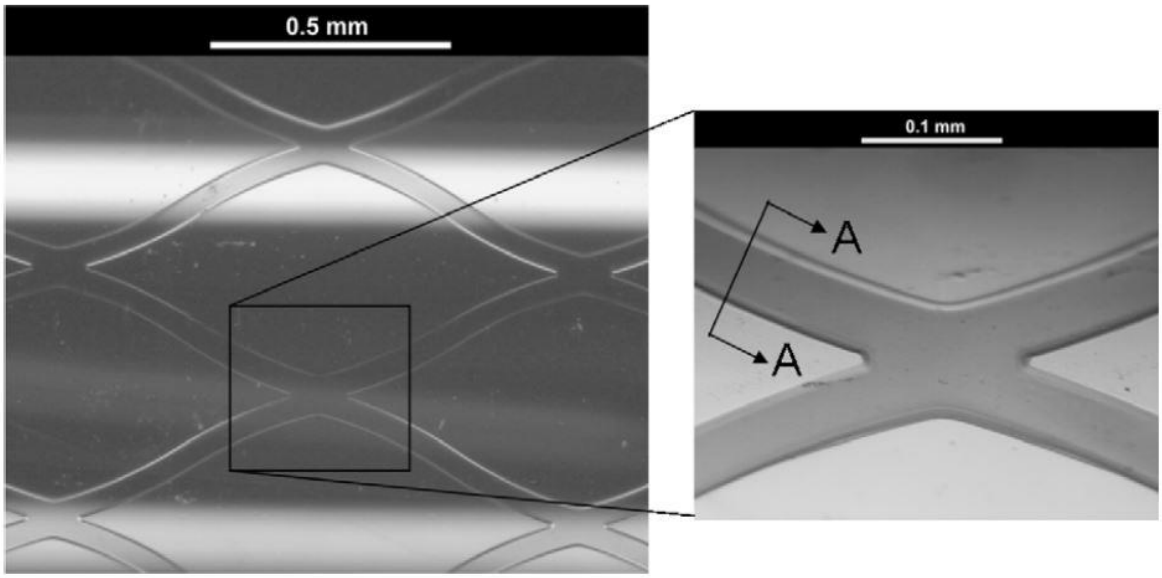

Figure 28 Optical micrograph from structured positive photo resist (AZ1518) on a TiNi cylindrical thin film [29]

1.2.3 Wet etching

Wet etching process is used to obtain the desired shape by eliminating the developed part of the photo resistant material and the NiTi down that surface. As the process is isotropic it causes some design limitations such as the feature resolution that is related to the thickness of the film and feature widths [29].

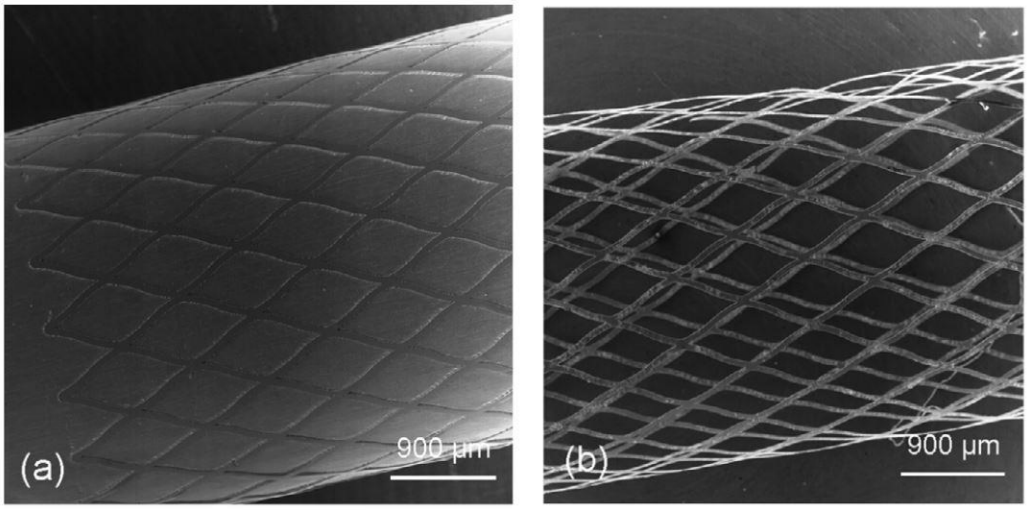

Figure 29 Structured TiNi cylindrical thin film: (a) before and (b) after sacrificial layers etching [29]

1.3 Advantages of using SMAs in terms of material properties and morphology possibilities

Sputtering of NiTi results in thin film with excellent properties such as:

- Superelasticity
- Shape memory effect
- Fatigue performance
- Biocompatibility
- Damping properties
- High cyclic stability of the elastocaloric effect

This properties originates from the extraordinary features of NiTi alloys and the purity of the sputtered film.

The deposition condition with said method results in a homogeneous normal flow of particle, focus ion beam (FIB) cross section revealed a very homogeneous growth of the NiTi film. [29]

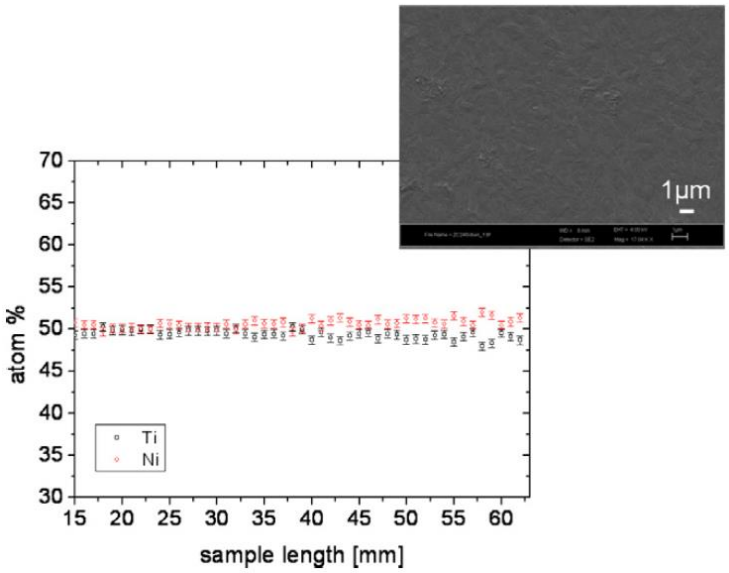

Figure 30 Example of stoichiometry of sputtered NiTi thin film [29]

Concerning phase transformations NiTi films show the transition temperature could be shifted by varying the composition of the alloy. The excess Nickel content out of equiatomic composition caused the transformation temperatures to drop, but excess titanium content did not affect the transformation temperatures as much. The transformation temperatures of titanium-rich NiTi films are within the range of human body temperature these values indicates the possibility of superelastic properties at blood heat (37C°). [33] This allows NiTi thin film to be part of several biomedical applications also for its high biocompatibility.

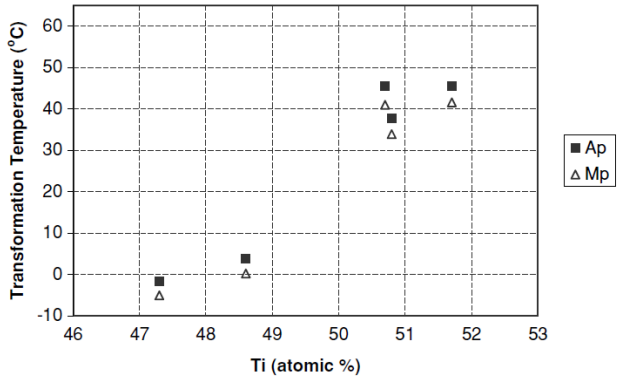

Figure 31 Variation of transformation temperatures with titanium content [33].

As shown in Figure 32 below light micrographs of titanium and NiTi and fluorescence micrographs at the surface of thin films. Human mesenchymal stem cells (HMSC) were incubated on the different samples for seven days and stained with cailceinAM (green) for living cells, and propidiumiodine (red) for dead cells. [34]

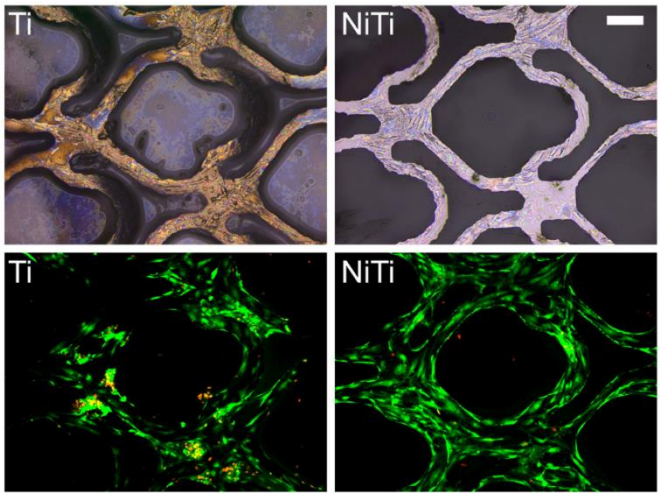

Figure 32 Micrographs of Ti and NiTi thin films of cultured HMSC [34]

Said thin films have also good mechanical properties such in terms of stress and strain in comparison to NiTi alloys made by casting.

If a comparison it's made between standard NiTi and sputtered thin film in terms of tensile test it appears that according to ASTM F2516 the second shows higher upper (UPS) and lower plateau (LPS) strength of 650/490 and 500/300 MPa. Furthermore a higher ultimate tensile strength (UTS) of 1600 versus 1400 MPa and higher uniform elongation from 22 to 17% but a lower Young's modulus for austenite (e.g., 30 versus 40 GPa) and martensite. The difference originates from a different temperature of transition of the austenite phase (Af) [35].

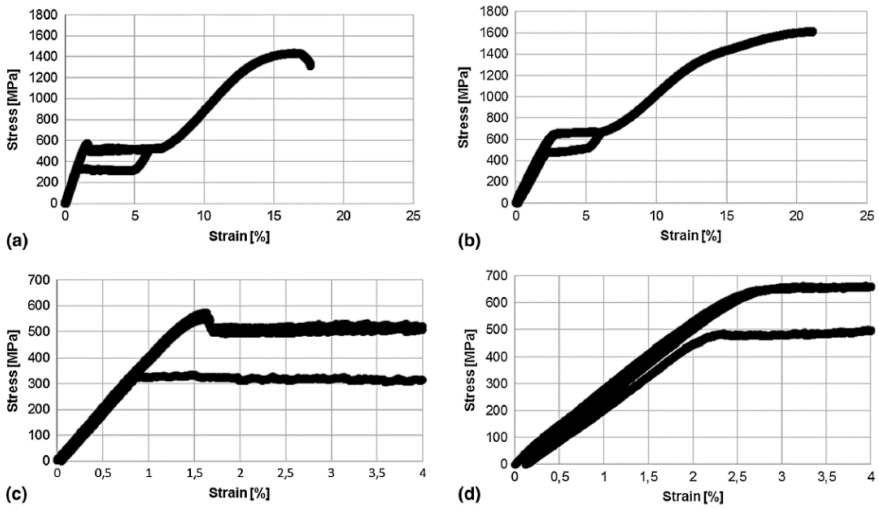

Figure 33 Comparison between stress/strain curves of standard and sputtered NiTi [35]

It is remarkably that also the dynamic behavior of the thin film is different. As it shows the Figure 34 below, after few cycles the residual strain is higher than in the standard alloy. The formation and accumulation of dislocations impede the correct transformation between austenite and martensite. This cause a cycle hardening and a narrowing of the hysteresis curve.

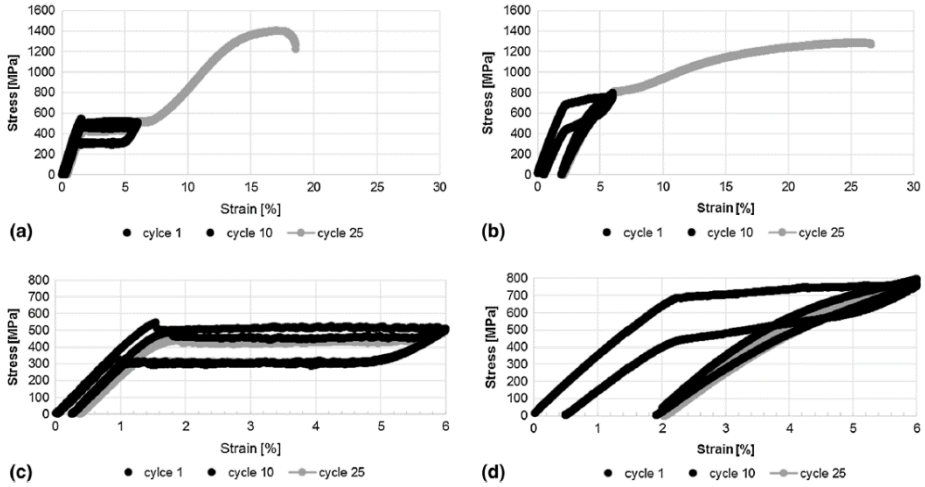

Figure 34 Dynamic tensile teste of standard and sputtered NiTi [35]

Another interesting feature of NiTi thin film is the damping properties. It is proved that a coat of sputtered NiTi improve eliminating vibration and undesired dynamics in a working tool. [36] In particular, it is proved that the damping coefficient is higher for coated tools with amorphous NiTi rather than with crystallized ones.

Più info paper 11 amourphous coated

The Figure 35 shows the damping coefficient in relation of a non-coated tool. [36]

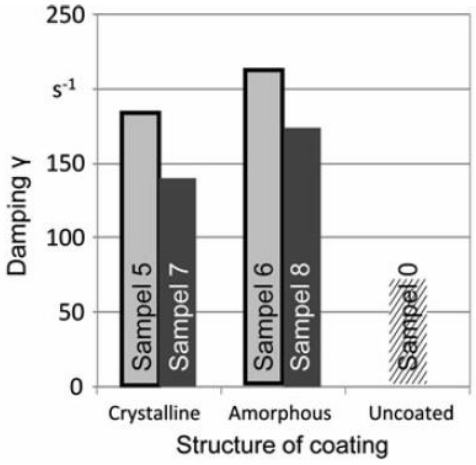

Figure 35 Damping coefficient in relation of the coating chosen [36]

During the martensitic transformation in shape occurs an interesting phenomena which is called elastocaloric effect. NiTi thin film shows high stability in the elasocaloric cycle, it means that there is slightly no changing in the shape of the hysteresis curve during several cycles. Measuring the changes in temperature during the stress induced transformation of martensite. The transformation is endothermic while going from austenite and exothermic while going back. [37]

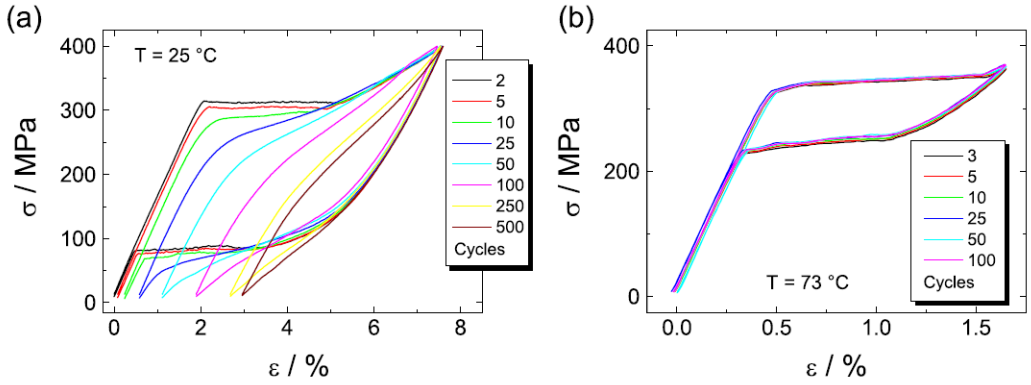

Figure 36 Comparison between binary (NiTi) and tertiary (NiTiCu) alloys in the elastocaloric effect. [37]

1.3.1 Properties of SMA sputtered NiTi films

With the process depicted, it is remarkable that there are not heat affected zone because there is not welding of the material, as the atoms of the material condensate on the substrate's surface. Remarkably nowadays laser cutting is the main process to obtain the desired shape of a NiTi film, especially for stents [28].

One alternative of sputtering used today is hot rolling a sheet of metal but this enhance anisotropy in the material due to the orientation of the same [13].

High aspect ratios can be achieved until a value of five, without losing resolution of the features.

When using a chromium covered quartz mask fabricated by electron beam writing, photolithography resolution can easily be improved to about 1 micrometer [38].

Aspect ratios, feature resolution and thickness of the film are parameters related to themselves, the maximum values are: 5, 5µm ± 3µm, 0.1 to 0.8µm ± 1%.

Other important parameters are: fracture strain (maximum 30% ± 5%), austenite peak (from –5°C to 100°C), tensile strength 1100-1500 MPa, elastic range 1-5%.

Due to the necessity of the material to be heated in order to show the shape memory effect, circuits can be integrated by applying a layer of copper between the materials itself, creating micro wires that forms micro-heaters.

1.3.2 Application of sputtered thin films

Shape memory thin film are suitable to most micro actuator application due to strokes and forces they can express with tiny volumes. Here are presented some application in non-medical fields such as: valves, microgrippers, pumps and micromirrors.

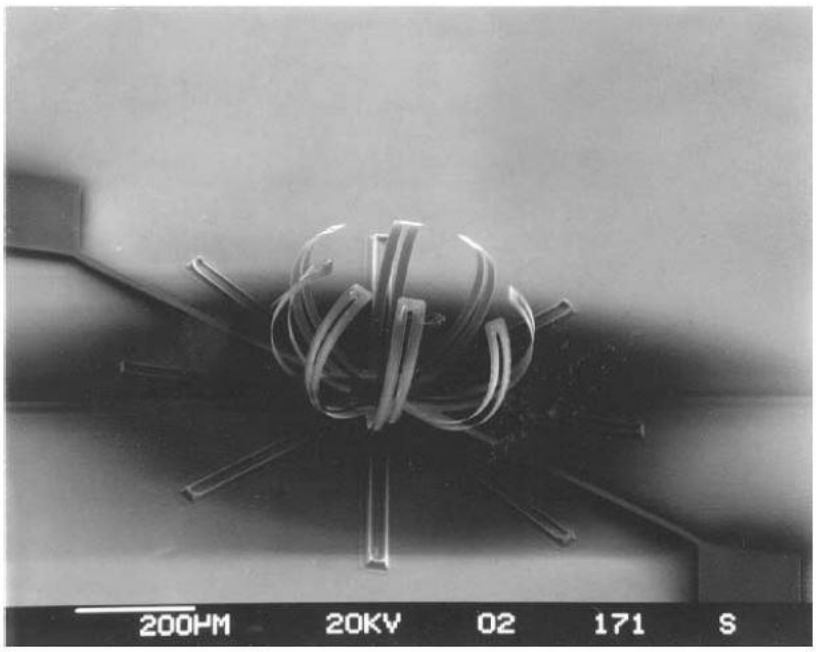

Figure 37 Microwrapper made of NiTi sputtered thin film [39]

Below is presented an interesting application for micropumping, by applying a sinusoidal current to the shape memory strip with joule effect it heat up and cold down at the same frequency (or slightly) of the current, doing so it is possible to have pressurization and depressurization inside the chamber of the pump to obtain the desired flow rate.

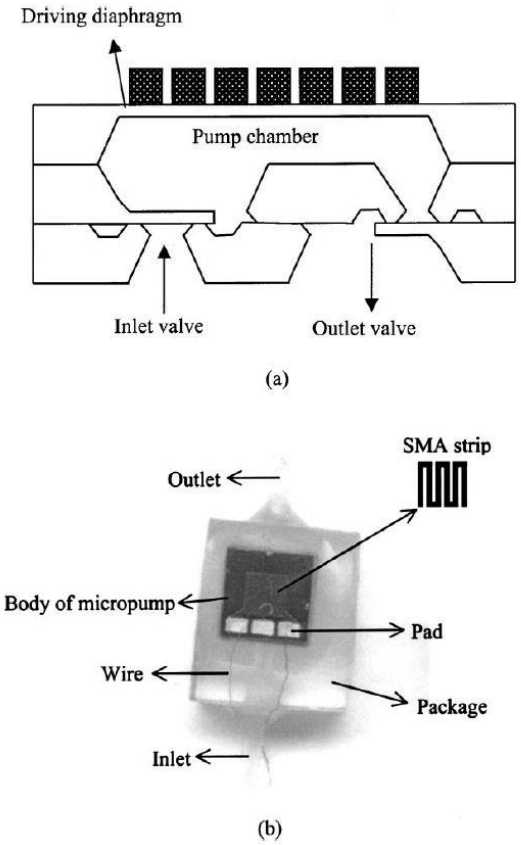

Figure 38 Schematic diagram (a) and photograph (b) of the micropump with NiTi/Silicon driving diaphragm micropump [40].

To have an idea of what are the possible shapes in Figure 39 is depicted a heart valve that can be used instead of biological valves coming from animals.

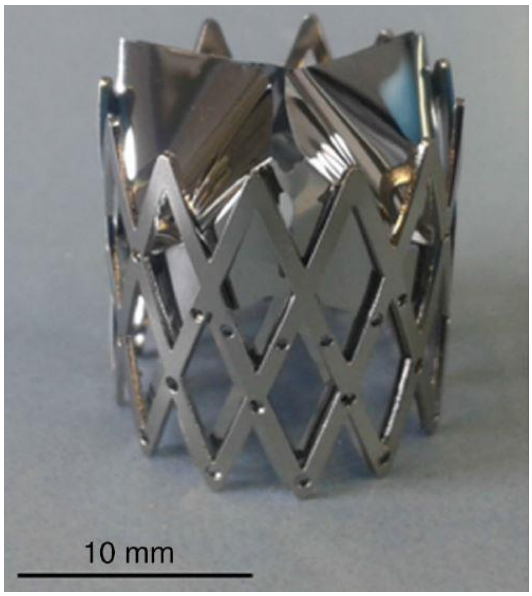

Figure 39 NiTi thin film heart valve design [41]

2 CHAPTER Case study: solenoid valve

Introduction

Fluid-o-tech, a company delivering innovation into the field of valves and pump, proposed the case study of this work consisting in designing a solenoid valve with outstanding performances.

In this chapter it is demonstrated that the field of solenoid valves is preferably to be chosen for a process of innovation. To show this possibility an analysis of patent filed from 1946 until January 2014 is provided. After choosing five relevant producers of solenoid valves, old and recent catalogs were collected and relevant data were fitted in a diagram showing the actual market of solenoid valves and it is evolutions in time. Furthermore, once defined a target in terms of performances, the design specifications, the mathematical models of shape memory alloys used to perform FEM analysis and the technological limitation of the fabrication process are framed.

2.1 Patent analysis and today's market

2.1.1 Patent analysis

Before starting the analysis, it is important to choose the right criteria to search for patents. The fields chosen are International Patent Classification (IPC) class, title, abstract, claims for the words "solenoid valve". The IPC class that best fits in this case is F16K, which describes valves, taps, cocks etc. Orbit is chosen as browser to perform the researches. To be sure, that the research is valid and it is not affected by "noise", in terms of accuracy of the results obtained, some patents were analyzed in details, in order not to count patents deriving from strategies such as fencing etc.

After having searched through various databases (US, EP, WO, JP, KR etc.), the data that best represent the history of the evolution of the patents were selected and divided by range of years (in groups of five). The cumulate is calculated and plotted with the program IIASA in order to show if there is any tendency in decreasing the number of patents filed by year. This would show that the technology is starting to be obsolete and it is luckily possible to make a leap in terms of innovation [42]. If a

technology is old there are not so many patents filed each years, in this sense the cumulate would starts to reach a saturation point.

In particular, with IIASA it is possible to fit the data in order to see if the tendency resembles a logistic curve, which has the typical "S shape.

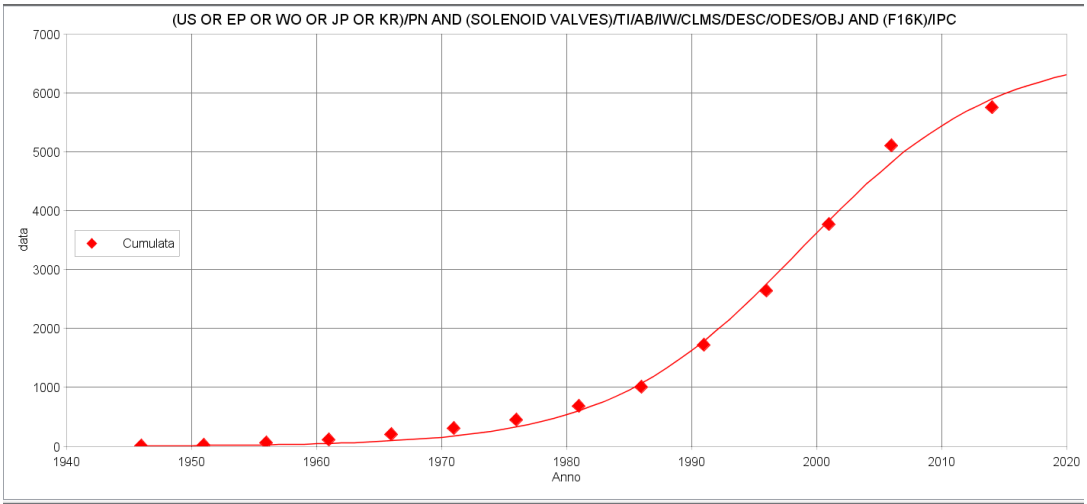

Info | Plot | Series | FitRange | Scenario | Fitpar

Fit Parameter

	Series	K	Tm (beta)	delta T	alpha	ObjFunc	Rsqare
Logistic	Cumulata	6,704.239	1,998.782	33.774	0.13	184,459.028	0.997
Gompertz	Cumulata	9,156.079	1,998.992	54.376		484,049.132	0.992
Sharif-Khabir	Cumulata	9,746.87	2,002.695	79.134		751,406.14	0.992
Floyd	Cumulata	11,775.298	2,004.099	118.242		942,559.314	0.99
Exponential	Cumulata		-173.787		0.091	186,822,350.551	0.459
Linear	Cumulata	-163,444.748			83.392	10,024,397.24	0.803

Figure 40 Data fitting of the patents filed from 1946 to 2014

As shown in the Figure 40 above, the data fit a logistic curve, the saturation point will luckily be reach in 2020, the inflection point (T_m) is at the year 1999. The results are interpreted as the possibility to start a process of innovation in this field because the number of patents filed per year is tending towards zero while the time is approaching the year 2020. Many researches are done varying the string of the search and the databases, the results are similar to the one presented. For example searching the same string with different databases the T_m reaches years 2003, with no substantial changes.

As told it is important to choose the correct keywords to perform this analysis. Actually, in the first researches, lots of patents were not related to solenoid valves, because in many cases producers use patent strategies such as fencing etc. to avoid the presence of other producers in the same application field. As an example, fencing consists in filing several patents concerning the same core invention but with little variations in other to prevent any other applicant to file a modified patent of the

core one. This method, widely used in Japan, spreads the number of patents filed creating false cumulates. This issue suggest to underestimate the number of patent filed which means decreasing the saturation point of the curve (seen as year).

Table 1 Research parameter

Database	US,EP,WO,JP,KR
Title (TI)	Solenoid valve
Abstract (AB)	
Index terms (IW)	
Claims (CLMS)	
Description(DES)	
Description in other languages (ODES)	
Object (OBJ)	
International Patent Classification(IPC)	F16K

The United States, European, Japanese, Korean and World Intellectual Property Organization were selected as databases.

In Table 1 are presented the value used to perform the researches on orbit, concerning the coverage of the database, FamPat which is the principal database covering more than 95 patent offices all over the world.

2.1.2 Review of two-way solenoid valves normally opened/closed

Once defined that the case study is a solenoid valve it is necessary to have an overview of the existing valves. In this work, the industrial partner is Fluid-o-tech, which is creating innovative valves ranging over various fields such as beverages and small valves for biomedical applications. For this reason, the research of catalogues aims to create a clear view of solenoid valves with small flow rates, small pressures and two-ways, which are the typical valves used in beverage and biomedical systems.

Main producers of valves in terms of importance and market influence have been selected: The Lee Company, Asco Numatics, Rotex, Parker, and Jefferson. Gathering catalogues is difficult if the purpose is to include also old ones, because companies usually do not keep information about the past. For this reason the research may not be thorough but it represents the state of the art nowadays.

From each catalogue were collected data representing for each application of the valves, (such as beverage, oil etc.), the best in class in terms of pressure (maximum pressure), flow rate (maximum possible), power (better efficiency) and volume (minimum dimensions of the overall volume).

Conversion makes it possible to evaluate valves from different producers. The most representative parameters to describe the ideal target of the possible innovative valve are flow rate ($\frac{m^3}{h}$) in comparison with the overall volume occupied by a valve in terms of the cube that fit the valve (mm^3). The technology leap would be to diminish the overall volume by keeping the same flow rate.

A graph is given in Figure 41 below, which contains the most relevant valves from each producer.

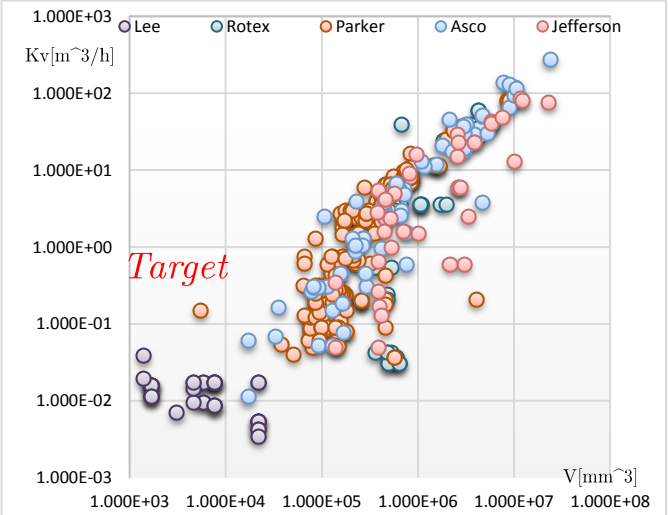

Figure 41 Data representing the valves with best performance divided by producer

Concerning the results, it is easy to see a linear tendency (with a bi-log scale) of the distribution of the valves (Figure 42). This behavior allows finding a target, in terms of the flow rate or volume to reach in order to make a product that is out of the ordinary standards of the valve sold today.

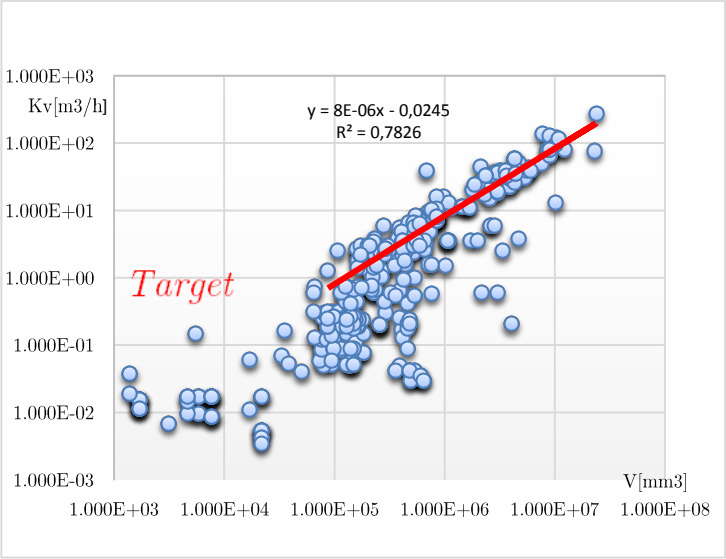

Figure 42 Linear fit of the valves parameters considering all the producers

The value of the R^2 is fair (0.8 while the maximum is 1) although there is dispersion of the points. The linear relation between the points allows to find a target valve which can be positioned outside the linear fit, it would means that provides performance that, if a parameter is fixed, gives better results than the ordinary

valves sold. The target point chosen is a flow rate of 1 m^3/h (16.6 l/min) with an overall volume of 3000 mm^3 (a cube with side of 14.5mm).

Another possible way to read the data is to divide them by range of years and to see if there are any changes between the linear fit of each group.

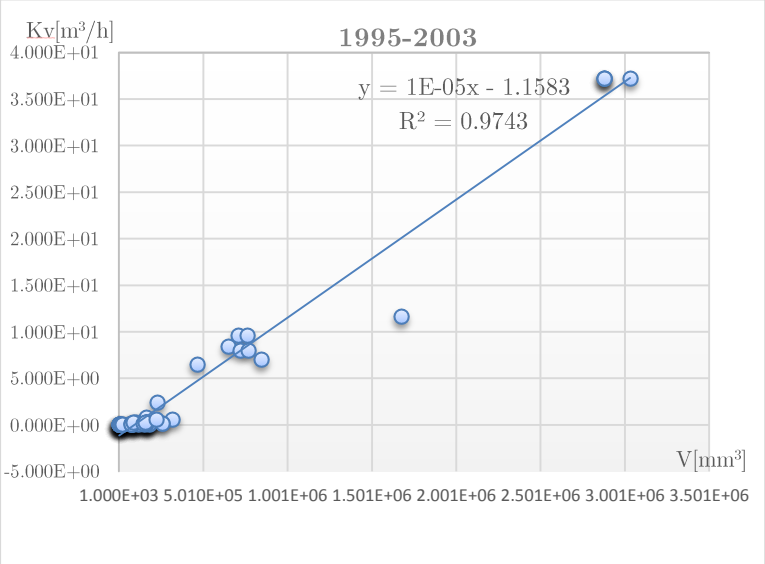

Figure 43 Linear fitting of the catalogues from 1995 to 2003

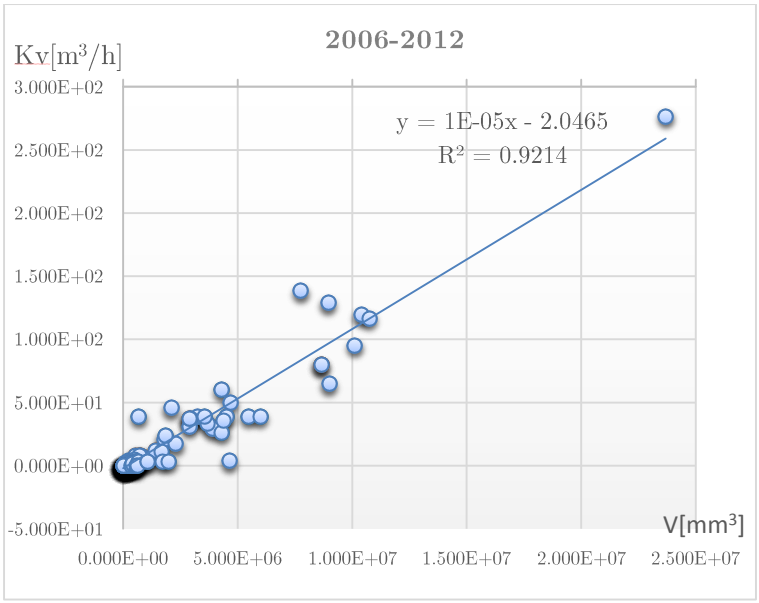

Figure 44 Linear fitting of the catalogues from 2006 to 2012

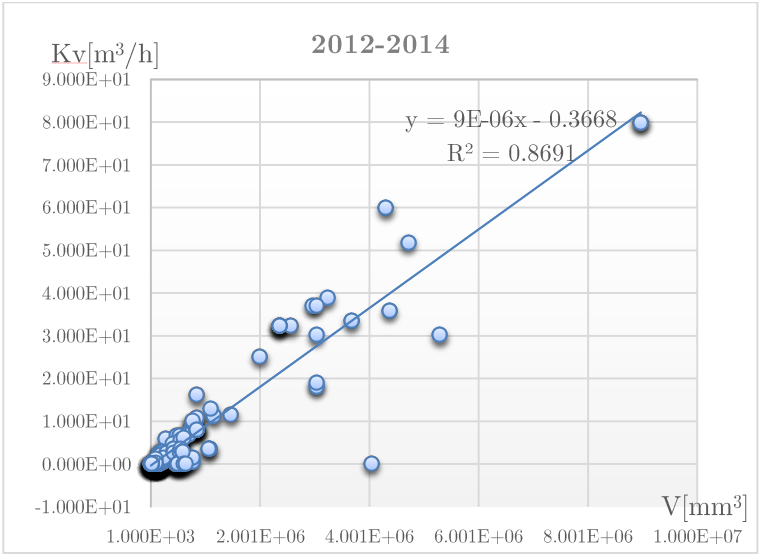

Figure 45 Linear fitting of the catalogues from 2012 to 2014

Concerning Figure 43 Figure 44 Figure 45 it can be seen that the R^2 values are similar and also the linear fits.

As shown in Figure 46 below, the linear fittings are slightly perfectly superposed, it means that the valves within the catalogues of those years are not changed through time. As a conclusion, the technology has not changed in the last years, so an innovation process is likely to be started in that field.

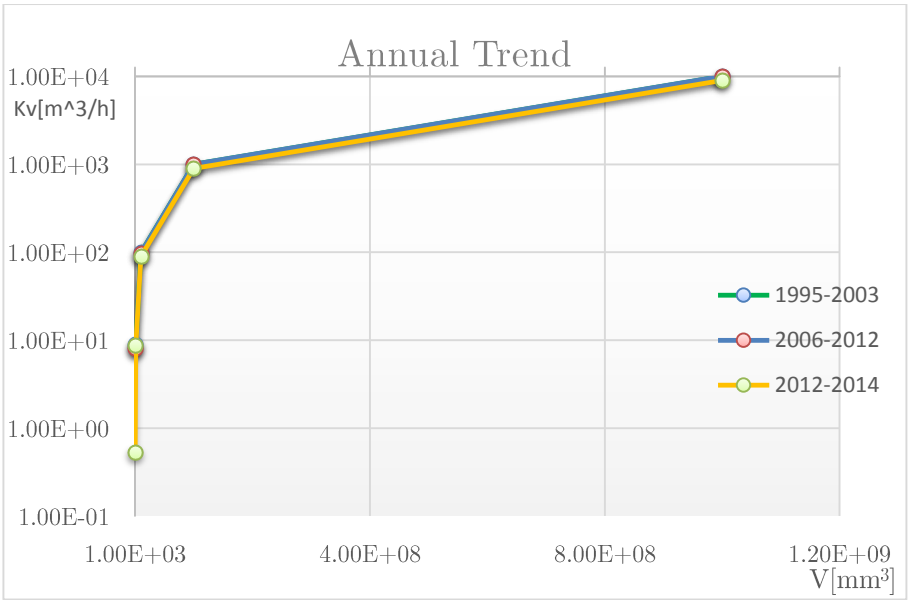

Figure 46 Superposition of the linear fittings obtained

2.1.3 Choice of the target features of the valve

As said earlier the target is achieved by maintaining a flow rate of $K_V = 1\frac{m^3}{h}$, keeping the overall volume minor or equal to $3 \cdot 10^3 m^3$ (see Figure 42Figure 41), this values are chosen to position the valve outside the linear fit, which represents the actual performances of solenoid valves. It means a flow rate of $16.6\frac{l}{min}$ for an overall volume equal to cube with a side of $14.5\, mm^3$. Therefore, the problem to be solved is how to create a valve with small overall volume and big flow rate. One possibility is to reduce the actuation part of a valve that has good flow rate in comparison of the volume occupied by the fluidic part. Considering the scheme of a typical two-way solenoid valve the actuator is represented by the solenoid and a metallic cylinder, which it has to have certain fixed dimension in order to reach the correct force with a certain amount of current in order not to burn the thin copper wires or to waste too much power. The functioning of the valve consist in, a current passing through the solenoid, transforming it into an electric-magnet which has the ability to lift the metallic cylinder opening the valve. While there is no current flowing through the solenoid a spring provide the sealing of the pilot channel.

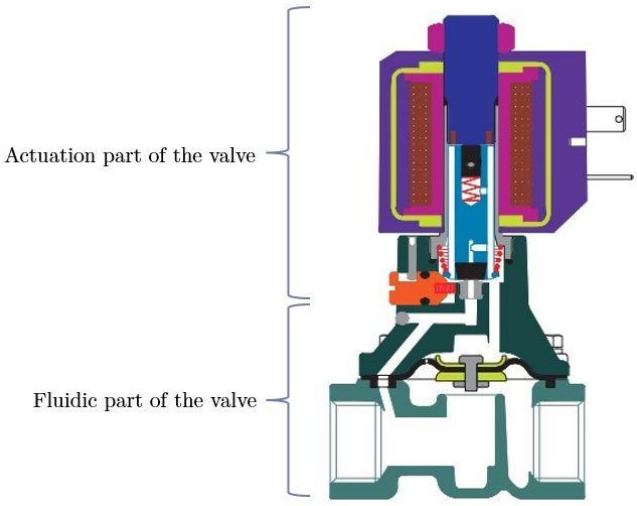

Figure 47 Two-way solenoid valves from Rotex catalogue [43].

Regarding Figure 47 is remarkable that the part involving the case and the solenoid itself represent slightly half of the total volume (actuation part). The purpose of the next chapters is to show a possible way to replace this technology with another one, which is less costing in terms of volume and more efficient in terms of power consumption.

2.2 Design specification and FEM model for shape memory alloys

2.2.1 Design specification

In order to obtain the best performance from the new valve, as decided with Fluid-o-tech, a pilot solenoid valve is chosen, because of the good flow rate that it provides having the same actuation part of the other two-way solenoid valve. In fact pilot valves can achieve high pressures and also high flow rate with relatively small actuation force. In such a valve, the membrane that helps closing the main channel is always in pressure equilibrium. The inner pressure is applied at both side of the membrane making the force needed to move it smaller than the one needed if it was not in equilibrium. A typical pilot valve design is provided below.

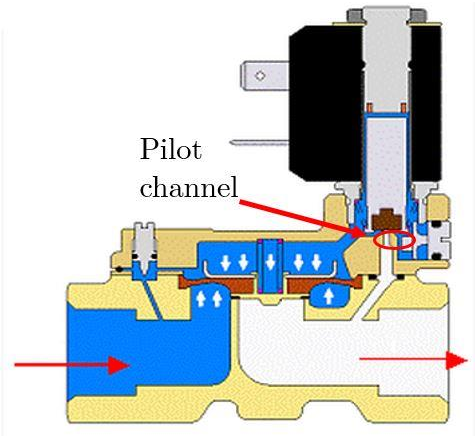

Figure 48 Example of pilot solenoid valve. [44]

As shown in Figure 48 the fluidic part, where effectively flows the fluid, is considerably bigger than the actuation part (black box), although the latter occupies a relevant volume compared to the whole valve.

In this context, the goal is to substitute the solenoid actuator that regulates the pilot channel with a Shape Memory Alloy actuator, to reduce the overall space occupied.

In order to validate the possibility to use a shape memory actuator, the next step is to create a model of this material in a finite element program and see if this material is able to achieve the right force and strains to guarantee the correct strokes.

In particular, Fluid-o-tech chose a general design of a pilot valve and technical requirements were given deriving from their expertise. The description is provided in Figure 49 below.

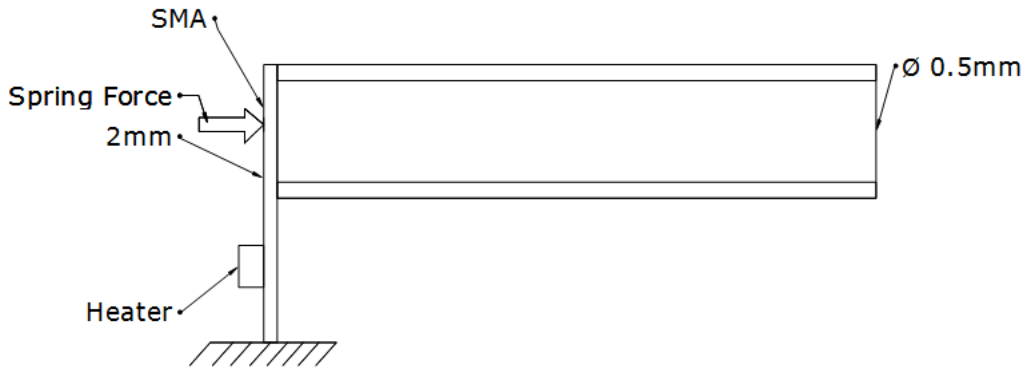

Figure 49 Technical requirements of the pilot channel

As shown in Figure 49 the task of the actuator is to achieve sealing a pipe of 0.5mm diameter, which represents the pilot channel, and to allow, applying a variation of temperature, a stroke of about 0.1mm. The maximum working pressure is estimated to be $5bar$. At first sight, a possible design could be a star-shaped actuator with three clamped legs made of SMA. In the further chapter the design is obtained by a process of optimization and numerical simulations.

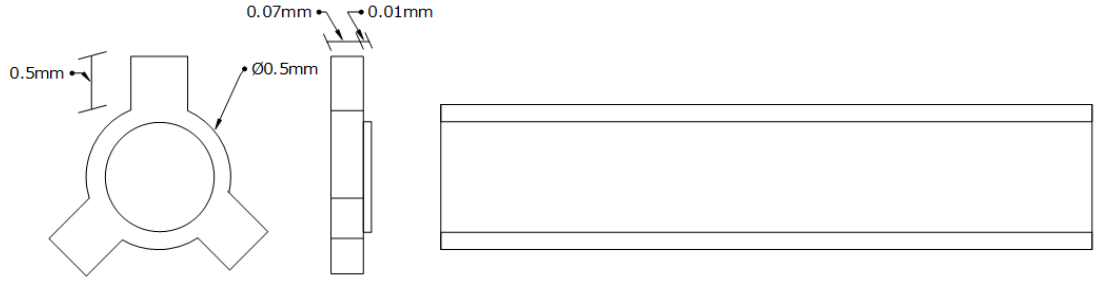

Figure 50 First attempt of design

The goal is understand the behavior of this material in order to avoid trial and error in the design phase. By means of numerical simulation is possible to predict the actuator's behavior before it is produced.

In the next paragraph are described the models used in the simulations.

2.2.2 Finite Elements Modeling

In the field of FEM analysis there are two way of modeling the thermos-mechanical behavior of shape memory alloys either by microscopic or macroscopic point of view [45]. There have been several attempts to build SMA constitutive models from the early phenomenological theories reviewed by Liang and Rogers (1990) till the latest paper of Auricchio et Al. (2014).

In this work, three models are chosen:

- A model based on varying the stiffness of the material between the two transition temperatures
- ABAQUS superelastic model [46]
- A three-dimensional model describing stress-temperature induced solid phase transformations [47]

The third model is implemented in a user material subroutines for ABAQUS, which is courtesy of prof. Ferdinando Auricchio (Full Professor of Mechanics of Solids and Head of the Department of Civil Engineering and Architecture, University of Pavia, Italy).

The main differences between them is that the first two are able to predict only pseudo-elastic behavior rather than the latter can predict also shape memory effect. The former represent an approximation of the real behavior of the material, in fact the parameters needed for this model are essentially the stiffness of martensite and austenite structures. The model considers the material as a subsequence of various elastic materials. The approximation can be made by only two stiffness (see Figure 51), but to better approximate the real behavior a linear variation with the temperature of the stiffness is applied.

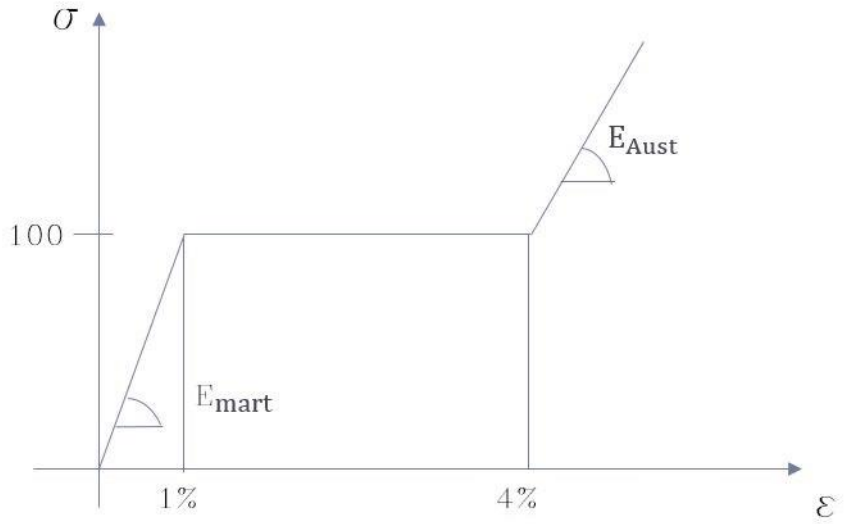

Figure 51 Model based on stiffness variation

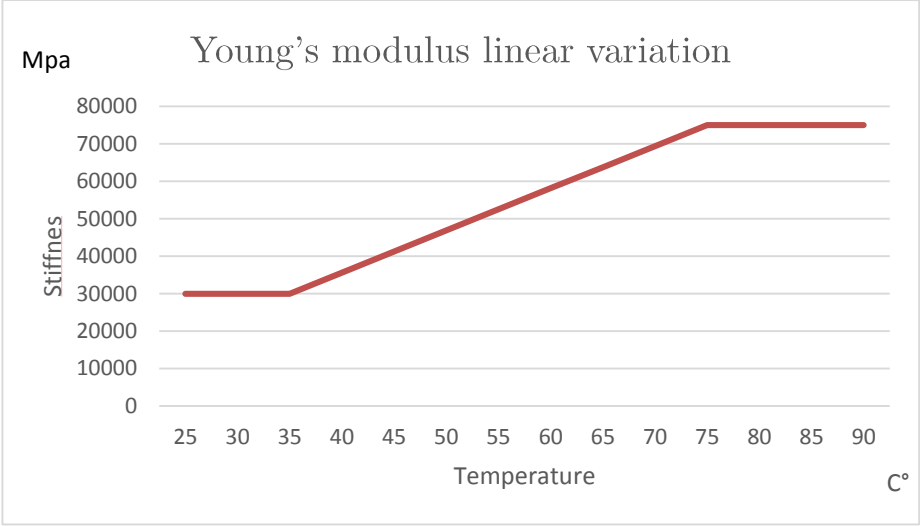

Figure 52 Linear variation of the stiffness for the first model

This model is used to check if the results of the latter two are aligned.

The model implemented in ABAQUS derives from the work of Auricchio Taylor et Al. [48]. With this model only isothermal analysis can be performed. By defining a stress-strain curve and "breakpoint" stresses shown on Figure 53 and Figure 54 below.

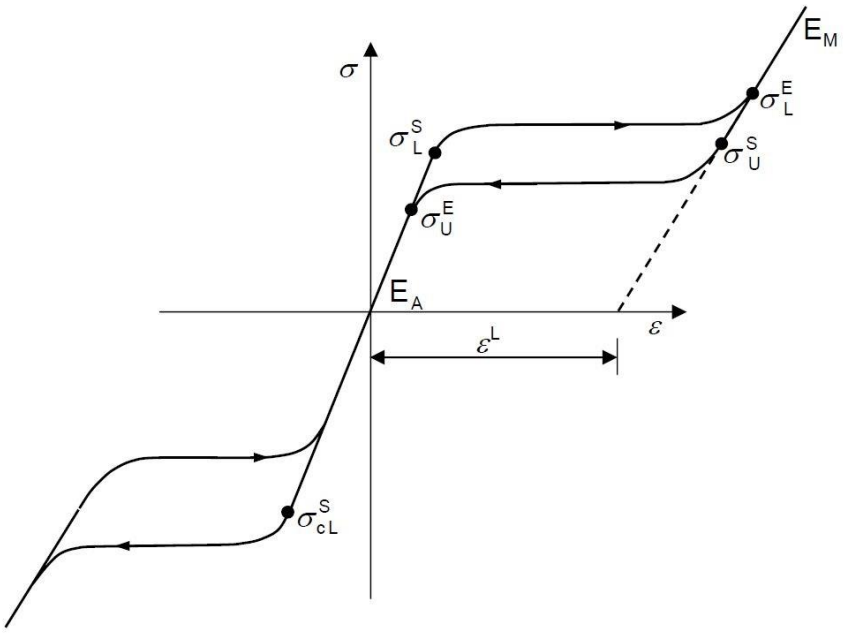

Figure 53 Stress-Strain curve of the ABAQUS superelastic model [46]

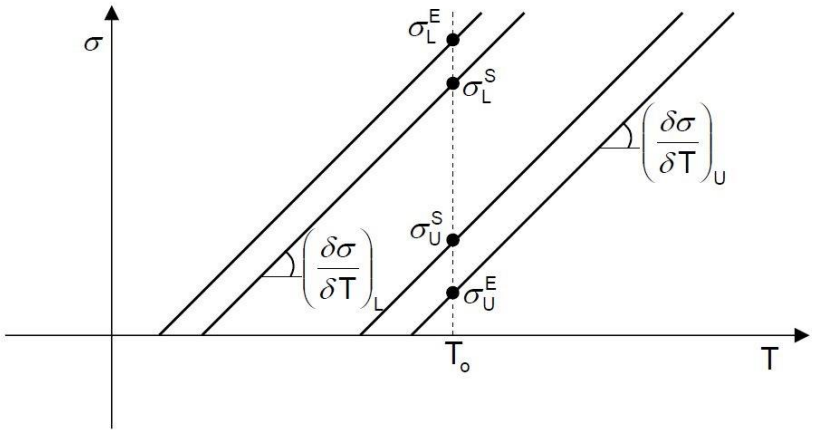

Figure 54 Stress-Temperature curve of the ABAQUS superelastic model [46]

The primary mechanical inputs to this model are two moduli of Elasticity, two Poisson ratios, a plateau transformation strain, and five stress breakpoints. Below is a list of the input parameters required to run this model in ABAQUS:

E_A = Austenitic Elastic Modulus

ν_A = Austenitic Poisson's ratio

E_M = Martensitic Elastic Modulus

ν_M = Martensitic Poisson's ratio

ε^L = Transformation strain

$(\delta\sigma/\delta T)_L$ = Loading $(\delta\sigma/\delta T)$

σ_L^S = Start of transformation stress during loading

σ_L^E = End of transformation stress during loading

$T0$ = Reference temperature

$(\delta\sigma/\delta T)_U$ = Unloading $(\delta\sigma/\delta T)$

σ_U^S = Start of transformation stress during unloading

σ_U^E = End of transformation stress during unloading

σ_{CL}^S = Start of transformation stress during compressive loading

The last model used is a three-dimensional model capable to describe the stress-temperature solid phase transformation. For this reason it can predict the shape memory behavior, which is fundamental to achieve the correct design process, because it can predict the stroke and the forces obtainable by the actuator. The model is based on the calculation of the free energy function Ψ for a polycrystalline SMA material through the following convex potential:

$$\psi(\varepsilon, e^{tr}, T) = \psi_{el} + \psi_{ch} + \psi_{tr} + \psi_{id} + \varphi_{\varepsilon L}(e^{tr}) \quad \cdot(1)$$

Where ψ_{el} is the elastic strain energy, ψ_{ch} is the chemical energy, ψ_{tr} is the transformation strain energy, ψ_{id} is the free energy and $\varphi_{\varepsilon L}(e^{tr})$ is an indicator function introduced to satisfy the constraint of the transformation strain norm. After the free energy is calculated it is possible to calculate the volumetric and deviatoric part of the stress (p and s), the entropy (μ) and the thermodynamic force (X) associated to the transformation strain.

To be thorough, below is provided the time continuous model.

TIME-CONTINUOUS MODEL FRAME [47]

External variable: $\varepsilon, \quad T$

Internal variable: e^{tr}

Constitutive equations:

$$\begin{cases} p = \dfrac{\partial \psi}{\partial \theta} = K[\theta - 3\alpha(T - T_0)] & \cdot(2) \\ s = \dfrac{\partial \psi}{\partial e} = 2G(e - e^{tr}) & \cdot(3) \\ \eta = \dfrac{\partial \psi}{\partial T} = \eta_0 + 3\alpha K\theta - \beta\|e^{tr}\|\dfrac{\langle T - M_f\rangle}{|T - M_f|} + c\ln\dfrac{T}{T_0} & \cdot(4) \\ X = -\dfrac{\partial \psi}{\partial e^{tr}} = s - \left[\langle\beta(T - M_f)\rangle + h\|e^{tr}\| + \gamma\right]\dfrac{\partial\|e^{tr}\|}{\partial e^{tr}} & \cdot(5) \end{cases}$$

With

$$\begin{cases} \gamma = 0 \quad if \quad 0 \le \|e^{tr}\| \le \varepsilon_L & \cdot(6) \\ \gamma \ge 0 \quad if \quad \|e^{tr}\| = \varepsilon_L & \cdot(7) \end{cases}$$

Limit function:

$$F(X) = \sqrt{2J_2} + m\frac{J_3}{J_2} - R \qquad \cdot(8)$$

Flow rule:

$$\dot{e^{tr}} = \dot{\zeta}\frac{\partial F(X)}{\partial \theta} \text{ with } \dot{\zeta} \ge 0, \qquad F \le 0, \qquad \dot{\zeta}F = 0 \qquad \cdot(9)$$

In order to be implemented in a user subroutine the model needs to be discretized in time, to make possible iterating step by step the equation. After the discretization, a method to solve the equation is chosen (solution algorithm), that helps the convergence of the equation into a result. In this paragraph, the purpose is only to show the differences between the models, for this reason the continuous model is simply described, just to understand which behavior can describe the model.

As comparison it is useful to say that the first model do not consider temperature dependency of the critic transformation stress, whereas in the second it is possible to set the temperature of the stress driven phase transformation as an initial condition.

The third one is able not only to simulate the pseudo-elastic effect but also the shape memory effect. The interest of the previous ones is that the difference between the Young's modulus of austenite and martensite are taken into account, whereas in the third there is only one stiffness. For this reason in the simulation process the Young's modulus it is chosen as an average on the martensite and austenite ones.

In the next chapter, in order to check if the actuator is able to seal the pilot channel in a low temperature state (martensite state), simulations are performed within the worst case of the maximum load (non-leaking simulations). This simulation are fundamental to define the thickness of the actuator. For this calculation, the second model will be used, in order to have the possibility to set an initial temperature of 25°C, which represent the working condition temperature.

2.2.3 Technological Limitations

It is fundamental not to lose the feasibility of the actuator in terms of technological limitations. One important point is that sputtering technology allows thickness of maximum 80 microns (or the process starts to be slow) and the structures that can be realized are 2.5D. It means that the volume created is not "completely 3D", because it is made by a superposition of consecutive layers. The growth of the material on the surface can be modified in some point by the usage of quartz masks during the process. The phase transition temperature can be set by varying the composition of the alloy but within a certain range (austenite peak from –5°C to 100°C).

Because sputtering is a process of growth from a substrate it is not easy to realize curves in z-axis (axis of the growth), it would means to have a mask, which is moving in time with a non-constant speed in another axis. For this reason it is difficult to realize fillets in the thickness plane, on the contrary with a curved mask it is possible to have fillets in the other planes.

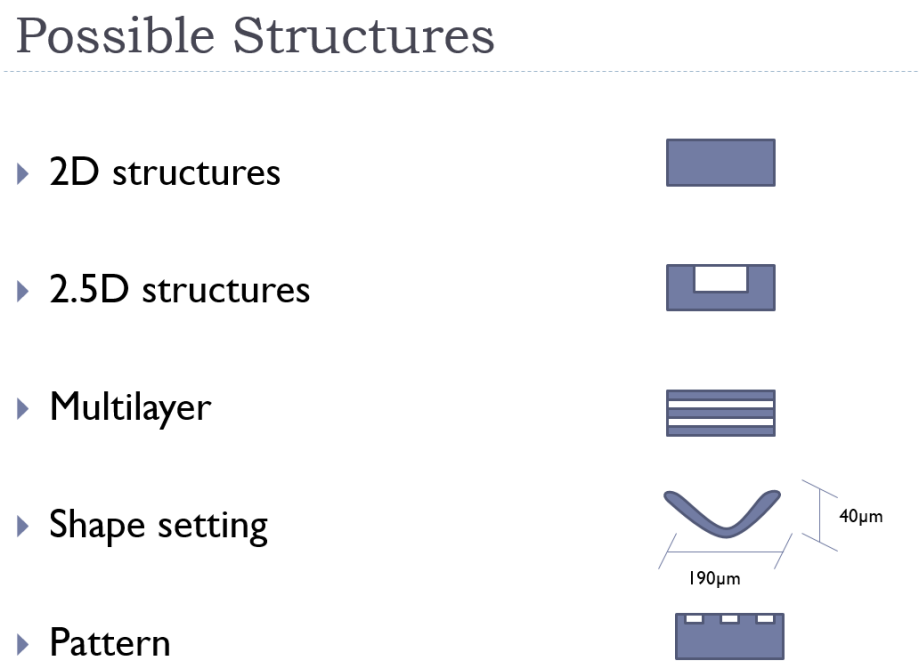

Figure 55 Feasible structures with sputtering process

The feature resolution is limited and it is connected to the thickness of the material.

Acquandas is the partner to produce the sputtered thin film, their great technological capabilities allows to choose the better design that fit the actuator within the boundaries of the sputtering process. Shape setting, for two-way actuators, is possible but it is preferable not to do it in order to make the process more cost efficient.

The multilayer capability allows creating electrical path between or on the surface of the actuator to have the possibility of direct heating of the film.

3 CHAPTER FEM simulations

Introduction

In this chapter is described the process used to reach the optimum shape for the actuator. Starting from the function of the NiTi thin film (SMA) in the valve, the technical requirements are decided, thanks to the expertise of Fluid-o-tech. Simulations starts from the simplest design which is a cantilever beam, increasing the complexity of the latter by optimizing parameter after parameter such as number of cantilevers, width and thickness of the material. The entire process described above helps defining the designs to produce, that increases strokes and forces of actuation. Acquandas, a German company, specialized in microsystem technology and sputtering process, is chosen to build the prototypes of the actuator. For this reason, the parameters of the material in the further simulations are as closed as possible to the standard alloy they use.

3.1 Evolution of the design

Sputtering process offers great advantages in terms of crystalline structure and in possible obtainable shape. The concept of the design originates from the necessity to seal and open the pilot channel of the valve; the movement that is performed is an axial displacement along the direction of the pipe (stroke). The first option considered is a cantilever beam (Figure 56).

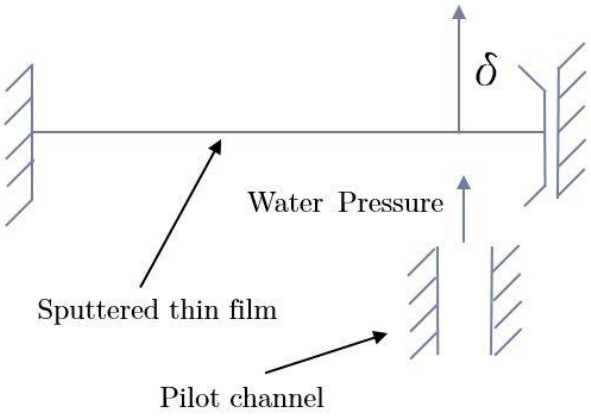

Figure 56 Cantilever beam design

It is easy to see that the slider pair at the end of the cantilever is difficult to produce also because the film is thinner than a sheet of paper. Therefore, to avoid adding this constraint it is preferable to have a symmetric structure, like a "bridge".

In order to prevent the forces to "slip" away from the side of the bridge a three-cantilever design is built, the so-called star shape design.

In the following chapter is discussed the optimization of length, thickness, number and position of the beams of this design.

Supposing that it is possible to make the temperature of the actuator changes as required, it has to be defined the position of the film at low and high temperature, considering that the design has to be the simplest as possible also in terms of the productive process. Firstly is decided that the position at low temperature corresponds to the position which has the channel sealed so, in order that if there is a loss of power occurs, the valve will stay closed. Low temperature means below the martensite finish temperature and high temperature means above austenite finish temperature.

Another degree of freedom is if the material is chosen to show one-way or two-way shape memory effect. As said in chapter one, one-way actuators allow to have elegant and simple design but training of the material is needed and the performances in terms of strokes and forces are lower. For that reason the two-way shape memory effect actuator is chosen.

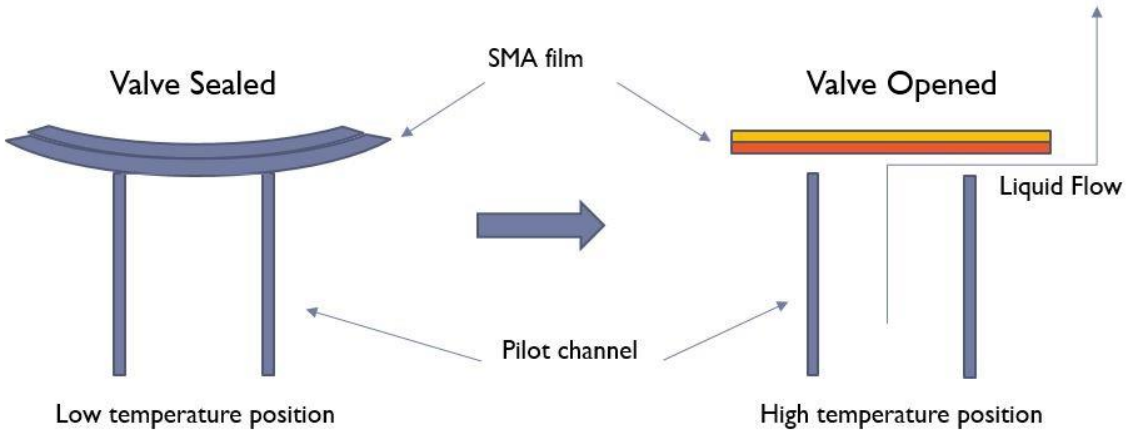

Figure 57 Valve's positions at low and high temperature

Another problem concerning material is that it is necessary, in order to have a recovery of the strain, to start heating the latter from a deformed configuration. The simplest way to deform the film is to apply a force in the center of the actuator. Two ways come up to apply the force, the former is to apply a thrust spring (Figure 58) and the latter is to use a super-elastic layer of the material already deformed and coupled or glued together at low temperature to obtain the deformed configuration (that in Figure 57).

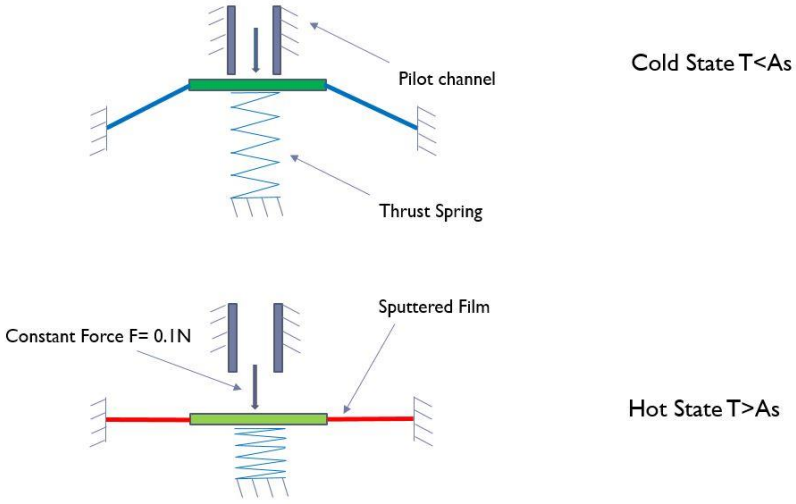

Figure 58 Position in the hot and cold state with the spring applied

To simplify the design the spring option is chosen, knowing that the spring in further works can be substituted with a more efficient superelastic layer, but for now simplicity drives the way of thinking, because it is a new field to explore for the companies.

Fixed specifications are also present such as maximum pressure, working temperature, diameter of the pilot channel, maximum thickness. To make easier the sealing of the pilot channel easier, the central part of the actuator is composed by a circular element connected to the beams to have a sealing surface preventing leakage. The number of "legs" of the star-shaped design becomes limited by the angular space, not to succumb to excessively thin cantilevers.

The goal of the shape optimization is to achieve the maximum difference of vertical displacement between the two configurations in order to create an easy passage for the fluid through the valve. In the next paragraphs, the spring is represented as a truss element (vertical), that provides only axial stiffness.

3.2 Mechanical model

In the case of the thrust spring, a mechanical model is used to predict the modulus of the stiffness and the forces needed to obtain a defined initial displacement at low temperature. The goal is to define the length of the beam that is more efficient to guarantee the maximum recovery of vertical displacement between the two working temperatures. In addition, the initial displacement of the beam is varied to obtain the perfect initial strain to have better performances. The purpose is to know, by always imposing the same vertical displacement of 1mm at the bottom of the truss, which is the stiffness that has to be applied to the truss in order to obtain a certain initial deformation in the cantilever beam.

As known from the theory, the transverse stiffness of a beam is:

$$E_B = \frac{12EI}{l^3} \tag{10}$$

Where E represent the Young's modulus of the film, I is the area moment of inertia and l is the length of the beam.

As said in this work, for simplicity, the spring is considered as a truss beam with only axial stiffness:

$$K_S = \frac{AE_S}{l_S} \tag{11}$$

In Figure 59 below are depicted the boundary constraints and the scheme of the model.

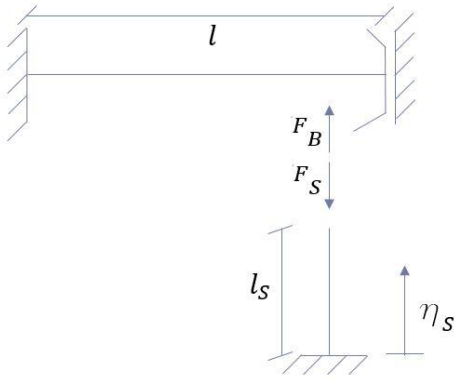

Figure 59 Initial configuration at low temperature

A displacement from the bottom of the spring is applied (η_S), as a consequence, a displacement at the end of the beam appears (η_B). The objective is, by varying the stiffness of the spring, to obtain the desired displacement of the actuator (η_B). This model is relevant because, during the simulation, it allows to predict the correct truss stiffness (E_S) to obtain the desired displacement. It is fundamental that for each length of the thin film beam (l_B) many initial displacement conditions (η_B) are tried in order to find which is the best situation to obtain the best performance in terms of force and vertical displacement.

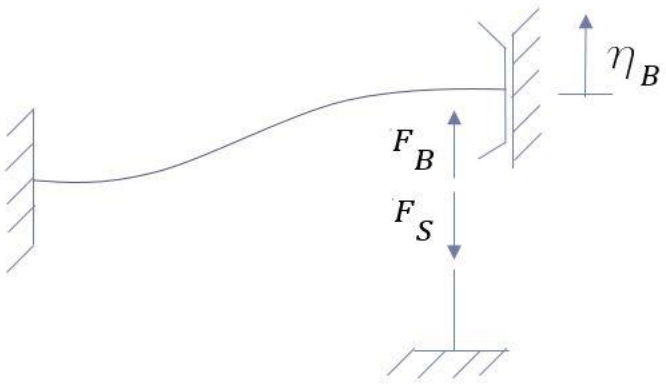

Figure 60 Deformed configuration after the spring displacement

Below is the equation to calculate the spring stiffness from the force equilibrium.

$$\eta_B \frac{12E_B J}{l_B^3} = (\eta_B - \eta_S)\frac{E_S A_S}{l_S} \tag{12}$$

Supposing that the displacement of the spring (η_S) is 1mm and the desired initial displacement of the actuator (η_B) is 0.5mm

$$E_S = \frac{12E_B J l_S}{l_B^3 A} \tag{13}$$

The equation (13) allows calculate the truss's stiffness (E_S) for a given vertical displacement of the truss and the beam.

3.3 Comparison between different models

The three models of the material, are analyzed in order to better understand the differences between them.

To make a comparison between different models it is necessary to define precisely the material that is used for each of them. Below is presented the material provided by Acquandas, which is one of the standard materials, they use to produce thin films.

Table 2 Material properties of the NiTi sputtered by Acquandas

	Unit	Austenite	Martensite
Thermal conductivity	W/mK	18	8.6
Specific heat	J/gK	0.45	0.45
Thermal exp. coeff	10-6/K	11	6.6
Clausius-Clapeyron	MPa/K	8	8
Young's modulus	GPa	75	30
Poisson's ratio		0.3	0.3
Shear modulus	GPa	28.8	10.8
Density	g/cm^3	6.45	6.45
Yield strength	MPa	550	100
Tensile strenth	MPa	1100	1100

Although models are describing the same material there are many differences in the parameter chosen to represent its behavior. For example, the first model, that is the simplest one, has only two parameters, the Young's modulus of the two phases of the material, instead the three-dimensional one has eleven (Table 3). For the simulation ABAQUS CAE is used as solver and, for the third model, a user material UMAT (courtesy of the Department of Civil Engineering and Architecture Pavia University) which implement the Souza Auricchio model is used. The latter combines the macroscopic model originally proposed by Souza, Mamiya, & Zouain [49] with the finite elements model proposed by Auricchio & Petrini [47]. The parameters of the material in the further simulations are as closed as possible to the standard alloy used by Acquandas, The values used in these simulations are:

Table 3 Material properties used for the Auriccho-Souza model

	Unit	Value
Young's modulus	MPa	53000
Poisson's coefficient		0.33
Hardening coeff.		1000
Saturation strain limit		0.056
Transformation temperature	K	323
Beta (temperature coeff)	GPa	6.1
Regularization coeff.		10-6
Critical stress	MPa	100
Current temperature	K	310
Tolerance for Newton cycle		10-6
Tolerance for F=|X_TR|-R		10-12

The values are chosen as tradeoff between the stability of the model (already tested values) and the reliability in terms of experimental results (material data given by Acquandas). For this reason, the value of the Young's modulus is the mean between the two phases of the material, and the value of Poisson's coefficient is the same as the real material. Remembering that any metal could be sputtered it is not fundamental which parameters are chosen unless are luckily to be an existing material.

To best characterize the behavior of the model a thin beam test in flection is performed. The section of the bar is rectangular 10x70 microns.

The model is imported in ABAQUS from Autodesk Inventor as IGES file, it is composed by: one elastic beam (4mm length) with rectangular section, a rigid body where is applied a truss (2mm length) with only axial stiffness (see Figure 61). The mesh is performed with C3D8 eight node linear brick.

Boundary condition applied are:

- At the left side surface of the beam the vertical (y-direction) and horizontal (x-direction) displacement are impeded to create a cantilever.
- At the right side surface of the beam only the vertical displacement is allowed, to create a slider pair.
- Between the beam and the rigid body, the connection is created by a tie function.
- The truss is coupled on the top with rigid MPC (multi point constraint) to the rigid body, at the bottom is allowed only vertical displacement.

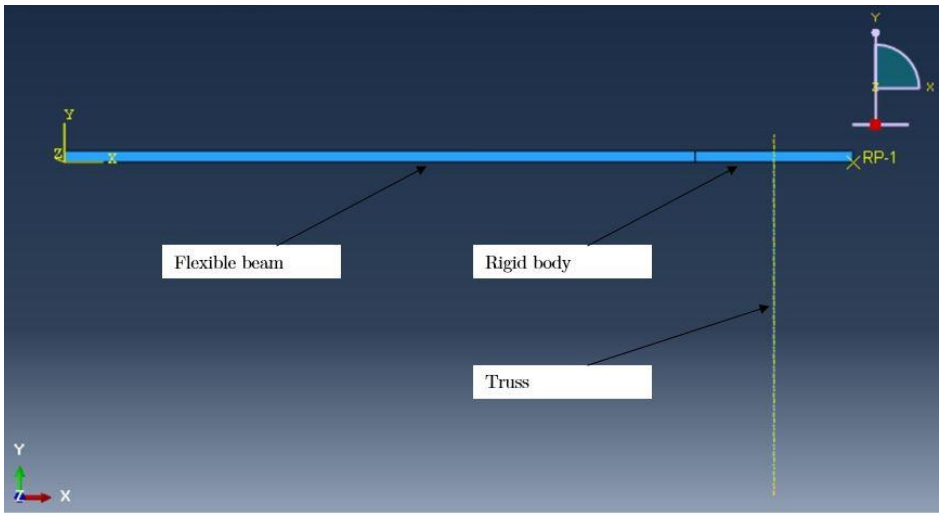

Figure 61 Undeformed configuration of the model

The step of the analysis are:

- Displacement in the y-direction of 1 mm applied at the bottom node of the truss
- The temperature rise above the transformation temperature

Results for the variable stiffness and the Souza-Auricchio are presented below in Figure 62 and Figure 63, the same data point is chosen. In the x-axis is plotted the time of the steps and in the y-axis the Von Mises stress and the y-displacement.

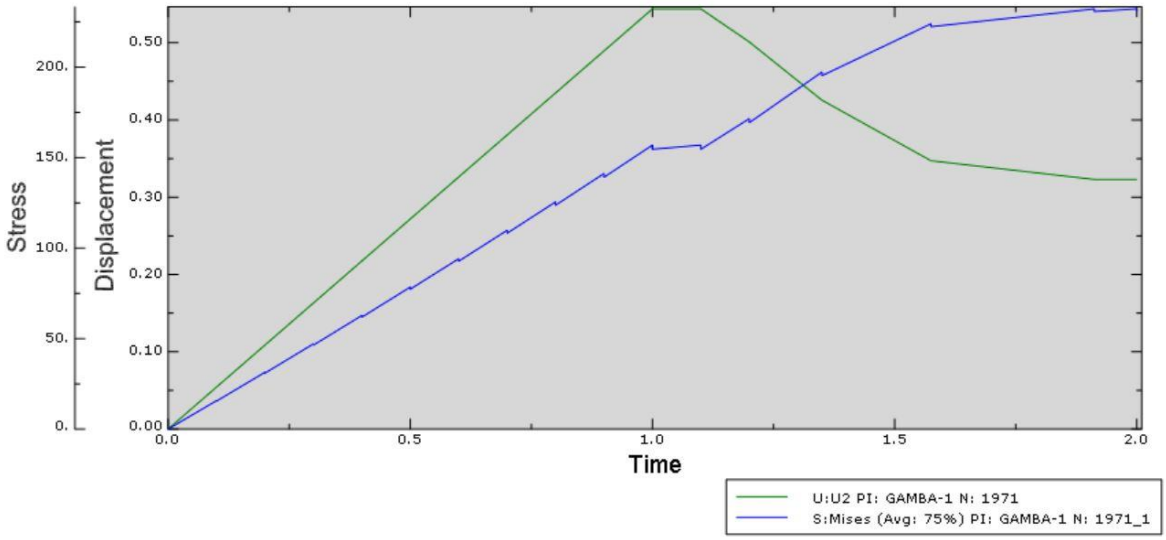

Figure 62 Plot in time of stress and displacement with the variable stiffness model

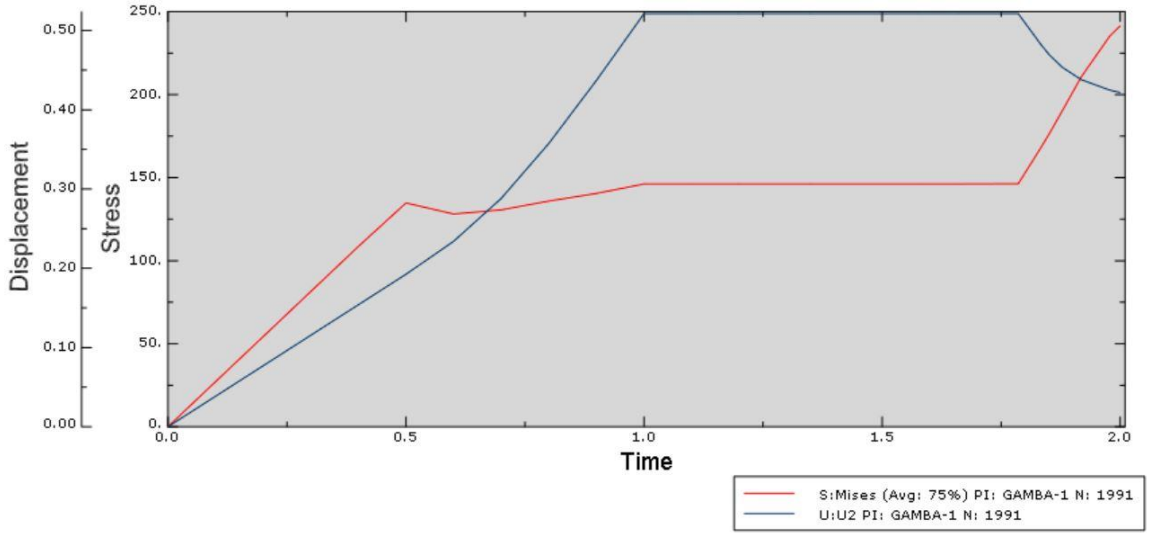

Figure 63 Plot in time of stress and displacement with the Souza-Auricchio model

As it is easy to see in Figure 63 the Sousa-Auricchio model provides smoother curves because the evolution in time of the equations that drive the solution have smaller steps. In the former model the stiffness varies abruptly, so when the temperature reaches the next step in stiffness, the material suddenly moves, this creates the shape of a saw tooth. Concerning the displacement the ramp up of the variable stiffness model is linear (Figure 62) as described by the mathematical model, in the latter the ramp is nonlinear (Figure 63), as the behavior of shape memory alloys.

The differences in the values of the maximum stress are not relevant: 241MPa (variable stiffness) 234MPa (Souza-Auricchio). The difference of the maximum

vertical displacement (0.544mm and 0.521mm) are not big but the recovery of vertical displacement, after heating the material, is different 0.221mm and 0.1mm for the first and the second model.

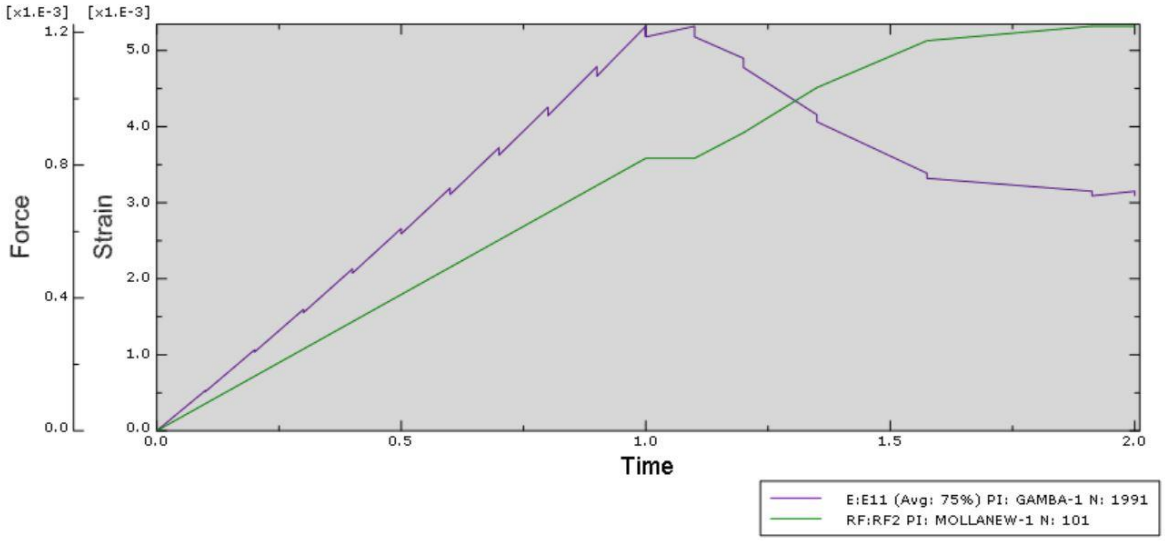

Figure 64 Plot in time of strain and force with the variable stiffness model

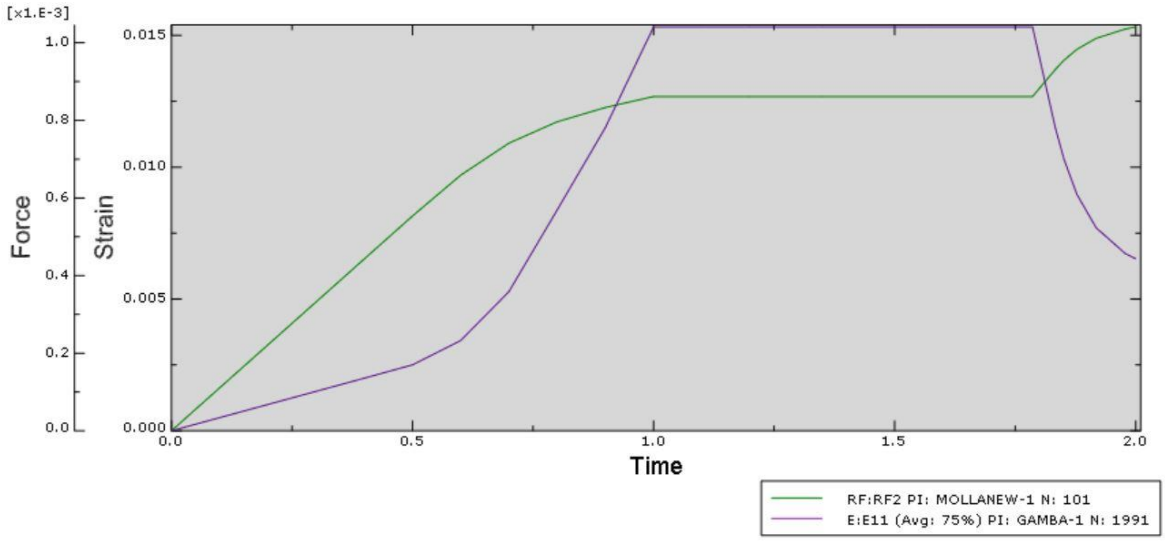

Figure 65 Plot in time of strain and force with the Souza-Auricchio model

If the strain are compared there is a sustancial difference because SMA material (Figure 65) allows elastic strain that are one order of magnitude more than a simple elastic material (Figure 64).

Comparing the forces there is no big difference ($0.82 \cdot 10^{-3}$ N and $0.86 \cdot 10^{-3} N$).
In conclusion the first model could be used to design a mechanical part knowing that the stresses and the forces expressed by the actuator are slightly affordable, but the recovery (different of vertical displacement before and after the temperature rises) and the strains not.

3.4 Optimization and sensitivity

The model used from now on is the Auricchio-Souza model, which is more precise in describing the behavior of the material.

An optimization process is started by varying the length of the elastic beam from 0.5mm to 5mm. As said, the maximum thickness obtainable by sputtering process is 80 microns so the section is modified to a 10x80 microns section. After the length optimization, the design is modified into a three legs star-shaped design and thickness and performance are tested. Later, a five legs design is tested to increase the actuation force and to see how the results change with respect to a width variation of the beams. Finally, the design with best performance is chosen, tested to prevent leakage and to choose the best way to embed it in the valve (clamping).

3.4.1 Simple beam optimization process

The aim of this process (see Figure 66) is to obtain not only the optimum length of the beam, but also the best initial configuration (displacement just before heating). Because of the fact that the recovery of the vertical displacement is driven by the presence of strains in the material at low temperature, it is necessary to know what is the initial displacement that reaches the best results. To do so the stiffness of the truss (spring) is varied to obtain for each length of the beam, displacement at low temperature from 0.1mm to 5mm. As said in the earlier paragraphs only the stiffness of the spring is changing because, the imposed displacement at the bottom of the spring to deform is remains always the same (1mm). The variation of the displacement and length ranges are set in the way that the material is tested from nearly zero stress to the maximum reachable. It is also fundamental to know which force is used to give the initial deformed configuration, for this reason the vertical displacement of the spring is fixed at 1mm. Only the stiffness varies in order to obtain different forces and therefore different initial conditions. Data are collected in the same point, node near the right end of the beam, for each length and for each displacement.

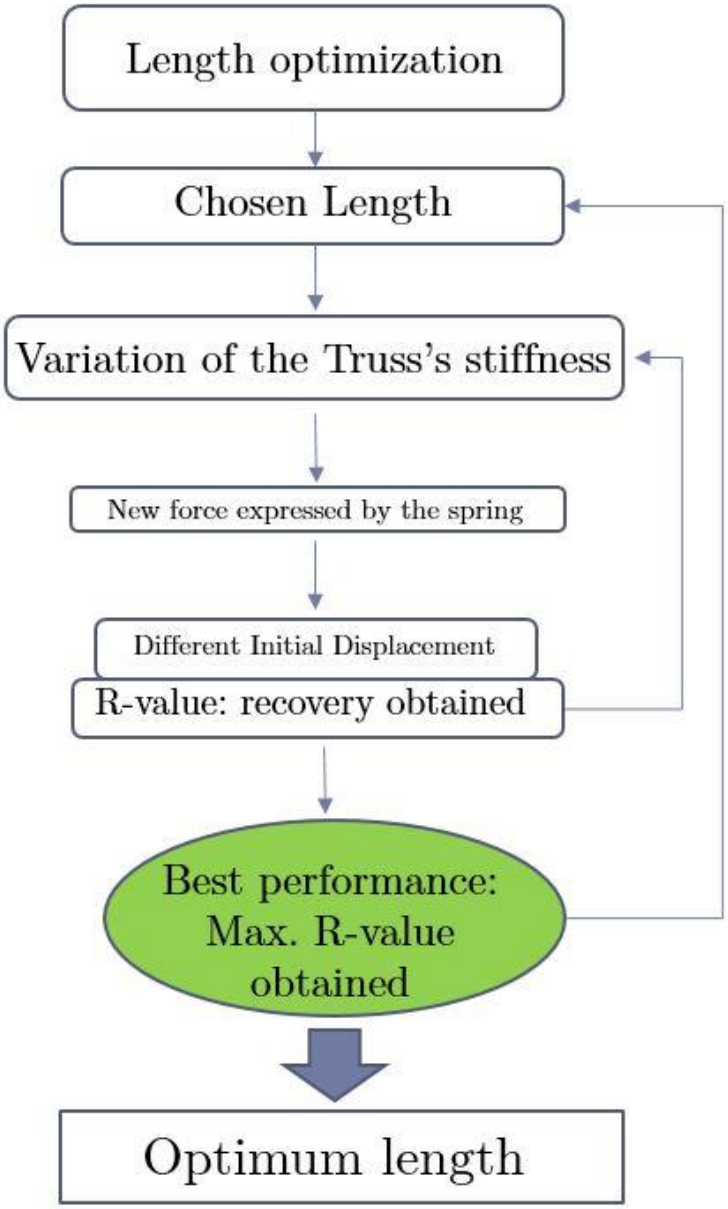

Figure 66 Description of the length's optimization process.

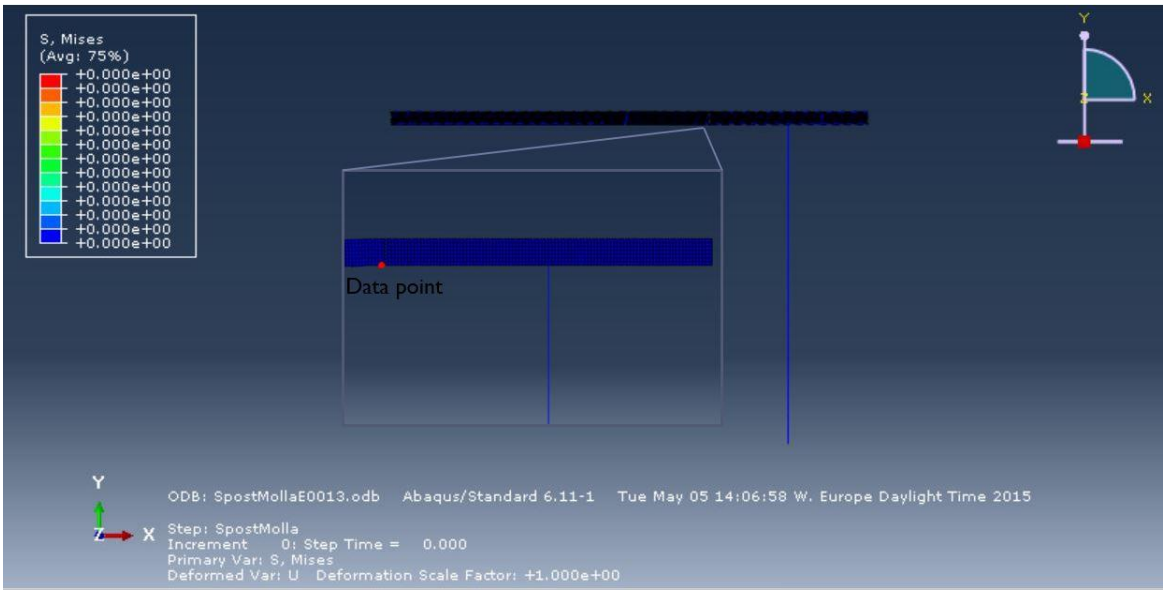

Figure 67 Position of the data point in the deformed configuration

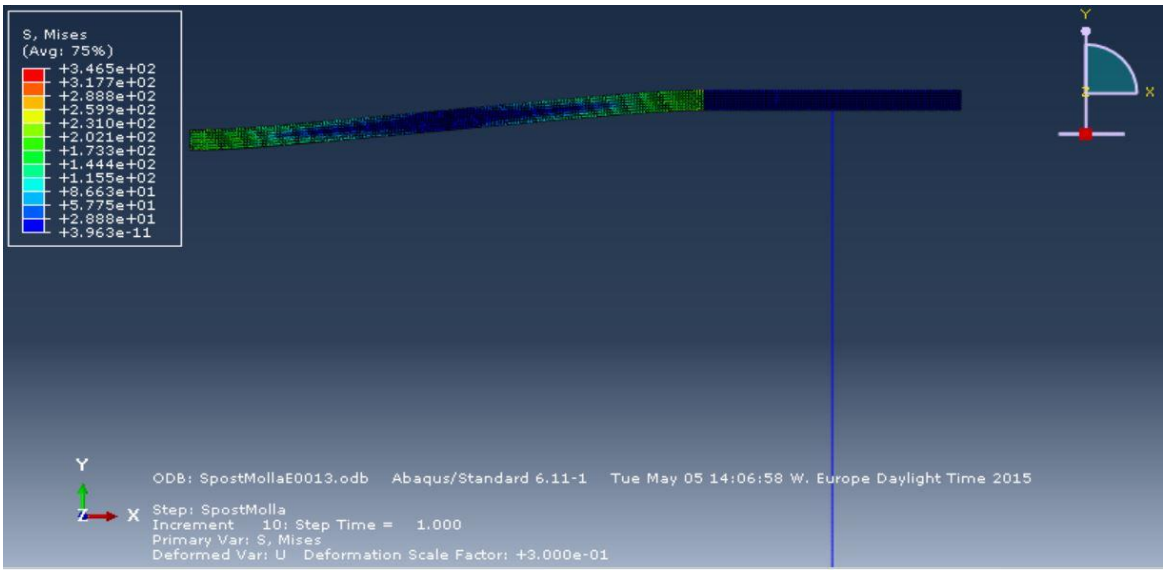

Figure 68 Deformed configuration at low temperature after the vertical displacement of the spring

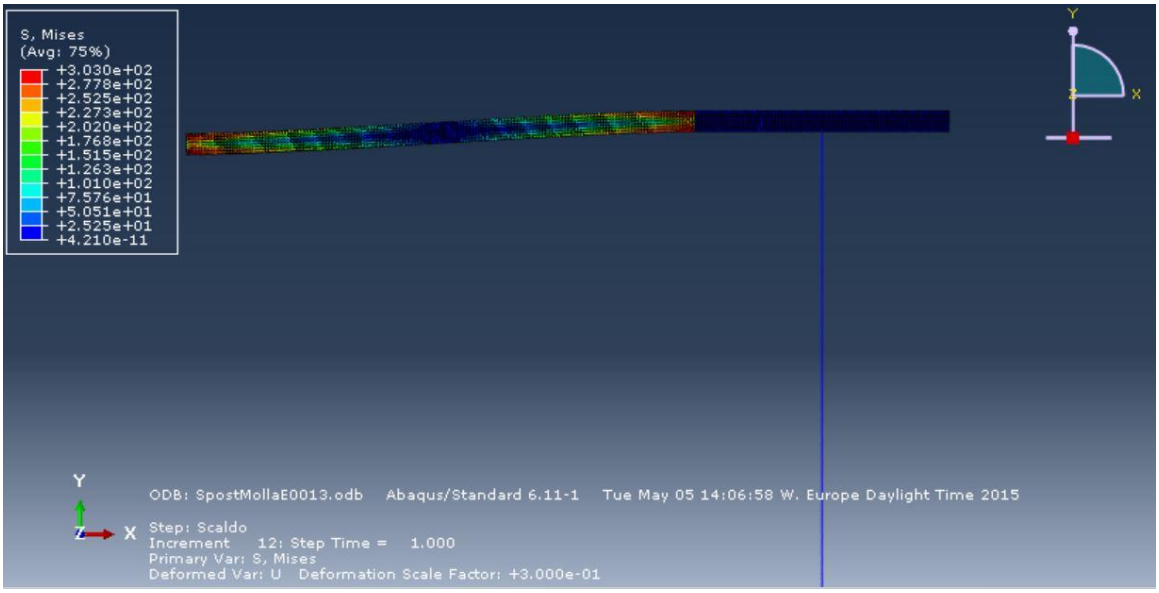

Figure 69 Deformed configuration at high temperature after heating the material above transformation temperature

In every analysis several data are collected including displacement, stress, strain, force at the bottom of the spring etc., doing so a graph is made representing on the x-axis the initial displacement and on the y-axis the differences between high and low temperature state (recovery R).

$$R = U_C - U_H \tag{14}$$

In Equation (14) U_C and U_H are respectively the vertical displacement (y-axis) below and above the transformation temperatures.

Figure 70 shows the relation occurring between the initial displacement U_C of the beam and the R parameter calculated. The process is reiterated so that each line represents a different length of the beam, this allows recognizing the best configuration of the actuator in terms of length of the beam and initial condition.

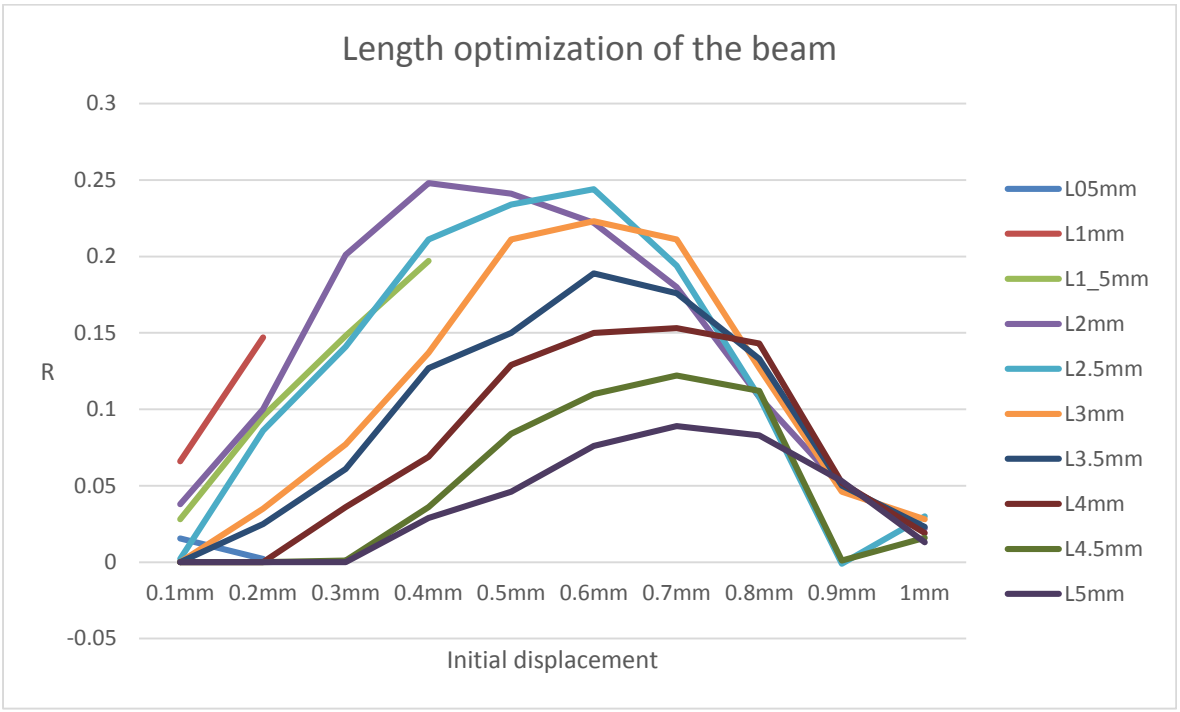

Figure 70 Optimization of the length of the beam by mean of the R parameter

As result from Figure 70 the best length in terms of performance are: 2mm and 2.5mm. The maximum value for the R parameter is 0.248mm.

In order to include the stress in the optimization process, a new parameter(R_s) is defined:

$$R_s = \frac{U_C - U_H}{\sigma_C} \tag{15}$$

Where σ_C is the stress that has the material under the transformation temperature, once deformed by the displacement of the truss.

The graph below (Figure 71) represents the variation of the parameter R_s with the length of the beam and different initial displacements.

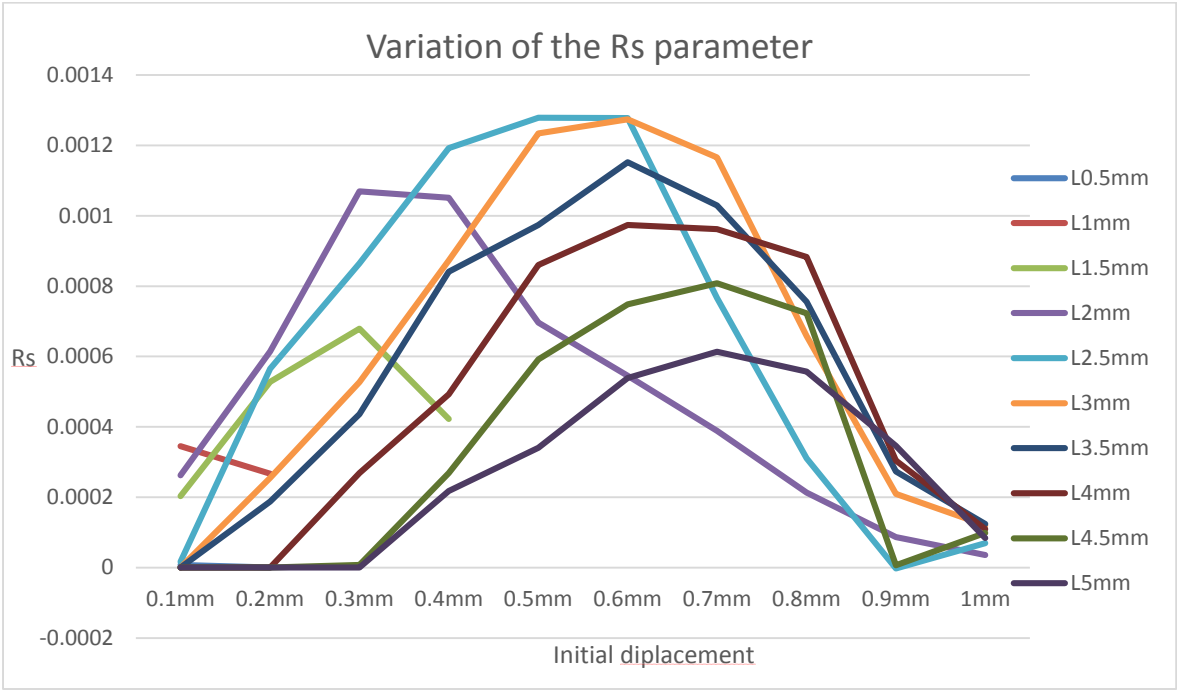

Figure 71 Optimization of the length of the beam by mean of the Rs parameter

In this case, another length appears to be competitive which is the 3mm beam. The maximum value for the R_s parameter is $0.0013\ mm/MPa$.

It is interesting to observe the behavior of the 1mm length, that seems to decrease while the other lines increase their values. This behavior appears because the curve has already reach his maximum outside the graph and, like the others, is starting to decrease.

In Table 4 are presented the first three best values for each parameters, but the data of all the combination are considered. Selecting the best results leads to choose only three principal beam's length. As result the parameter's range is reduced and so the number of combination possible for each value, reducing the overall time of the optimization process.

Table 4 Results of the beams optimization

Beam's length	Max R value	Max Rs value
2 mm	0.248mm	0.00107mm/MPa
2.5 mm	0.244mm	0.00128mm/MPa
3 mm.	0.223mm	0.00127mm/MPa

Finally, three lengths are chosen: 2mm, 2.5mm and 3mm, which are the values used from now on.

3.4.2 Three beams star-shaped design

Once the optimum length is find, the design defined in chapter 2.2.1, is tested.

Using the star-shaped design with three "legs" (beams); a new optimization process starts to obtain the best initial configuration (always varying the stiffness of the spring), and to verify if the best thickness is the maximum achievable by sputtering (80microns). Three thickness are tested (60, 70 and 80 microns) for the design in Figure 72, if there is little differences between the results it could be useful to use the thinner in order shortens the sputtering process or the thicker to have a more rigid actuator. In addition, it is possible that the optimum values of the parameters are different for the three thickness, for this reason are worthy to be tested.

The optimization of the leg's width is object of further simulation.

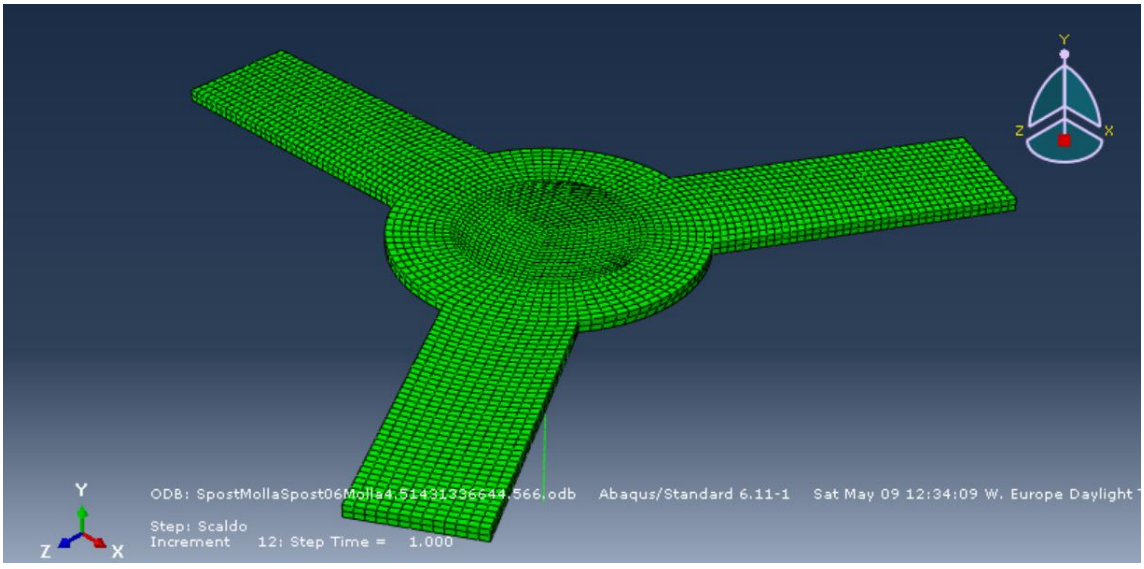

Figure 72 Undeformed star-shaped design with three beams.

With the same method, results are collected, but this time only the length that represents the optimum for the simple beam simulations are tested which are: 2mm, 2.5mm and 3mm.

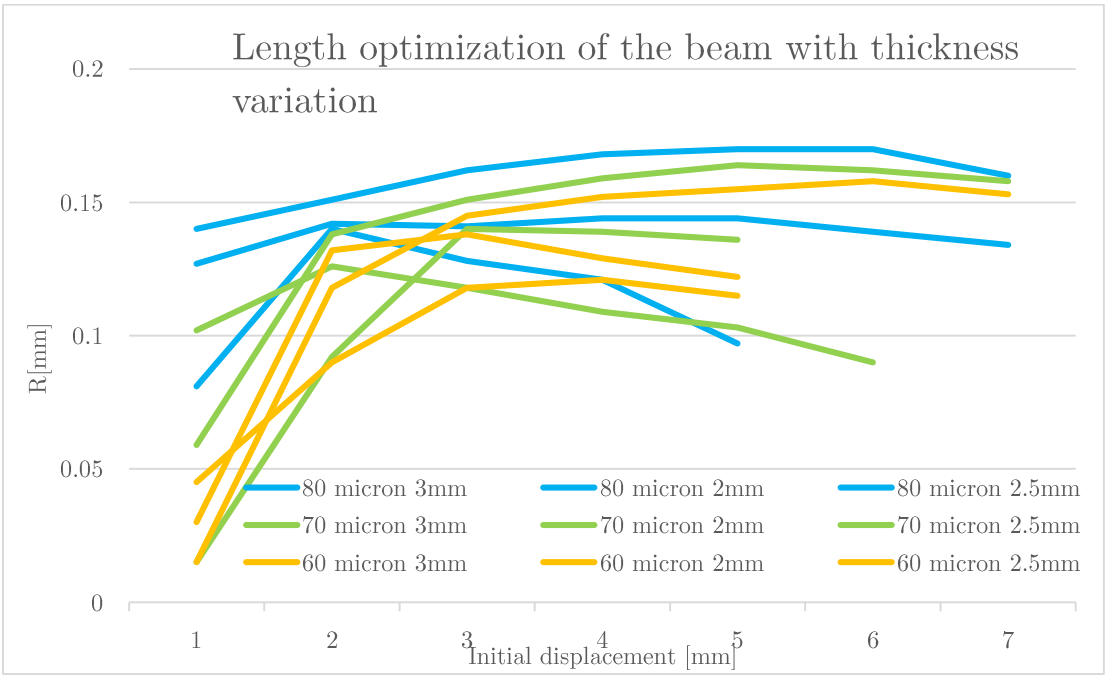

Figure 73 Length optimization of the three legs star-shaped design with thickness variation

The best data for each different thickness are now selected from Figure 73.

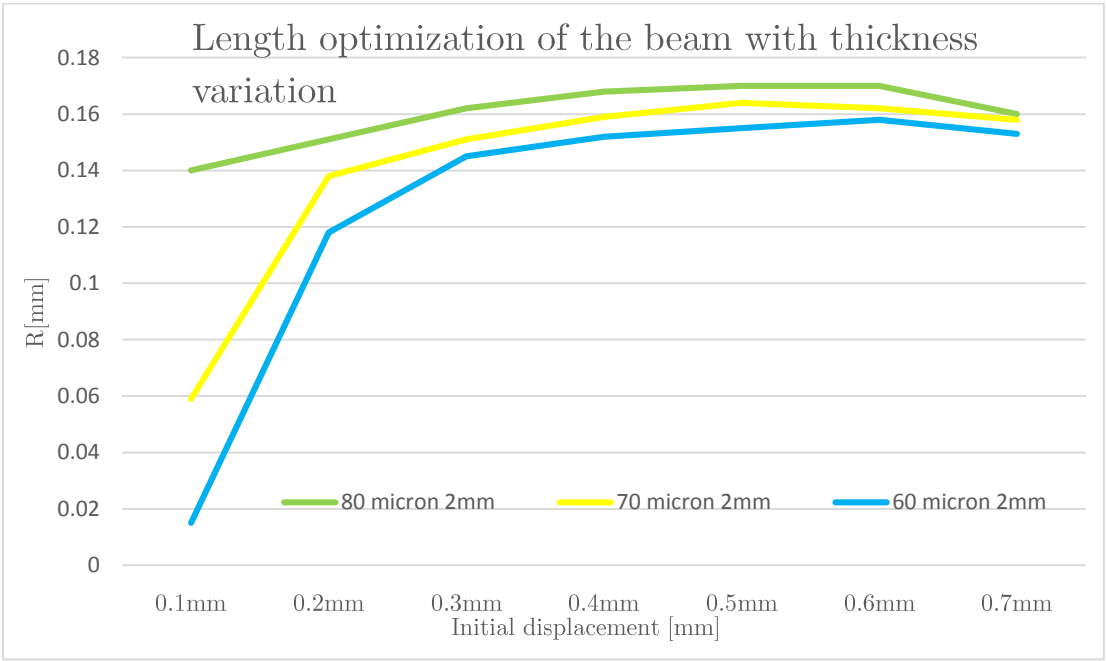

Figure 74 Selected data length optimization of the three legs star-shaped design with thickness variation

As it is clear the best thickness is the bigger one ($80\mu m$) also because it has greater stiffness that allows better performance preventing the leakage of the valve (holding still the position at low temperature while the maximum pressure is applied).

Another parameter tested is the force (F) that can be express by the design. This derives from the stiffness but also from the percentage of transformed Martensite, which depends on the initial configuration. Below is presented the F parameter.

$$F = F_H - F_C \tag{16}$$

Where F_H and F_C are respectively the forces measured at the bottom of the truss in the hot state and in the cold state in respect with the transformation temperature.

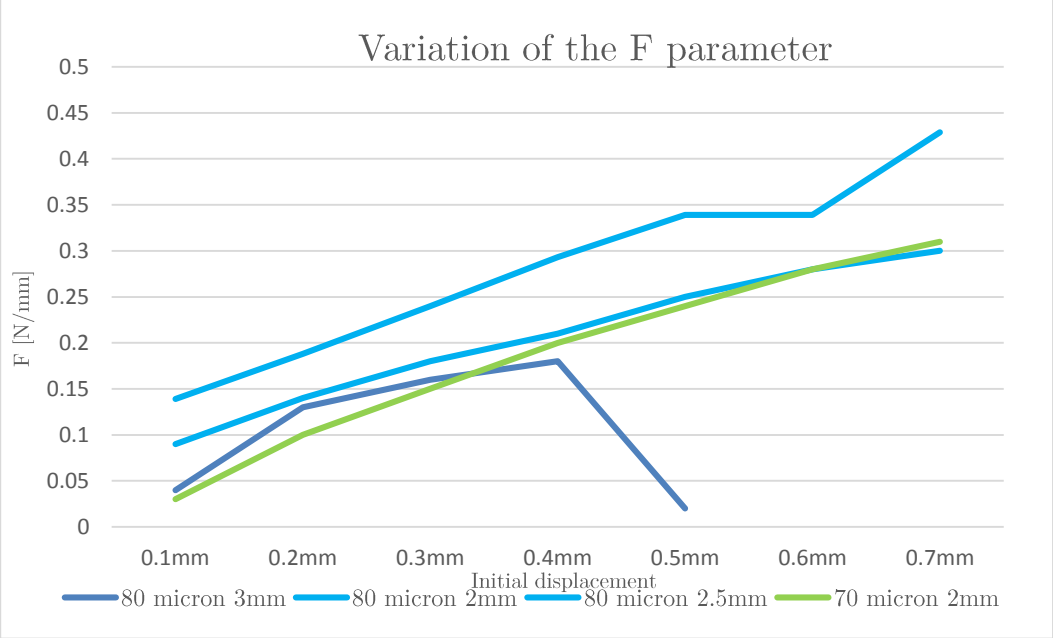

Figure 75 Variation of the F parameter varying the initial condition

The maximum of the F parameter is obtained with the stiffer configuration that is the one with 2mm leg. As results from Figure 74, Figure 75, it is clear that the best length is 2mm and the best thickness is, as expected, 80µm.

Table 5 Results of the three beam star-shaped design

Beam's thickness	Max R value	Max F value
0µm	0.170mm	$0.34N$
70µm	0.164mm	$0.31N$
60µm	0.158mm	$0.20N$

3.4.3 Five beams star-shaped design

To improve the force provided by the actuator another design with five beams is tested (Figure 76).

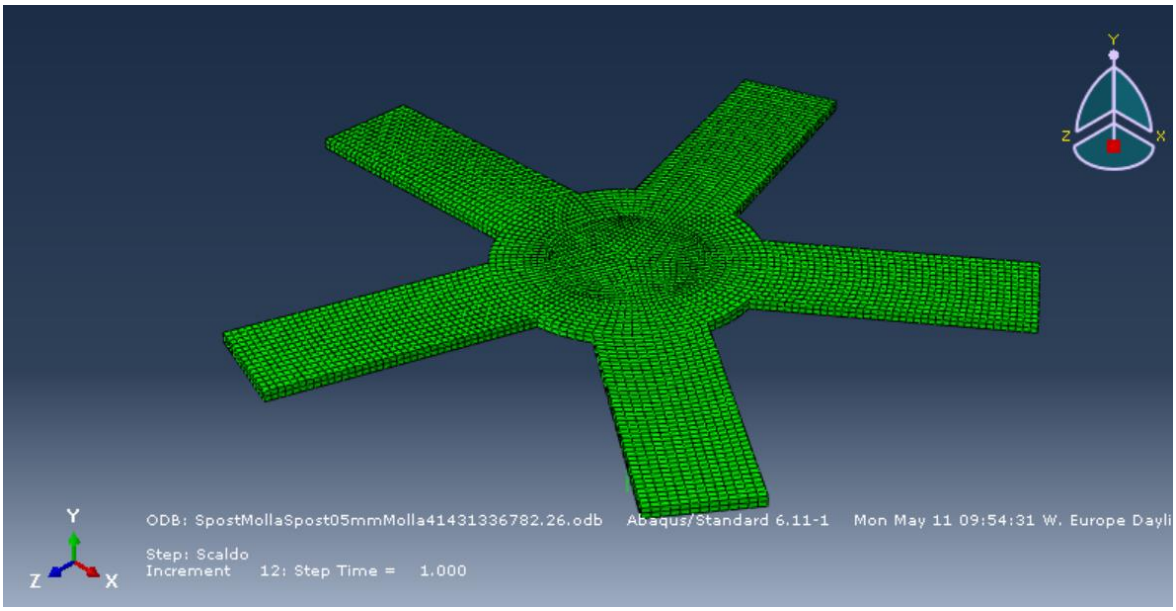

Figure 76 Undeformed star-shaped design with five beams.

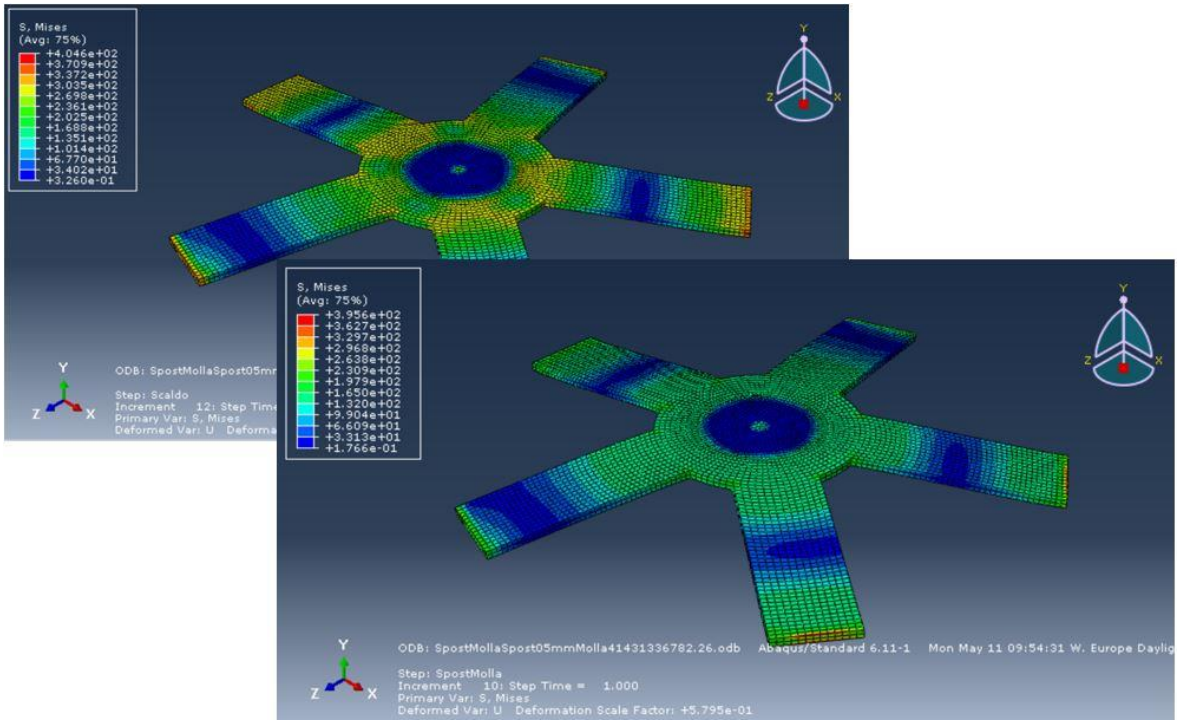

Figure 77 Deformed configurations star-shaped design with five beams.

The same optimization process is done but this time only the initial displacement is varied because the length is already the optimum one (2mm). This process is done to see what is the maximum performance obtainable from this design.

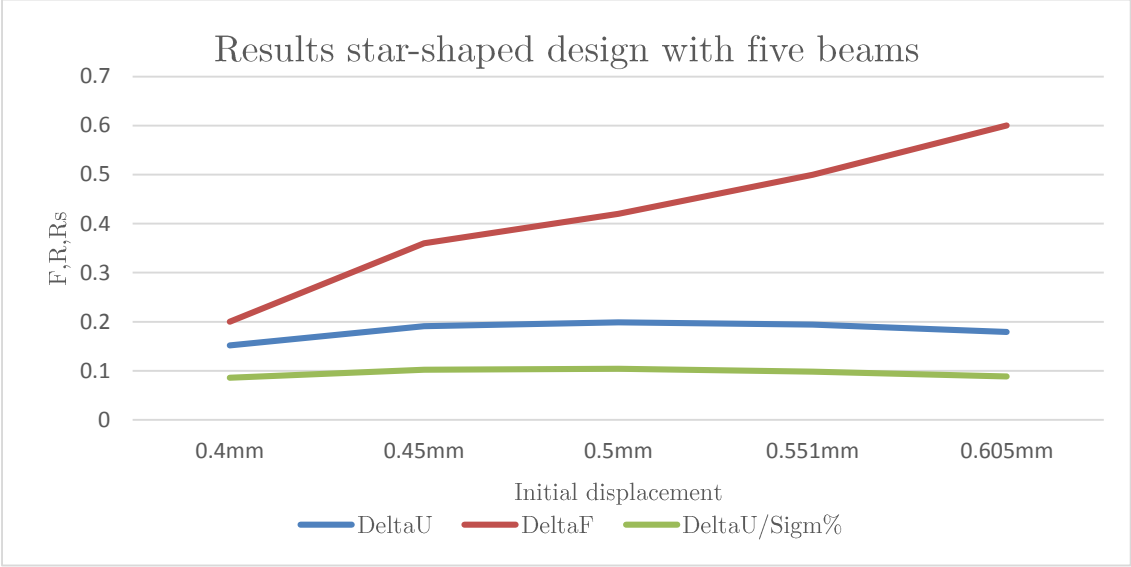

Figure 78 Results for star-shaped design with five beams 80microns thickness 2mm leg.

As result the maximum value of the R parameter is $0.199mm$, the maximum value for the F parameter is $0.6N$.

The last dimension to be varied is the width, in this case three values are chosen:

$0.6mm$, $0.8mm$ and $1mm$.

The motivation of the chosen values is that less than 0.6mm it appears that the stiffness is not sufficient, and more than 1mm width, obliges to increase the dimension of the inner diameter, wasting material and making the actuator too rigid.

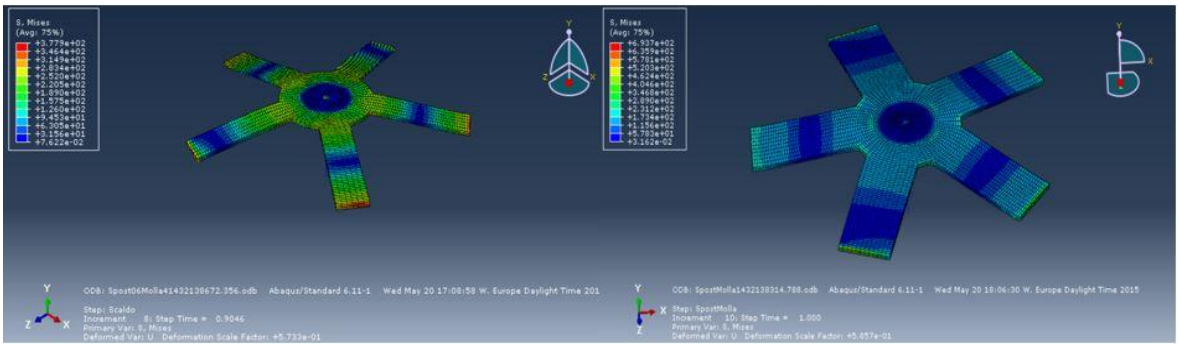

Figure 79 Width variation for the five beams star-shaped design.

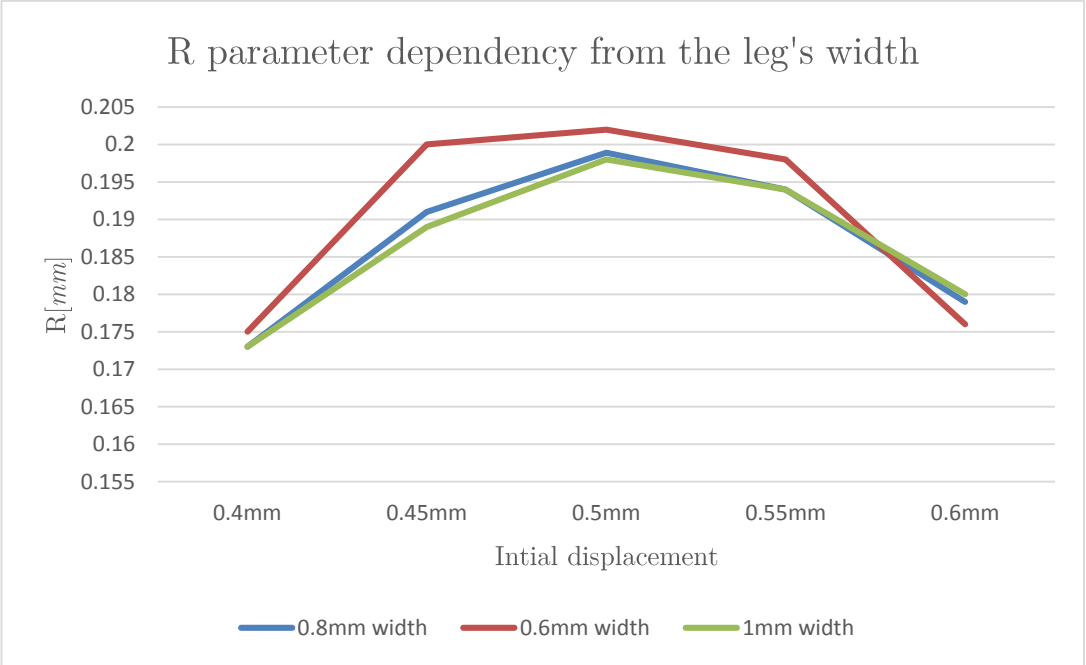

Figure 80 R parameter dependency from leg's width

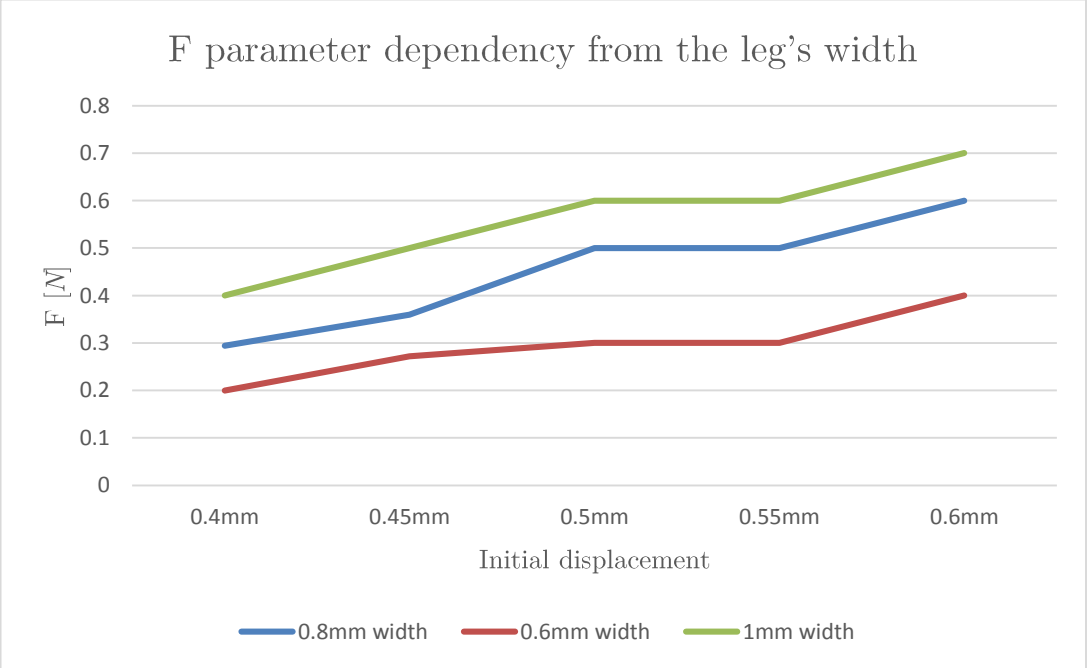

Figure 81 F parameter dependency from leg's width.

As shown in Figure 80 above, the best R-value (0.202mm) is obtained with a width of 0.6mm and the best F value (0.7N) for the one of 1mm. It is remarkable also, that the R parameter shows no big difference between the configurations with 0.8mm and 1mm. In order not to have a too stiff actuator, could be a good design those with

0.8mm, because the one with 0.6mm it's not enough rigid to guarantee that the valve stays closed while a pressure is applied.

In order to find the optimum initial displacement for the R parameter the range of displacement in figure 80 is limited to the values that include the best one. In order to choose the optimum configuration the designs have to be tested also with the non leaking simulation (see Figure 82), which can lead changes to the optimum design, because also the stiffness of the actuator is involved. Having greater values in terms of stiffness, allows not to move while the pressure is applied, but on the contrary, it limits the recovery of the displacement (R parameter).

Table 6 Results of the five beam star-shaped design

Beam's width	Max R value	Max F value
0.6mm	$0.202mm$	$0.3N$
0.8mm	$0.199mm$	$0.5N$
1mm.	$0.198mm$	$0.6N$

3.5 Non leaking test

Non-leaking test consist in simulating the actuator while the maximum working pressure (5bar) is applied. The goal is to verify that the thin film does not move while the pressure is applied; "doesn't move" means that the vertical displacement is one order of magnitude less than the R parameter, but it allows good strokes letting easily flow the fluid through the pilot channel.

The setup of the simulation is presented below.

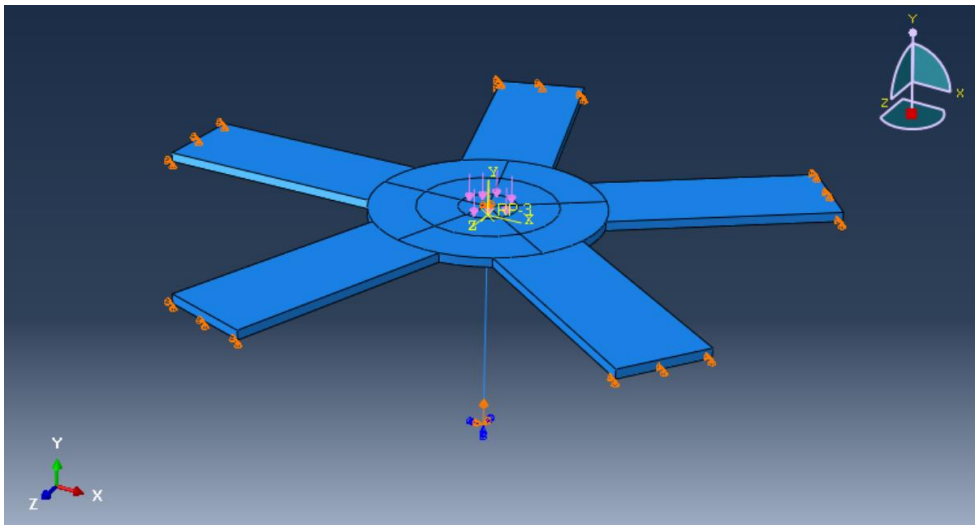

Figure 82 Non-leaking simulation of the valve

In Figure 82, the pressure is represented by purple arrows, which works in the opposite direction with respect to the spring. The pressure represents the action of the fluid while the valve is closed. Finally to evaluate, which is the model that best fit this type of simulation, the three models are used to describe the material, one simple elastic set at the value of the martensite phase (30000MPa), the superelastic model set at the same value and the Souza-Auricchio (53000MPa).

For the first two model the step of the simulations are:

- Initial temperature is set at 243K
- Vertical displacement of the spring
- Linear rising of the pressure until the value of 5bar (0.5MPa).

For the third one:

- Initial temperature is set at 243K
- Vertical displacement of the spring
- Linear rising of the pressure until the value of 5bar (0.5MPa).
- The temperature rises linearly to 373K

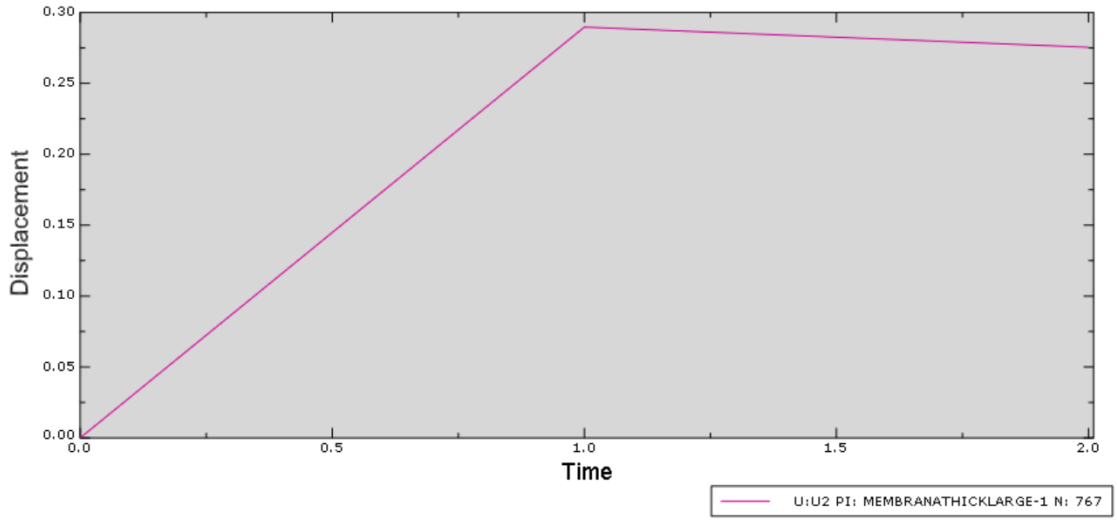

Figure 83 Result of non-leaking test with the simple elastic model.

In Figure 83 the vertical displacement as result of the application of the pressure is 0.014mm.

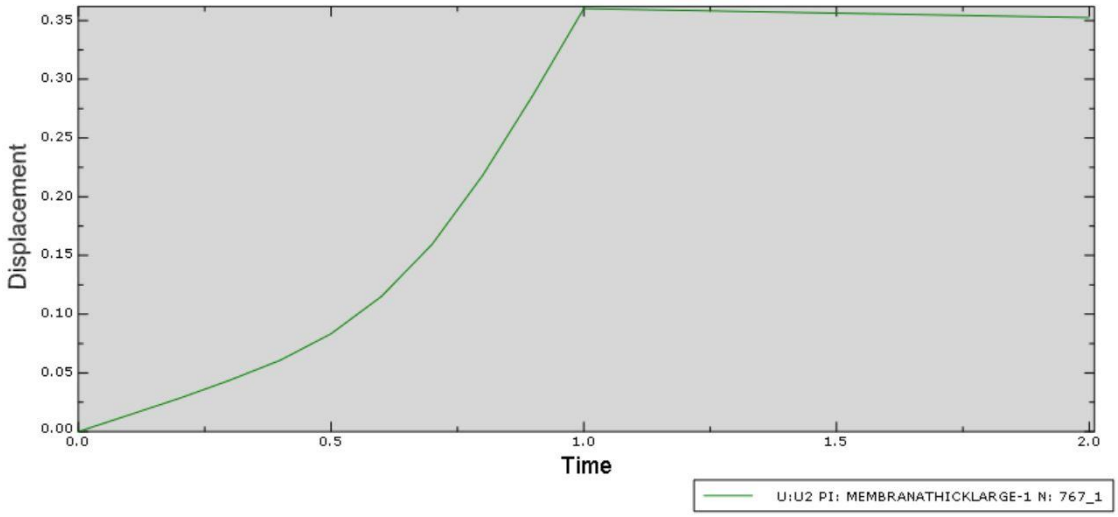

Figure 84 Result of non-leaking test with the superelastic elastic model

It is important to focus on the ramp up of the displacement, that in opposition with the former result where is linear (Figure 83), in Figure 84 it is nonlinear.

In (Figure 83) where is depicted a linear-elastic model, the relation between strain and stress is linear on the contrary in the second model, the superelastic one, the displacement is nonlinear because of the constitutive relation of the shape memory alloys; Below the displacement due to the pressure is 0.0077~0.01mm

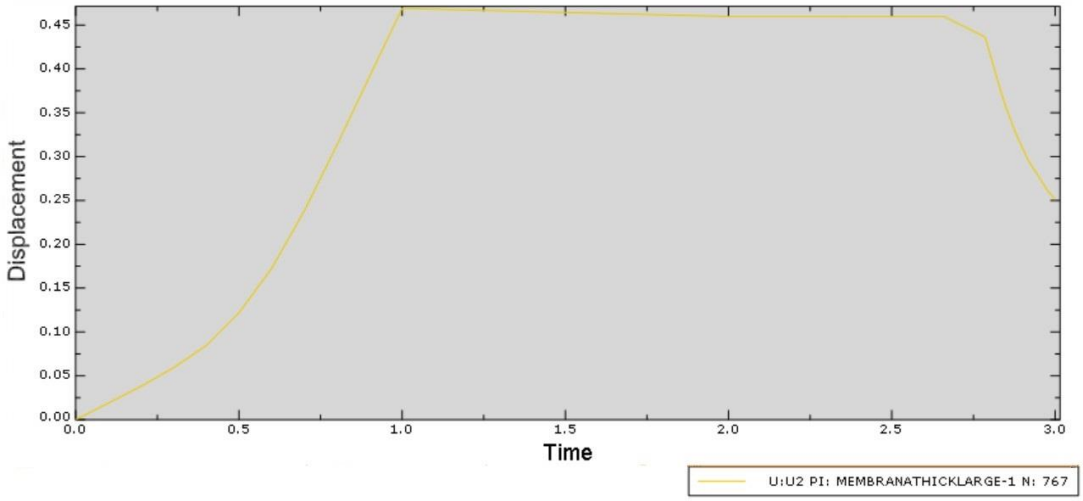

Figure 85 Result of non-leaking test with the Souza-Auricchio model

With the Souza-Auricchio model, the displacement due to the pressure is: 0.009mm. It is also possible to see the magnitude of the R factor, which is 0.218mm.

As conclusion the third model is used for the further simulations because of the agreement obtained with respect to the values of the other models and due to the fact that is more complete allowing to measure the R factor.

Concluding as it can be seen from Figure 83, Figure 84, Figure 85, the simple elastic model and the superelastic one cannot predict the shape memory effect. The superelastic achieves to describe the nonlinear behavior of the phase transformation, but the third one is more accurate predicting also the material's transformation while being heated (SME).

Table 7 Comparison of the results from the three model used for the non-leaking test

Model	Nonlinear Behavior	SME	Leaking test	R value
Simple elastic (Figure 83)	No	No	$0.014mm$	NaN
Superelastic (Figure 84)	Yes	No	$0.010mm$	NaN
Souza Auricchio (Figure 85)	Yes	Yes	$0.009mm$	$0.218mm$

3.5.1 Non leaking test with width variation

Another important comparison that has to be done is between the three widths already tested in order to see which is the best design. Remarkably these simulations are not only leakage test, but also simulations involving phase transformation, representing, as close as possible, the real environment the actuator is put through.

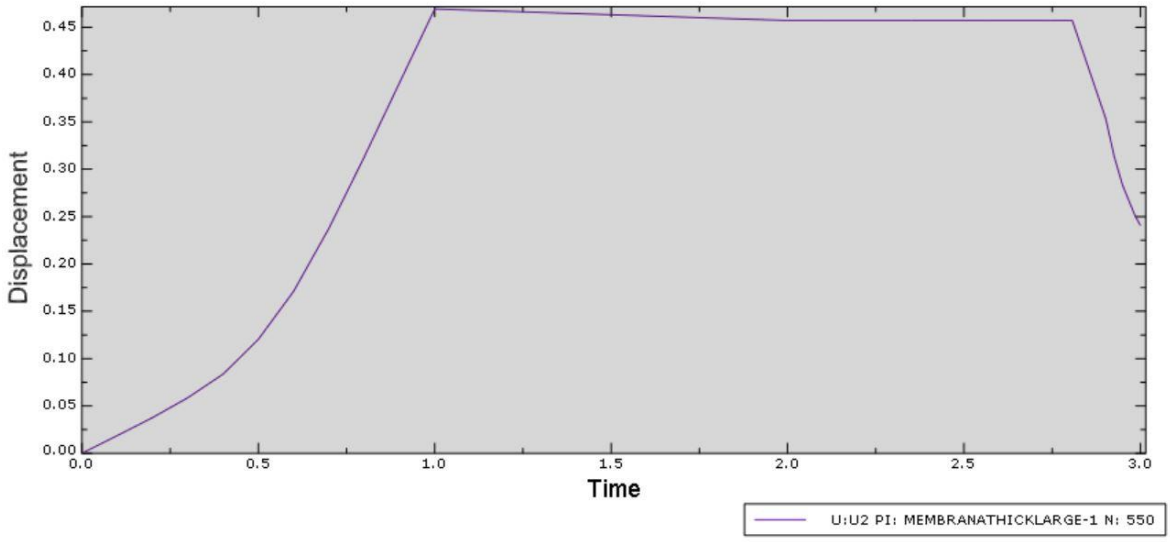

Figure 86 Result of non-leaking test with 0.6mm width beam

The 0.6mm width design is the less rigid, so it is expected to show larger displacement while the pressure is applied, but also greater R values, in comparison with those of 0.8mm (see Table 8).

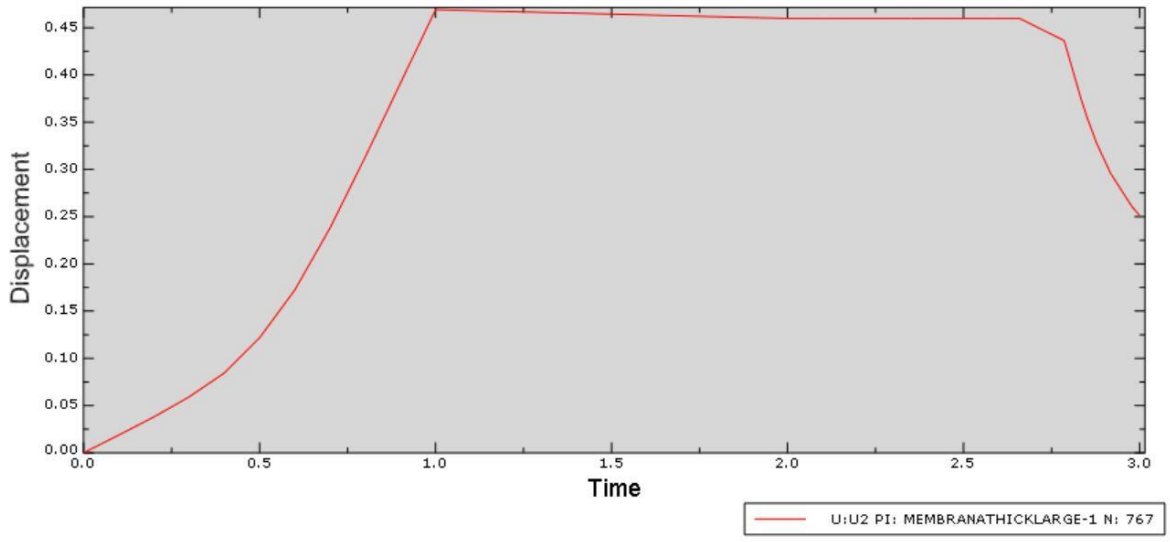

Figure 87 Result of non-leaking test with 0.8mm width beam

The results presented in Figure 87 above are intermediate and it can be seen as a tradeoff between the R values and the leakage parameter, although there is not such a difference between the results in general.

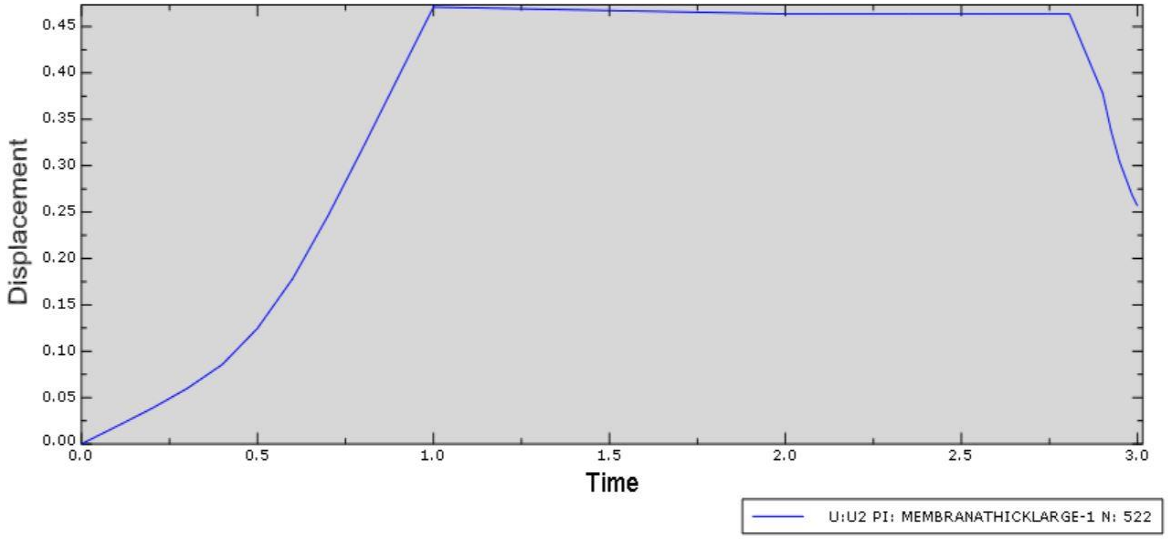

Figure 88 Result of non-leaking test with 1mm width beam

The results of Figure 88 above are of the stiffer design, as expected the displacement due to the application of the pressure is less than in the other cases, but the vertical recovery (R) is also smaller.

Table 8 Results of the width optimization for the five beams star-shaped design

Width	Initial disp.	Leakage	R value
$0.6mm$	$0.469mm$	$0.012mm$	$0.224mm$
$0.8\ mm$	$0.469mm$	$0.009mm$	$0.218mm$
$1\ mm.$	$0.471mm$	$0.007mm$	$0.214mm$

As it can be seen from Table 8 the differences between the three cases are not relevant, it means that exists a certain degree of freedom in choosing the design. A design with 0.8mm width is chosen because it allows having good performances in comparison with the maximum obtainable, without hinder other parameters such as leakage.

3.6 Clamping and location in the valve

The optimum configuration is defined:

- 80 microns thick
- 2mm leg's length
- 0.8mm width or 1mm width
- Five legs

The aim of this paragraph is to understand how to hold the actuator in position while working and where to place it in the innovative valve.

Concerning the constraints, from the expertise of Acquandas, clamping the thin film with two metallic plate by means of pinholes is recommended to prevent undesired movements. This method seems to be the best one, because gluing is considered less reliable than a geometric constraint like the one presented. In addition, glue is less efficient from the production point of view, because it means more operation to assemble the valve. In addition is not always compatible with hostile working environment such as temperature changing and contact with fluids.

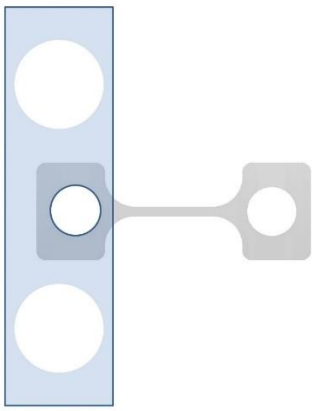

Figure 89 Clamping system for sputtered thin films (Courtesy of Aquandas).

3.6.1 Modification and performance of the clamped design

An external ring of material is added to make the assembling and handling of the actuator easier. As result it makes grow the external diameter also decreasing the stresses on the pinholes.

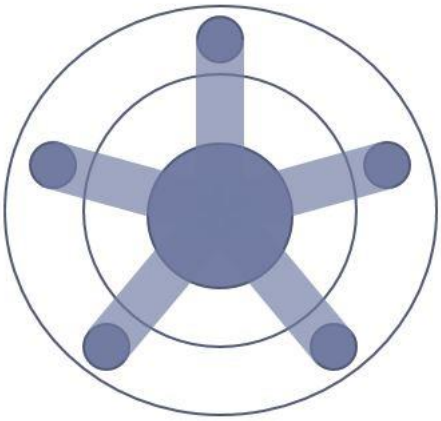

Figure 90 Clamping pinholes with external ring for the star-shaped design

Now that the geometry of the design is changed is preferable to verify it with new simulations. Two clamped design are tested, one with the external ring and one without, to understand which one is suitable for the application.

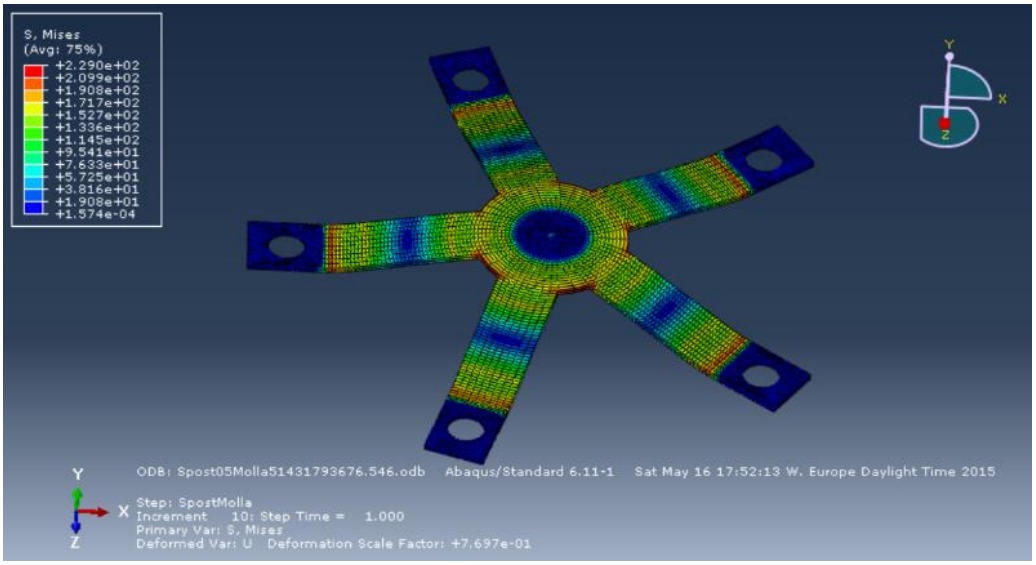

Figure 91 Clamped design without external ring.

The results are presented in Figure 92:

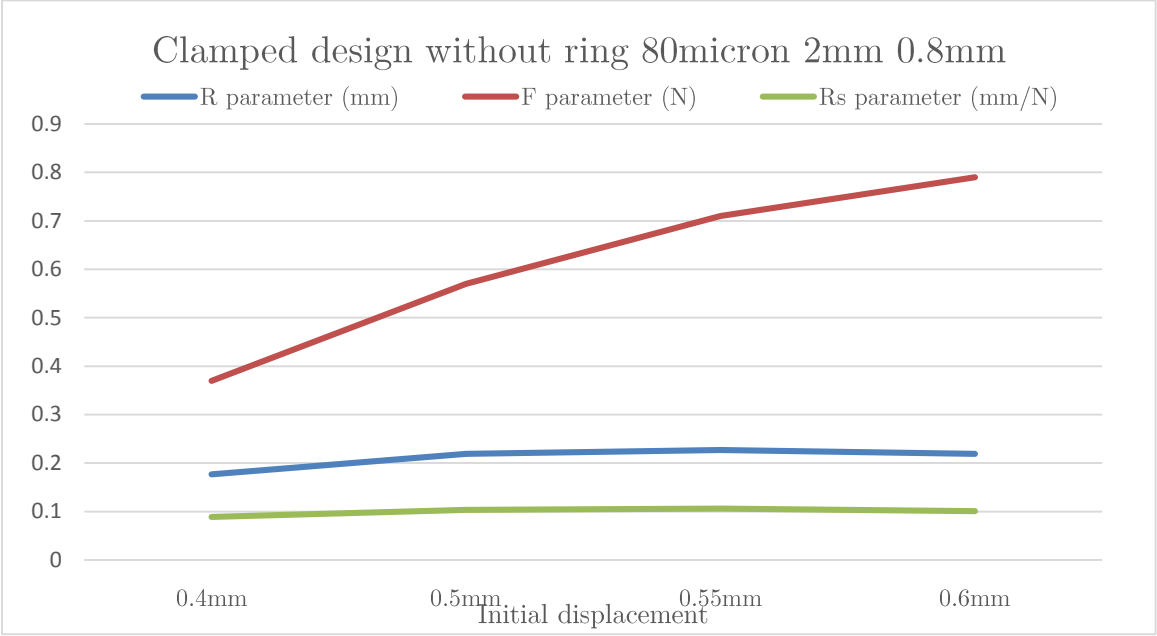

Figure 92 Results for clamped design 80microns thick, 2mm leg's length, and 0.8mm width

The Figure 92 above shows that the maximum of the R value is 0.227mm

Another simulation is performed to see the behavior with the working pressure applied.

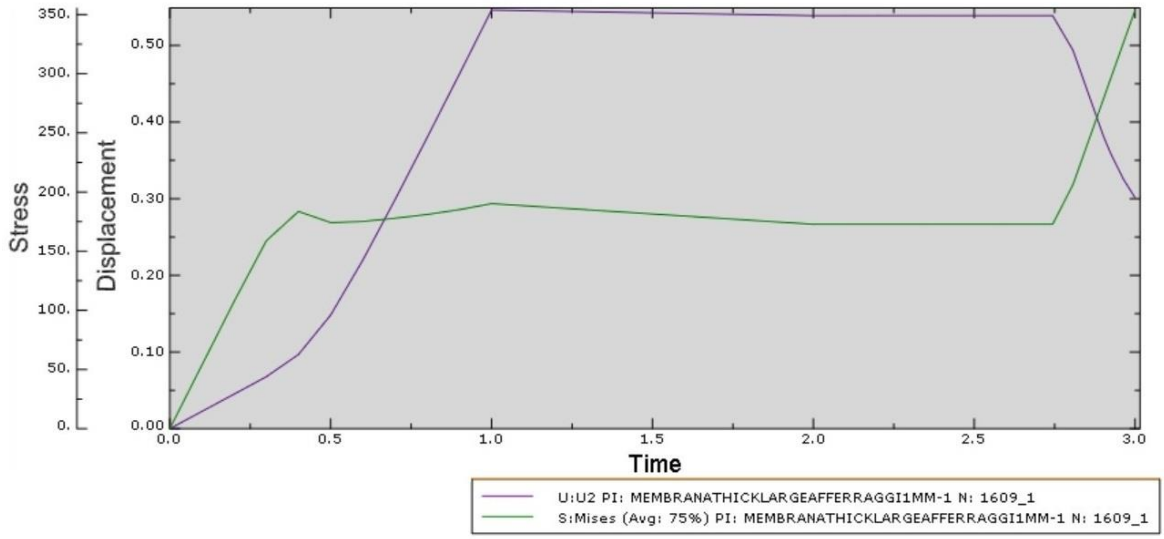

Figure 93 results for clamped design without external ring.

As result, the vertical displacement due to the pressure is 0.007mm and the R value is 0.245mm.

Now it is useful to verify the clamped design with external ring for two different boundary conditions: ring totally fixed and ring with fixed pinholes.

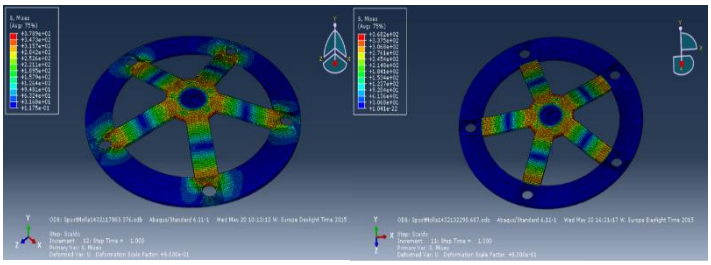

Figure 94 Boundary conditions for the clamped design with external ring

As shown in Figure 94, the result for the boundary condition on the left (clamped pinholes) is a pressure displacement of 0.0080mm. The latter on the right (camped ring) achieves 0.0079mm. The maximum R values are 0.21mm and 0.244mm respectively.

Concerning the results it is clear that is better to clamp not only the pin but also the external ring.

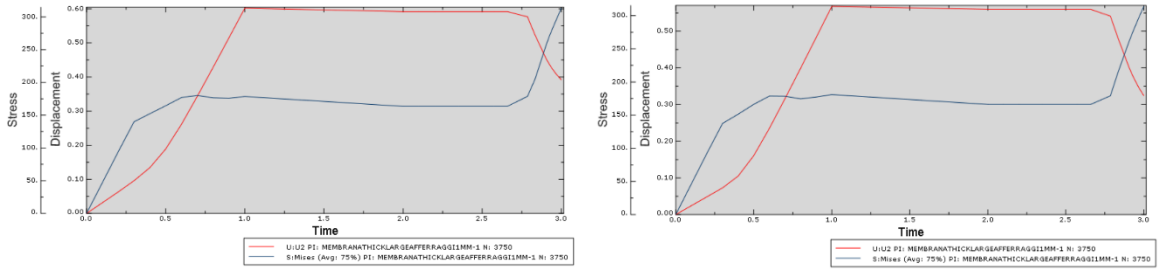

Figure 95 Results for different boundaries conditions clamped design with external ring

If the same simulation is carried out at the same conditions but with the width of 1mm the results are near in value but worse.

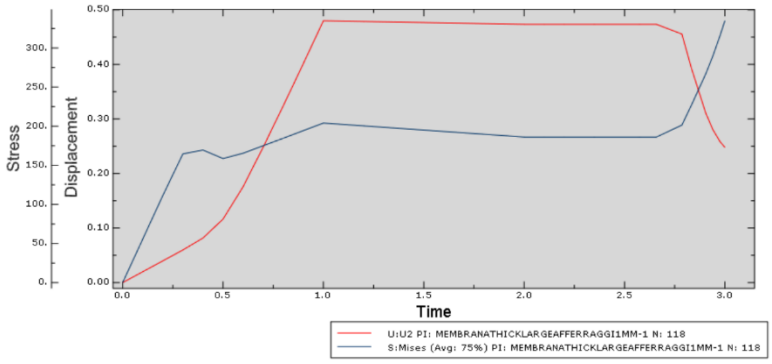

Figure 96 Results for clamped ring configuration with varied width of 1mm

As it can be seen in Figure 96 the maximum R value for the clamped ring with $1mm$ width is 0.233 in comparison with the previous one of 0.244mm. The displacement due to the pressure is better for the former 0.007mm instead of 0.008mm for the latter. Because it is considered more important for the valve to have more stroke than to gain 0.001mm while the maximum pressure is applied ($5bar$), the optimum design is defined to be the one with 0.8mm leg's width.

3.6.2 Actuator's position in the valve

The position inside the valve of the actuator is determined by the function it has, which is to seal and open the pilot channel.

Below in Figure 91 is presented the position of the actuator in a pilot valve, for future works it has to be considered also the possibility to reshape the geometry of the valve.

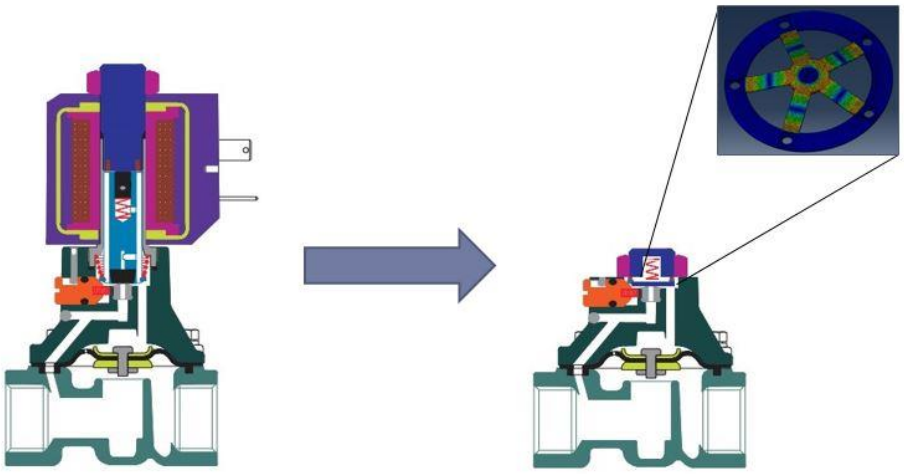

Figure 97 Position for the SMA actuator in a pilot valve

Looking at Figure 97 helps to understand how with the same fluidic part, which means same flow rate, the volume is nearly half of the conventional solenoid valve overall volume. This innovation process could continue by modifying also the fluidic part, improving the performance of the valve. Considered that the actuator need DC current with nearly no electronics, it has to be considered a small volume for housing batteries or an AC/DC converter.

3.7 Choice of the final design

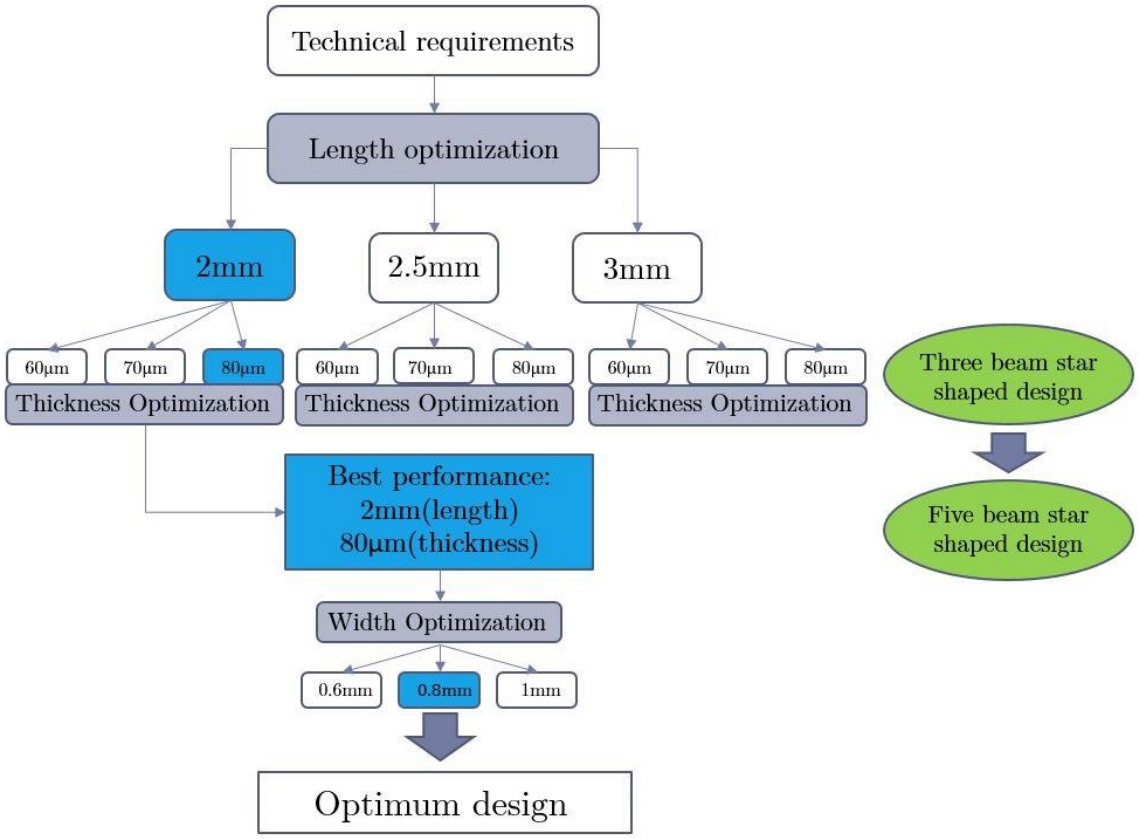

Figure 98 Diagram of the overall optimization process.

In Figure 98 is depicted the whole process that leads to the optimum design. In the first part (length optimization) several analysis were performed in order to reach the maximum R parameter for each beam's length by varying the initial displacement.

After deciding a first attempt three beams star-shaped design, the thickness optimization starts, which is quite trivial, because, as expected, 80µm allows superior performances in flection. Concerning width optimization seeing Table 8 the differences between the three configurations are small (microns), but it is possible to trim the design to obtain either bigger R parameter (0.6mm) or smaller displacement (non leaking tests).

In Figure 98 purple indicates the parameter chosen for the optimization, green stands for changes in the number of beams used; light blue represents the chosen configuration after each process.

Below it is presented the final optimum design.

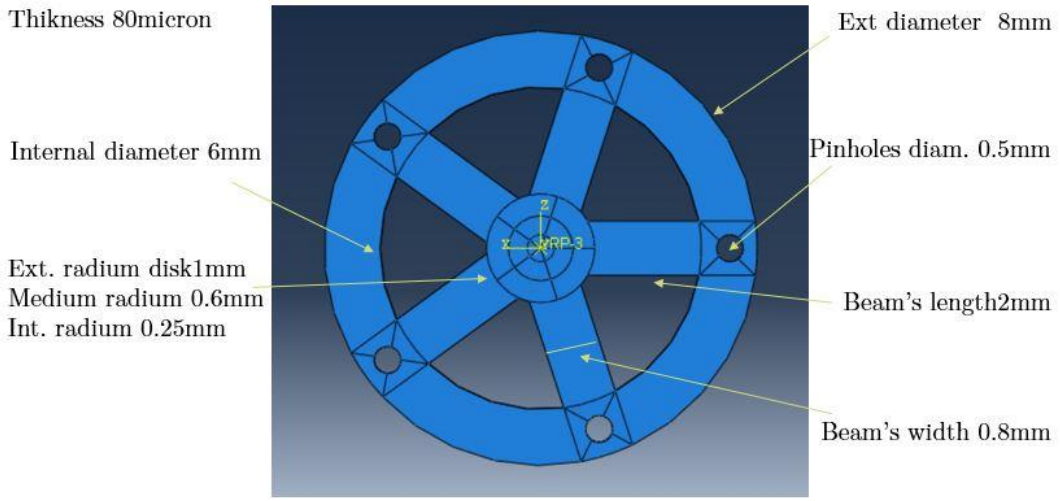

Figure 99 Final optimum design.

In order to understand which are the performance of the final design, in Figure 100 are plotted the vertical displacement and the force measured at the bottom of the truss, this values are compared with those coming from the experimental setup.

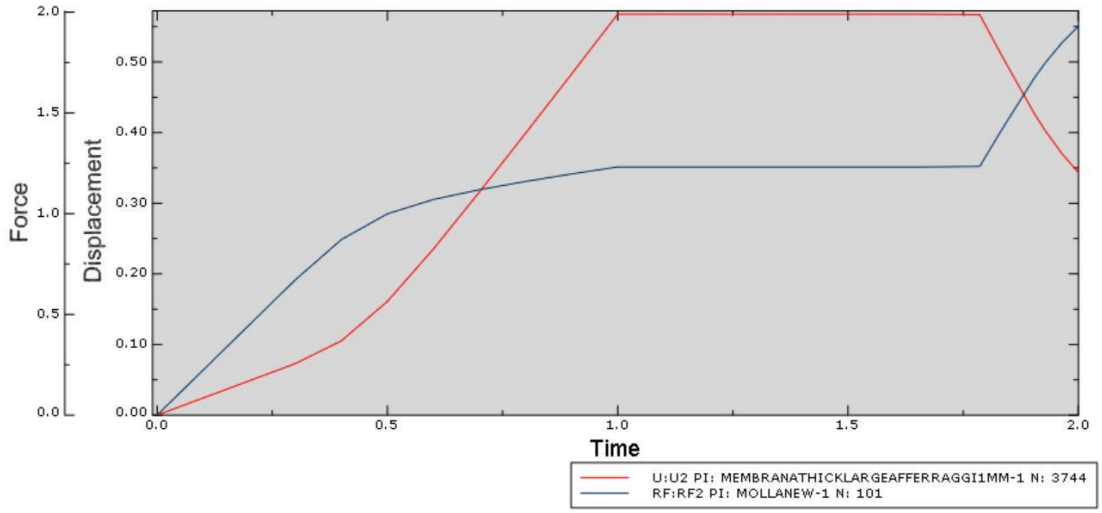

Figure 100 Performances for the final optimum design.

In Table 9 are provided the results achieved by the best design. These values are compared in the next chapter with the experimental setup.

Table 9 Results of the optimum five beams star-shaped design

	Best initial disp	Max R param.	Max F param.	Max Stress
Opt. Design	$0.568mm$	$0.224\ mm$	$0.7N$	$377MPa$

To obtain better performances of the actuator a $0.6mm$ initial displacement must be provided, the R parameter as seen from Table 9 is near to the best value of all, which belongs to the 0.6mm width, the F parameter is one of the biggest and the maximum force that can be provided by the actuator is $1.9N$. Observing the stresses it can be seen that are below the yield stress but greater that the transformation stress ($100MPa$), which means that the actuator works properly and in the material occurs phase transformation.

4 CHAPTER Production and tests

4.1 Designs for testing

To have an experimental proof that the behavior of the valve is correctly depicted by the numerical simulations, some designs are selected to be produced and tested.

To consider the possibility that the parameters of the model are not precisely those of the real material, from the optimum design and its best performance, other designs are chosen by diminishing by twenty per cent the best value. The aim is to find designs that can reach the performance of the varied best values, reconsidering every parameter earlier optimized. The purpose is to produce not only the best design but also some others prototypes, which have fair performances in case there is a systematic error in the simulations performed. For all the designs, a fillet with radius of 0.5mm is applied to the edges in order to increase fatigue performance. This are not applied to the simulation, in order to have volumes easily divisible into shapes easy to mesh, to decrease the time of execution and to increase mesh precision. Another reason is that the model cannot predict fatigue behavior.

The following results are obtained:

- The thickness chosen for all the designs is 80 microns due to the fact that allows best performance for all the parameters
- The optimum leg's length is 2mm
- The best value for the R parameter is obtained with 0.6mm width, but it is dangerous due to the lack of stiffness (difficult to hold the position while the pressure is applied)
- Varying by 20% the best R value two more beam's length are obtained: 1.5mm and 2.5mm
- Varying the best F parameter a width of 0.8mm is obtained

Combining these data a table is created (Table 10) with all the possible combinations of length and width, but not all of them are worth to be produced.

These are the four principal designs, to be sputtered:

- Firstly, of course the optimum design, in case model and material are perfectly aligned.
- The best R parameter is provided by the length of 2mm and the width of 0.6mm
- Two design respond with the diminished R values which are: for a beam's length of 2.5mm a width of 0.8mm and 1mm

In the worst case of great differences between the model and the real material (experimental data), the stiffer and more flexible (1.5mm length/1mm width and 2.5mm length/0.6mm width) are produced, to understand in which direction the optimum performance is shifted.

Table 10 Table of the designs for production

Width/Length	1.5mm	2mm	2.5mm
0.6mm		x	x
0.8mm		x	x
1mm	x		x

It is decided to start with the four principal designs and, if necessary, to produce the other two if the results are not satisfying.

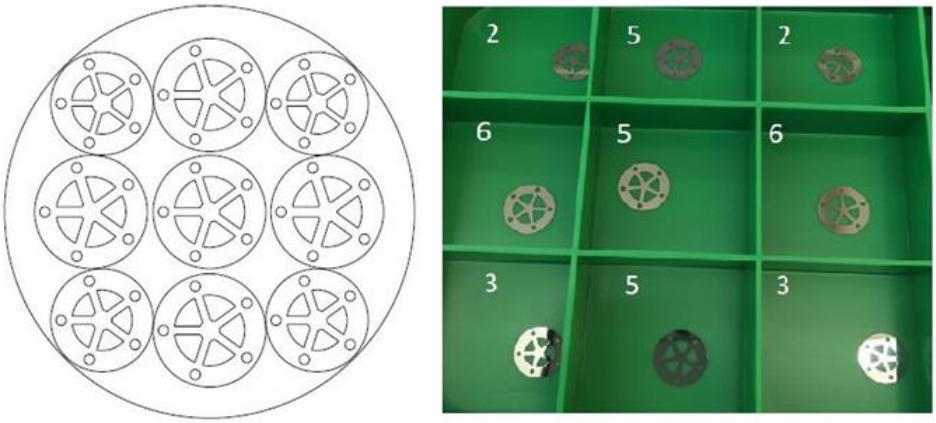

Figure 101 Wafer layout and sputtered prototypes

Because of the production process of the actuators, there is the possibility to sputter on top of the NiTi layer another layer, which is composed of metallic elements placed on top of the beams of the star-shaped design.

These elements (micro-heaters) are connected to a power supply, which allows heating them with electrical current. Two sets of actuators are produced: one with micro-heaters and another one without.

Figure 102 Prototypes with and without microheaters

4.2 Experimental set-up

The aim of this paragraph is to describe an experimental set-up suitable to validate the results of the proposed simulations. In particular, it is necessary to have proof of the strokes and forces provided by the actuator. In this way, it would be possible to determine also, what is the most reliable model and to identify the error.

For both the experiments the material required is:

- Laser range sensor
- Oscilloscope
- 0.5mm diameter screws
- Thermocouple
- Force sensor
- Lever

The laser sensor is positioned with its axis perpendicular to the actuator to allow measuring the vertical displacement. The NiTi layer is clamped with five $0.5mm$ diameter screws to a metal plate, which has a hole in line with of the center of the actuator.

The force sensor could be piezoelectric; the main characteristic is that it has to be flat in shape, because it has to be positioned in contact with the spring.

Two setups are described; the difference between them is the way the thrust force (spring) is provided and how it is measured. The former occupies a lever, which is in contact with a compression spring and the actuator; the latter has a different concept of springs in fact the force is provided by a cantilever beam. The two setup are described in the next paragraphs. Each setup has two variation: testing the film with or without micro-heaters. The former, without micro-heaters is aimed to give a material characterization (comparison with simulations results); the latter is to measure the performance of the actuator proposed. For this reason the results of the former will be compared with those of the CHAPTER 3; on the contrary the experimental evidence obtained with the second are used to show the functional relation between input (temperature, current) and output of the actuator

(displacement, actuation force). It is remarkable also that the design of the micro-heaters is to be validated and it must be checked if it can provide the correct heat flow to reach the correct temperature of the beam without melting the micro-wires.

4.2.1 Spring and lever design

In this experiment, a first type lever connects the actuator to the thrust spring, to allow using bigger springs than the ideal springs of the simulations, which have diameter less than $2mm$. In this case, the spring is not directly under the film, which causes severe volume limitations and assembling problems, so its force is transferred in space by the lever allowing displacing the spring aside the actuator. Below are listed the parameters of the spring as in the simulations (Table 11). For each configuration is used a different spring, here is considered the spring for the optimum configuration.

Table 11 Spring's parameter

Stiffness	6N/mm
Free length	2mm
Compressed length	1.6mm
Force	1N

Due to the thickness of the material, it is complicated to apply a coil spring on the center of the actuator, especially thinking about the end of the spring. On the market a spring is chosen with the correct stiffness ($6\ N/mm$), but different characteristics in terms of free length and dimension. In order to guarantee the same forces applying the same displacement provided by the truss in the simulations, a lever system is chosen to transmit the force from the spring to the model.

Table 12 Datasheet of the chosen commercially available spring

Stiffness (Spring rate)	6N/mm
Free length	2mm
Compressed length	1.6mm
Force	1N
Wire diameter	1mm
Outer diameter	11mm
Inner diameter	9mm
Free length	5mm
Active coils	1.7
Total coils	3.7
Solid height	3.7mm
End type	Closed and grounded
Maximum Load	7.575N

In Figure 103 is depicted the experimental setup, the spring on the left is a commercial spring produced by Acxess spring (Table 12). On top of the spring a force sensor is glued, which is fixed on a plate, which has the possibility to move up and down by means of a screw.

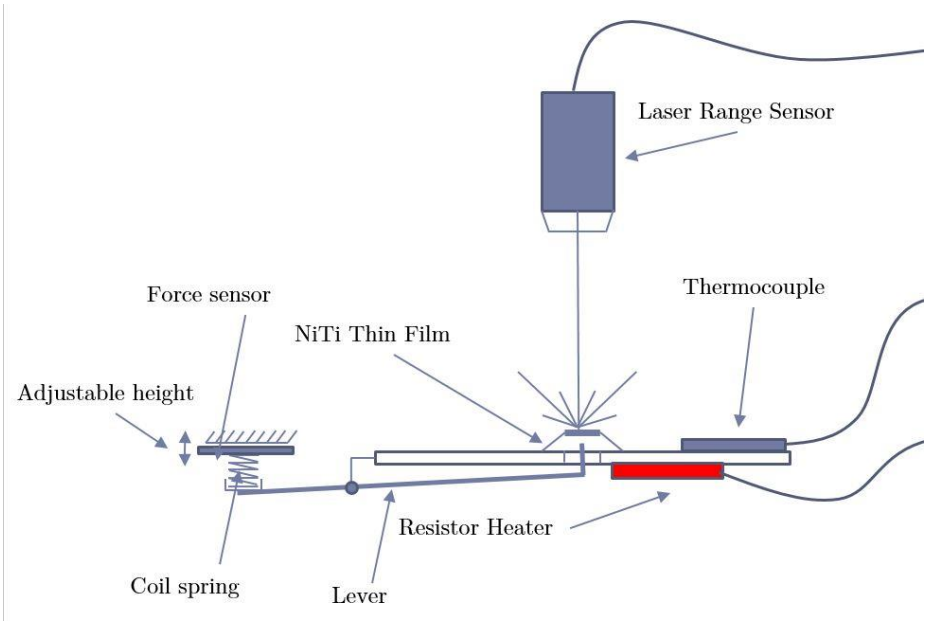

Figure 103 Experimental setup

From the theory of levers, it is possible to calculate the correct position of the fulcrum to obtain the desired ratio between forces and displacements. However knowing that the stiffness of the ideal and real springs is the same it is useful to place the fulcrum in the middle of the lever in order to measure directly the force of the actuator and to have the same displacement. In this way using a laser sensor and start adjusting the position of the force sensor, compressing the spring (see Figure 103) it is possible to obtain the desired initial configuration of the actuator.

The stiffness of lever have to ensure that the measure is not affected by its deformations. The displacement at each end of the lever must be at least one order of magnitude less than the measured displacements. The deflection of a beam is calculated as follows, from the equation of the elastic curve.

$$\delta = -\frac{Pl^3}{3EI} \tag{17}$$

As maximum value for the load is chosen $5N$, which is, five times more than the maximum value $1N$.

The lever is $10cm$ long in order to place the spring aside from the actuator but sufficiently far not to be affected by the heat comings from the resistor heater. The length of the freestanding beam (l) is half of the total, because the fulcrum is placed on the center of the lever. Supposing that the section of the lever is circular with a diameter of $5mm$ its area moment of inertia is calculated below.

$$I = \frac{\pi r^4}{4} \tag{18}$$

The material chosen for the lever is FE510, which has a Young's modulus equal to 210000 MPa.

Applying a load of $5N$ results in a $\delta = 2\mu m$, considering that the displacement of the actuator is around $0.20mm$ ($200\,\mu m$), there are two order of magnitude of difference which means that the lever can be treated as a rigid body. Concerning the force sensor to whom is attached the spring, the deformability is in the order of few micron because it is composed by a piezoelectric crystal which is extremely rigid. An example of force sensor is provided below in Figure 104.

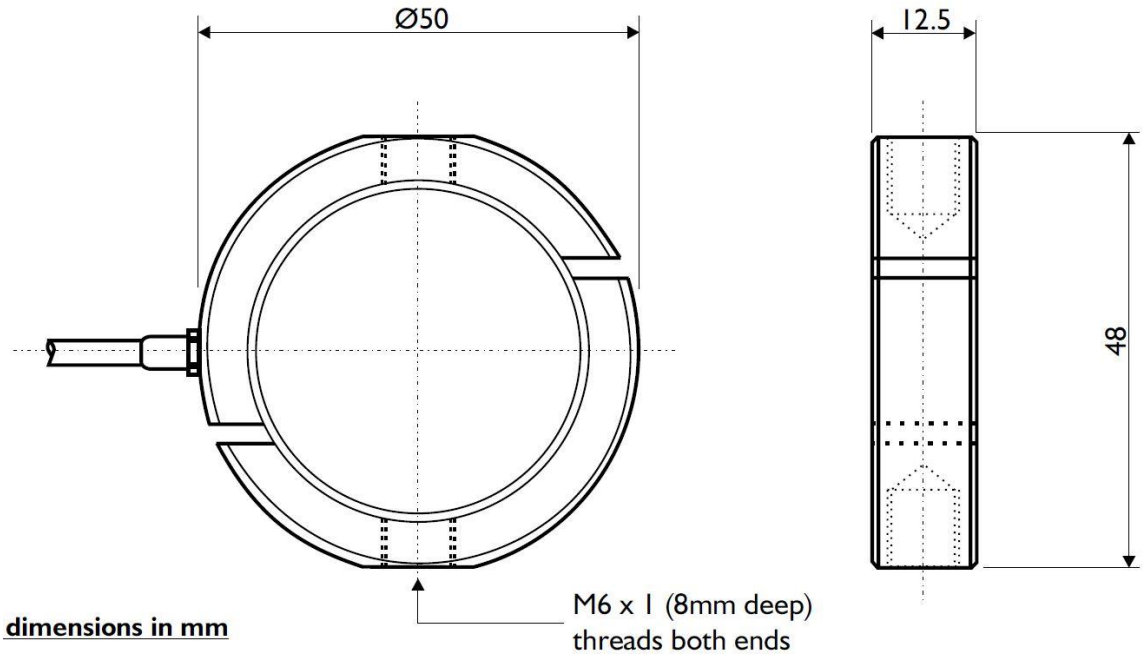

Figure 104 Example of a load cell suitable for the experimental setup.

4.2.2 Cantilever spring design

The setup described in the last paragraph is suitable to measure the forces and the displacements of the actuator while the temperature is changing, but it has the inconvenient to change the spring whenever is changing the design tested. For this reason it is designed a setup with variable length cantilever spring in order to be able to apply the spring force in the center of the actuator with a flat surface. By varying the length of the beam, a variation of stiffness is obtained following the needs of any configuration tested. In this configuration either a slider constraint or various positions to fix the cantilever are required, because varying the length of the free standing part of the beam requires also to adjust its position with respect of the actuator. If the beam is fixed with a screw would guarantee better results because it could appear a rotational stiffness with the slider.

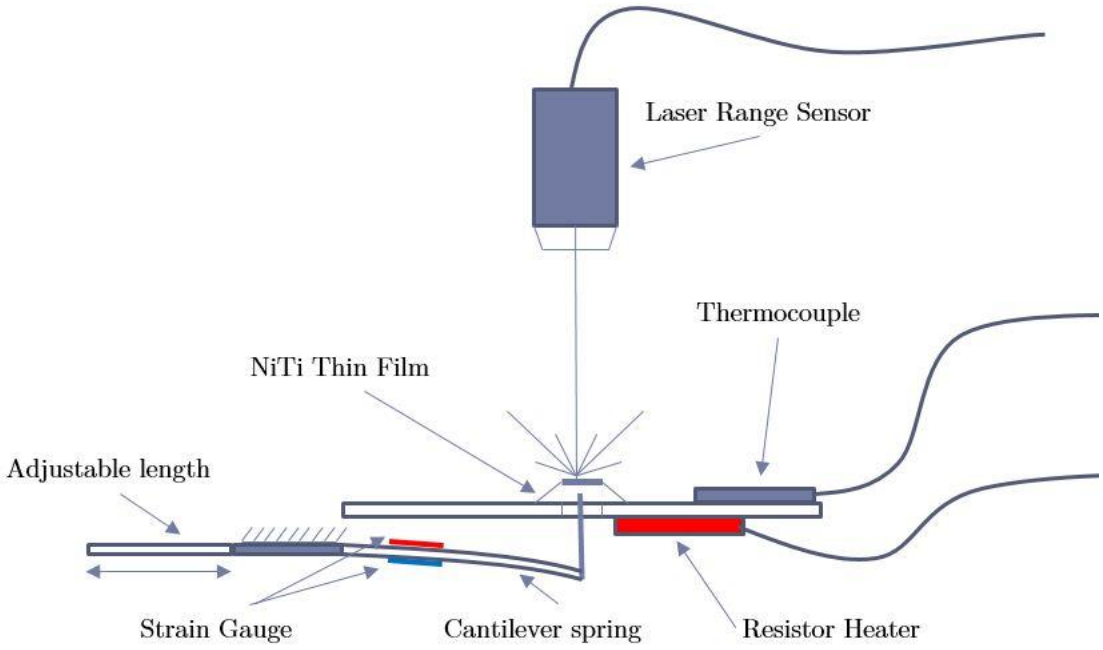

Figure 105 Cantilever beam setup.

To define the length, the beam must have to guarantee the needed stiffness, the deflection of a cantilever beam is calculated with Equation (17). Using the equation of the elastic curve and the concept of spring rate, the stiffness of a cantilever beam loaded at the end is calculated:

$$k = \frac{P}{\delta} = \frac{3EI}{l^3} \tag{19}$$

It is important to draw attention to the fact that Equation (17) is valid below the hypothesis of small displacements, so it has to be defined, for this application, which deflection can be accepted as small displacement. The maximum deflection of the beam is represented by the bigger initial displacement required, which is below $1mm$ ($0.6mm$). Knowing that the free length is $5cm$=$50mm$, it can be considered that the beam is in condition of small displacements, because the vertical displacement provided is nearly two order of magnitude less, than the length of the beam.

The stiffness necessary is the one in Table 11 ($6N$). The material of the beam is the same of the previous setup (FE510), which has a Young's modulus of $210000MPa$. The section is chosen rectangular to allow better deflection in the y-axis; the thickness and the width is tailored according to the area momentum needed. The length is chosen equal to the previous setup ($5cm$) in order not to be too close to the heater (excessively stiff), nor to occupy space where not needed. From Equation (19) is obtained the area momentum, which is equal to $I = 1.2mm^4$, knowing that for a rectangular section is:

$$I = \frac{bh^3}{12} \tag{20}$$

The width (b) of the cantilever beam is chosen 2mm as the diameter of the circular part of the actuator to foster a proper contact between them. Now it is possible to calculate the correct thickness to achieve the desired stiffness. The thickness results to be $h = 1.93mm$ which can be approximated to $2mm$. Defined the section and the length of the bar, with the same equations is possible to calculate the distances needed to gather the required stiffness for the other designs.

In this setup, if the force sensor is fixed to the bar with glue, it is not possible to adjust the length of the beam, and if it is placed between the bar and the metal plate with a screw, would read the force provided by the latter. Another solution possible is to apply strain gauges to the beam, converting the cantilever beam into a force sensor like most of the load cells. With a configuration composed by one strain gauge on the top surface of the beam and one on the bottom (see Figure 105),

reading the compression strain on the lower face and the traction strain on the upper surface it is possible to calculate the load applied at the end of the beam. From the theory of the Wheatstone bridge, it is possible to compensate the distortion due to the temperature variations and those of the axial stresses. The amplification factor is 2, if the signal amplification is not sufficient, a factor 4 is achieved with four strain gauge.

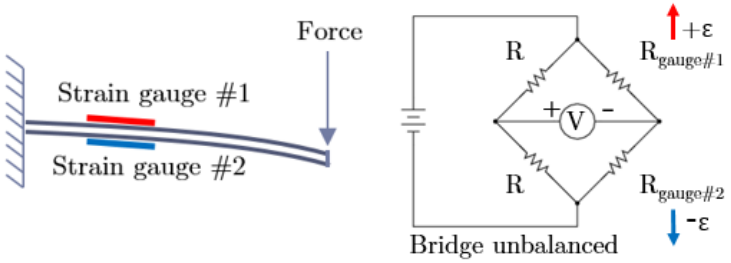

Figure 106 Operation and position of strain gauges.

From the Equation (21) of the Wheatstone's bridge for half bridge is possible to calculate the strain present in the material:

$$\varepsilon = \frac{-2V_r}{GF}\left(1 + \frac{R_L}{R_S}\right) \tag{21}$$

Where V_r represents the voltage ratio that is used in the voltage-to-strain conversion, GF is the gauge factor specified by the gauge manufacturer, R_L is the lead resistance if the connecting cables have a non-negligible resistance. R_S is the nominal gauge resistance (also specified by the manufacturer).

V_r is calculated with Equation (22).

$$V_r = \left(\frac{V_{CH}(strained) - V_{CH}(unstrained)}{V_{EX}}\right) \tag{22}$$

Where $V_{CH}$is the measured signal's voltage and V_{EX} is the excitation voltage.

With the stress strain law of the material is it possible to obtain from the value of the strain present in the material the stress.

$$\sigma = E \cdot \varepsilon \tag{23}$$

To calculate the force applied is sufficient to know the free length of the beam and the point where the force is applied (b). The maximum stress is on the surface of the beam, that it is possible to obtain with Equation (24)

$$\sigma_{max} = \frac{M_f}{I}\frac{h}{2} \tag{24}$$

Where M_f is the moment generated by the force applied at the end of the beam, h is the thickness of the material, I is the area momentum already calculated.

Finally, it is possible to obtain the force provided by the actuator with Equation (25)

$$M_f = F \cdot b \tag{25}$$

Where b is the distance between the point load of the force and the position if the strain gauge.

Once the force is calculated and the displacements are read from the laser range sensor, it is possible to compare the results with the FEM simulations of the chapter three.

4.2.3 Experimental set-up without micro-heaters

Remembering that two sets of actuator are sputtered (with and without microheaters), here is presented the sagacity to adopt to test the NiTi layer without mircoheaters, keeping the setup as described earlier (paragraphs 4.2.1, 4.2.2).

In this case, the actuator has just one layer of NiTi in order to make it reaches the phase transformation, the temperature of the material must rise. The actuator is heated by conduction from the metal plate on which it is fixed. A resistor heater positioned on the lower surface heats the metal plate. A thermocouple placed on the top of the plate, near the NiTi film, measures the temperature. By the time that temperature rises, the laser sensor and the force sensor record the data of vertical displacement and force.

The metal plate is made by a conductive metal in order to guarantee homogeneous temperature on the upper surface, the mass of the plate has to be greater than those of the film in order to have greater thermal inertia to be sure they have slightly the same temperature. The material has transition temperatures that has to be reached in order to make it transform. In case that the temperatures rises above them it would be sure that the thin film has changed structure, for this reason it is not necessary to achieve the precise transformation temperature but it is sufficient just to rise above it.

The thermocouple is positioned on the upper surface of the metal plate. Because this ensemble is thermodynamically not determined is preferable to position the data point (thermocouple) on the upper surface, doing so it would measure a temperature of a surface directly connected with the temperature of the actuator.

Results has to be compared with the Figure 100 of chapter three, which represent the simulation correspondent to this experimental setup.

4.2.4 Experimental set-up with micro-heaters

Maintaining the same experimental setup described (paragraphs 4.2.1, 4.2.2), additional material is required:

- DC power supply
- Ammeter

Due to the presence of the microheaters on the surface of the actuator, it is sufficient to connect it to the DC supply by welding. Starting the alimentation of the micro-heaters the temperature rises locally and the actuator begins to respond, force and displacement are measured. A graph with current on the x-axis and displacement or force in the y-axis is created. Other interesting data to collect is temperature in comparison with stroke and force. Thermodynamically speaking the behavior of the design is unknown, it is interesting to see with an IR camera the temperature distribution, to verify that the position and the configuration of the micro-heaters is correct. The experiment consists in increasing the current from zero until the actuator stops moving, this means that the structure of the material is transformed into austenite and the transformation temperature is reached. This experimental setup is meant to test the performance of the actuator as it is while embedded into the valve's body.

4.2.5 Possible problems

Concerning the spring-lever setup the friction of the lever in the pivot point represents a possible problem; this can be solved by holding it up on a single point by mean of a blade placed under it. The shape of the lever must be modified by adding a notch in order to hold it in the correct position. Another possible problem concerning the lever is its balancing, because to fix the spring a plate must be applied to the left arm of the lever, so a weight has to be applied on the other side for balancing.

Regarding the second experiment (with micro-heaters) an issue is how to know the current needed to reach a certain temperature of the actuator. The temperature of the film is related to several variables such as temperature of the environment, convection ect., so to calculate it precisely a thermocamera would be necessary, also to validate the design and the position of the heaters. Is possible to determine when to stop increasing the current by observing the displacement of the actuator, when the displacement stops decreasing (while the material stops recovering the deformations), the current must be stopped in order not to melt the micro wires.

Another type of problem is to verify the rate of the commercial springs (in the first setup), which is solved using defined weight and by measuring the displacement with the laser once positioned on the top of the spring. In this way a graph is created which links force and displacement. The rate is obtained by measuring the slope of the curve.

Concerning the first setup, heat transfer from the resistor heater to other parts of the model can be problem if the spring expands due to the rising of the temperature. This is solved by positioning the spring sufficiently far from the resistor, at a distance of $10cm$

4.3 Possible applications

Concerning possible applications, it is useful to think about the functions nowadays possessed by solenoid valves. The presented actuator is installed in a valve, which has the same fluidic part of a two-way normally closed valve, but with reduced volume and increased performance. The applications are firstly those who needs reduced volume, low power consumption and weight such as valves for dialysis machine (biomedical field), that could be portable with this technology or professional Inkjet in the way of reduced volumes. In general, other applications are beverage, especially cold, but also any application who need to regulate a flow of liquid or gases such as in oil and gas applications, which is one of the principal field of solenoid valves.

This actuator is aimed to fit in a valve, but the parameters optimized are strokes and forces, which can suit in every other application, who needs a linear displacement, such as switch controller or pumps. The limit is only the creativity of the designer in deciding what kind of engineering need satisfy with this product.

5 Conclusion and further work

This work is a practical example of an unconventional way to design an innovative actuator. From the patent analysis performed, it can be seen that patents filing concerning solenoid valves in the past seventy years follows a logistic curve with saturation point set around the year 2020. This can be interpreted as a sign of an obsolete technology ready to be redesigned. The catalogue research conducted, underlines that the performance of the current market of solenoid valves, if classified by flow rate and overall volume, shows a linear trend. To go beyond the current performance in that field, a flow rate of $K_V = 1\frac{m^3}{h}$ is chosen with an overall volume of $V = 3 \cdot 10^3 m^3$. Once the target values are chosen, the overall volume is reduced by replacing the solenoid actuation part that seals the pilot channel, with an SMA thin film. A one-way shape memory effect actuator is designed instead of a two-way one, because of its better mechanical behavior. According to, the thrust force of a spring, is needed to initially deform the actuator in order to allow it to recover the deformation upon heating. The difference between the vertical displacement (y-axis), before and after the temperature rises is called R parameter.

The optimum shape for the film is deduced by means of an unusual, but strongly logic, optimization process with finite element simulations, which consists in optimizing one parameter at a time, increasing the complexity of the design only after the best possible value is achieved. A truss (an element with only axial stiffness) provides the spring force. Simulations starts from the simplest possible design (embedded beam), to understand the behavior of the material. Various lengths are tested from $1mm$ to $5mm$. The optimum length for a thin cantilever beam made of SMA that achieve the best recovery in terms of displacement (R parameter) is $2mm$. The R parameter is influenced not only by length, but also by the initial displacement, which varies for each length to achieve the best performance. The force needed for the different initial deformation of the material, is provided by changing the stiffness of the spring, always keeping the same displacement to compress it. As the stiffness of the actuator changes with the length of the beams so the stiffness of the spring must change accordingly; as a consequence, each design needs a different spring to achieve the optimum initial displacement.

Another parameter considered in the optimization is represented by the difference of the vertical force expressed by the actuator at low and high temperature (F parameter). Considering the influence of the stresses, the R parameter of each length is divided by the stress inside the material, so if the stress is lower, the parameter's value increases. By choosing the greatest value obtainable for each length, two more configurations are to be considered, that is $2.5mm$ and $3mm$, which accomplish Rs=0.00128mm/MPa and Rs=0.00127mm/MPa, respectively. The complexity of the design increases as a first attempt is made to test a three-beams star-shaped design. The star shape is chosen in order to allow better stability when a force is applied in the center of the actuator. With the last design, three thicknesses are considered and, as expected, the bigger one ($80\mu m$) shows better results. To optimize the number of legs, a five-beams star-shaped design is also tested, which increases the performance from an R value of $0.17mm$ (three beams) to a $0.199mm$ for an initial displacement of $0.6mm$. As a result, this design is chosen for the subsequent simulations. Three widths of beam are tested: $0.6mm$, $0.8mm$, $1mm$, the first of which gives the best R-value (0.202mm) while the last yields the best F value ($0.6N$). Clamping is the method chosen to hold the actuator into position in the valve's body. To allow fixing the thin film to the valve's body, its geometry is modified with an external ring. After modifying it, new simulations are performed to guarantee that the actuator can hold its position while the maximum working pressure of the valve ($5bar$) is applied at low temperature (no-leak condition simulations). Reconsidering the width optimization, a $0.8mm$ width is chosen after no leak simulation on account of its fair R-value ($0.199mm$) and its capability to hold the deformed position while an external pressure is applied (leakage value of $0.009mm$). The other two widths are discarded because the bigger one shows a lower recovery of the vertical displacement while the smaller one results in a bigger displacement for the no leak condition simulations. After all the possible geometrical dimension are chosen, the optimum design is found (see Table 13 below); namely that with the external ring, which achieves an R-value of $0.244mm$.

Table 13 Geometrical dimension of the optimum design

Parameter	Value
Beam's length	2 mm
Thickness	80 μm
Number of legs	5
Beam's width	0.8mm

After the optimum design is achieved, in the event of a systematic error, in the simulations performed, that shifts the optimum to other configurations with different geometrical parameters, other designs are produced. Other designs are chosen by decreasing by twenty percent the best (R) and (F) value, obtained in the optimum case. The sputtering process allows also to sputter on top of the NiTi film another layer of a desired metallic material to create an electrical path on the surface to allow direct-heating of the material (micro-heaters, see Figure 102). Two experimental setups are provided promoting the simplicity and the effectiveness of the measuring process. In the former the thrust force is given by a spring using a lever, while the latter employs a cantilever beam spring. There are some problems to solve, namely how to position the thrust spring in contact with the film without damaging it, how to solve the variability of the stiffness for each design and how to find a spring with tiny dimensions (the stroke is about 1mm) and a rate of 6N/mm. Regarding the spring-lever design, a lever is positioned in contact with the actuator and a spring, which is positioned to the side of the actuator in order to gain space to allow using a "normal" spring. In addition, the stiffness ensured the spring is precisely the one needed, because the currently marketed springs have the required stiffness, although it is necessary to buy a different spring for every configuration tested (no variable stiffness). To solve the issue related to variable stiffness it is necessary to change the experimental setup. The cantilever spring setup, which ensure a stiffness that varies with deformation, by adjusting the free length of the spring, allows adaptation to any design that has to be tested, but it is valid only under the assumption of a small displacement, which is the case.

Following the conclusion of this dissertation, it is useful to apply the proposed experimental setup to verify the behavior of the material in comparison with the models used. The innovation process could be enriched with biomimicry researches

on AskNature, to see how nature solved the problem of regulating a liquid flow, and with TRIZ methods. Concerning the type of actuation instead of a spring a prestrained superelastic layer could be applied, to make the design more compact.

The simulations performed are only one aspect of the complex environment of the valve, reducing the issue related to electro-thermal-mechanical problem to a simply mechanical problem, which is sufficient to optimize the shape, but it could be useful to perform a simulation with heat transfer involved or simulated electric current through the model, to optimize the model with new parameters.

New materials can be applied to the actuator part such as shape memory composites or shape memory polymers (which could automatically seal the valve). To continue the process of innovation the valve's body could be modified, its shape linearized, because the actuation part could be embedded in the fluidic part. Finally, various types of power supply can be tested to provide power to the micro-heaters, such as AC current or different types current signal shape, in order to choose the supply that reduces power consumption guaranteeing the proper working temperatures.

To conclude, this study demonstrates that, through the process presented, using SMA as a smart material, this study demonstrates that it is possible to design an innovative valve with outstanding performance in terms of power consumption, weight, flow rate and volume. It is up to the creativity of the mechanical designer to spread its applications in the field of engineering.

6 Bibliography

[1] R. S. S. M. Z. G. Wei, «Shape-memory materials and hybrid composites for smart systems,» *JOURNAL OF MATERIALS SCIENCE* , vol. 33, 1998.

[2] O. K. a. W. C. M., Shape Memory Materials, Cambridge University Press, 1999.

[3] M. L. A. S. M. A. G. Jaronie Mohd Jani, A review of shape memory alloy research, applications and opportunities, Elsevier, 2013.

[4] T. K. Kazuhiro Otsuka, Science and Technology of Shape-Memory Alloys: New Developments, MRS BULLETIN, 2002.

[5] M. J. M. a. M. D. Reginald DesRoches, «Cyclic Properties of Superelastic Shape Memory Alloy Wires and Bars,» *JOURNAL OF STRUCTURAL ENGINEERING,* 2004.

[6] H. W. M. D. Z. Z. Y. W. C. C. P. H. T. C. Sun L., Stimulus-responsive shape memory materials: A review, Elsevier, 2011 .

[7] V. D. R. C. A. R. E. V. F. A. G. G. Annamaria Lisotti, Educational pathways through nanoscience: nitinol as a paradigmatic smart material, IOP, 2013.

[8] Z. W. H. G. X. Y. HuangW M, «Micro mirror based on surface relief phenomenon in shape memory alloys,» *SPIE.*

[9] W. M. H. M. H. H. M. J. W. Y. Q. F. QHe, «Characterization of sputtering deposited NiTi shape memory thin films using a temperature controllable atomic force microscope,» in *SMART MATERIALS AND STRUCTURES*, INSTITUTE OF PHYSICS PUBLISHING, 2004.

[10] X. R. K. Otsuka, «Physical metallurgy of Ti–Ni-based shape memory alloys,» *Progress inMaterials Science,* n. 50, 2005.

[11] M. S. T. K. T. S. Akira Ishida, «Effects of composition and annealing on shape memory behavior of Ti-rich Ti-Ni films formed by sputtering,» *Materials transactions,* vol. 42, n. 6, p. 1060 to 1067, 2001.

[12] H. W. Gao XY, Thermomechanical behavior of shape memory alloys under non-proportional load., SPIE, 2002.

[13] Y. Bellouard, «Shape memory alloys for microsystems: A review from a material research perspective,» *Materials Science and Engineering,* 2008.

[14] W. T. W. HUANG, «Training two-way shape memory alloy by reheat treatment,» *JOURNAL OF MATERIALS SCIENCE LETTERS,* 2000.

[15] «Linear and Non-Linear Superelasticity in NiTi,» *MRS Shape Memory Materials,* vol. 9, p. 201-209, 1989.

[16] W. Y. Dieter Stoeckel, Superelastic Ni-Ti Wire, WIRE JOUANAllNTERNATIONAl, 1991.

[17] U. o. Cambridge, «Doitpoms,» [Online]. Available: http://www.doitpoms.ac.uk/tlplib/superelasticity/limits.php.

[18] F. H. E, Shape Memory Alloys Vol. 1 Precision Machinery and Robotics, Taylor & Francis, 1987.

[19] C. J. Harsh Deep Chopra, «Magnetic-field-induced twin boundary motion in magnetic shape-memory alloys,» *The American Physical Society,* 2000.

[20] F. butera, «Shape memory actuators for automotive applications,» *shape memory alloys advances in modeling and applications,* 2001.

[21] H. W., «On the selection of shape memory alloys for actuators,» *Mater Des,* vol. 23, pp. 11-9, 2002.

[22] Y. Bellouard, «PhD Dissertation no. 2308,» Lausanne, 2000.

[23] A. L. P. R. J. T. J. H. P. Krulevitch, «Thin film shape-memory alloy microactuators,» *J. MEMS,* 1996.

[24] Y. B. E. B. R. C. A.-N. P. D. H. H. Zhang, «Robotics and Automation,» in *IEEE International Conference on Robotics and Automation*, 2004.

[25] S. L. Wu MH, «Industrial applications for shape memory alloys,» in *International conference on shape memory and superelastic technologies,*, Pacific Grove, California, USA, 2000.

[26] W. T. Stoeckel D, «Use of Ni–Ti shape memory alloys for thermal sensoractuators,» in *Active and adaptive optical components*, San Diego, CA,, 1992.

[27] Y. Q. F. a. W. M. H. Shuichi Miyazaki, Thin Film Shape Memory Alloys: Fundamentals and Device Applications, Cambridge University Press, 2009.

[28] E. L. C. Adam W. Martinez, «Microfabrication and Nanotechnology in Stent Design,» National Institute of Health, 2011.

[29] C. Z. a. E. Q. R Lima de Miranda, Fabrication of TiNi thin film stents, IOP PUBLISHING, 2009.

[30] I. Micro Magnetics, «directvacuum,» [Online]. Available: http://www.directvacuum.com/pdf/what_is_sputtering.pdf.

[31] V. M. Akira Ishida, Sputter-Deposited Shape-Memory Alloy Thin Films: Properties and Applications, MRS BULLETIN, 2002.

[32] M. B. A. I. V. E.-C. H. C. V. T. J.L. Seguin, «Low temperature crystallised Ti-rich NiTi shape memory alloy films for microactuators,» *Sensors and Actuators,* vol. 74, pp. 65-69, 1999.

[33] C. Y. K. E Wibowo, Fabrication and characterization of sputtered NiTi shape memory thin films, JOURNAL OF MICROMECHANICS AND MICROENGINEERING, 2005.

[34] R. D. M. C. Z. E. Q. C. G. T. S. M. K. T. Habijan, The biocompatibility and mechanical properties of cylindrical NiTi thin films produced by magnetron sputtering, Elsevier, 2011.

[35] A. S. R. L. d. M. a. E. Q. Gerd Siekmeyer, «Comparison of the Fatigue Performance of Commercially Produced Nitinol Samples versus Sputter-Deposited Nitinol,» *Journal of Materials Engineering and Performance,* vol. 23, n. 6, 2014.

[36] R. L. d. M. T. S. C. Z. C. M. D. B. a. E. Q. F. Kahleyss, «Processing and Damping Properties of Sputtered NiTi Thin Films for Tools in Machining Processes,» *Journal of Materials Engineering and Performance,* vol. 20, 2011.

[37] C. C. R. L. d. M. a. E. Q. C. Bechtold, «High cyclic stability of the elastocaloric effect in sputtered TiNiCu shape memory films,» *Applied Physics Letters,* vol. 101, 2012.

[38] V. W. C. Z. E. Q. Holger Rumpf, «Near Net-Shape Fabrication of Superelastic NiTi Devices by Sputtering and Photoetching,» in *Materials Transactions*, The Japan Institute of Metals, 2006, pp. 523-526.

[39] D. T. C. L. A. M. G. P. C. John J. Gill, «Manufacturing issues of thin NiTi microwrapper,» *Sensor and Actuators,* vol. A, n. 93, pp. 148-156, 2001.

[40] L. W. G. D. Y. Z. A. Y. B. C. Dong Xu, «Charcteristics and fabrication of NiTi/Si diaphragm micropump,» *Sensor and actuators,* vol. 93, pp. 87-92, 2001.

[41] R. L. D. M. A. E. M. M.-B. H. G. L. E. Q. K. LOGER, «Fabrication and Evaluation of Nitinol Thin Film Heart Valves,» *Cardiovascular Engineering and Technology,* 2014.

[42] R. d. C. J. C. G. S. R. M. M. Nikulin C., «Anticipation of technological change through patent analysis and logistic growth curve,» *Proceedings of the Institute of Behavioral and Applied Management',* 2011.

[43] R. catalogue, Fluid control system E-%, 2014.

[44] «Mga Controls,» 2015. [Online]. Available: http://www.mgacontrols.com/mm-international-two-way-solenoid-valves-pilot-operated/#prettyPhoto[737]/0/.

[45] A. P. L. P. B.-N. MARCELO A. SAVI, «Phenomenological Modeling and Numerical Simulation of Shape Memory Alloys: A Thermo-plastic-phase Transformation Coupled Model,» *JOURNAL OF INTELLIGENT MATERIAL SYSTEMS AND STRUCTURES,* vol. 13, 2002.

[46] «ABAQUS User's Manual,» 2004.

[47] L. P. Ferdinando Auricchio, «A three-dimensional model describing stress-temperature induced solid phase transformations: solution algorithm and boundary value problems,» *INTERNATIONAL JOURNAL FOR NUMERICAL METHODS IN ENGINEERING,* 2004.

[48] R. L. T. J. L. Ferdinando Auricchio, «Shape-memory alloys: macromodelling and numerical simulations of the superelastic behavior,» *Computer methods in applied mechanics and engineering,* 1997.

[49] E. N. M. N. Z. Angela C. Souza, Three-dimensional model for solids undergoing stress-induced phase transformations, Elsevier, 1998.

[50] F. Auricchio, «A robust integration-algorithm for a finite-strain shape-memory-alloy superelastic model,» *International journal of plasticity* , vol. 17, pp. 971-990, 2001.

[51] J. W. Y. Sanjay Choudhry, «A General Thermo-Mechanical Shape Memory Alloy Model: Formulation and Applications,» 2003.